Investigating natural killer cell-derived extracellular vesicles using clinically relevant TNBC models

Melanie Kirkby

Thesis submitted to the University of Ottawa

in partial fulfillment of the requirements for the

Master's degree in Microbiology and Immunology

Department of Biochemistry, Microbiology, and Immunology

Faculty of Medicine

University of Ottawa

uOttawa

Abstract

Triple-negative breast cancer (TNBC) is the most aggressive subtype of breast cancer with the worst overall survival, yet viable treatment options are limited. The majority of TNBC patients rely on chemotherapy, which has several side effects and limitations. For example, chemotherapy enriches cancer stem cells (CSCs), a subpopulation of cells with a vast potential for self-renewal and cell proliferation. CSCs are highly chemoresistant, contributing to tumour recurrence and metastasis. Thus, the development of novel therapies for TNBC is a critical area of research. In this regard, natural killer (NK) cell-derived extracellular vesicles (NK-EVs) have emerged as a promising anti-cancer immunotherapeutic. As NK-EVs are derived from NK cells, they are naturally cytotoxic against cancerous cells. The objective of this project is to evaluate the efficacy of NK-EVs against TNBC. This study demonstrated that NK-EVs exhibit a short-term dose-dependent cytotoxic effect on TNBC cell viability through the activation of both apoptotic and necrotic cell death pathways. For the first time, this study demonstrated that NK-EV treatment was also effective at suppressing TNBC CSC functionality and viability. Additionally, patient-derived xenograft (PDX), a three-dimensional tumour model that originates from human patients post-surgery, were used to validate NK-EV cytotoxicity in a clinically relevant *ex vivo* TNBC model for the first time. Finally, in a TNBC PDX mouse model, NK-EVs administered intratumorally accumulated primarily in the tumours. Conversely, intravenous injection of NK-EVs resulted in a more systemic distribution of NK-EVs throughout the body, with the major sites of accumulation being the liver, spleen, tumour, and lungs at 24 hours. Altogether, these findings suggest that NK-EVs may have broad implications for the treatment of TNBC and, with further research, could potentially improve the prognosis of TNBC patients worldwide.

Acknowledgements

I would like to thank my supervisors, Dr. Lisheng Wang and Dr. Jessie Lavoie, for their continued guidance and motivation over the entirety of my master's project. I started working in Dr. Wang's lab as an undergraduate student, and he has always been an amazing mentor who has helped shape the researcher that I am today. Now, getting to also work with Dr. Lavoie at Health Canada has been a deeply enriching experience where I've benefited from her expertise and passion for research. I'd also like to thank the members of my TAC, Dr. Seung-Hwan Lee and Dr. Derrick Gibbings, for their guidance and expertise. Their feedback has been instrumental in shaping the course of my research project.

I would like to thank Frederic St-Denis-Bissonnette for his mentorship and feedback over the entirety of my master's project. Having the opportunity to work alongside him and receive invaluable feedback has helped shape me as a researcher, and I'm very thankful for the experience. I'd also like to thank Karan Mediratta, who was my first mentor as an undergraduate student, and Marena Diab for their feedback and aid over the entirety of this project. Additionally, I'd like to thank all my lab members, as well as the undergraduate students I had the pleasure of mentoring, for all their help over the years. Without all of you, this research would not be possible, and I'm incredibly grateful to the people who have helped make it happen.

I'd like to personally thank my parents, Paul and Van, my siblings Sean and Kim, and my partner Ben. Their encouragement and continuous aid have meant the world to me, and I would not be the person I am today without all of them. Words could never express how grateful I am to have each and every one of you in my life.

Table of Contents

List of Tables

List of Figures

List of Supplemental Tables

List of Supplemental Figures

List of Abbreviations

293F-EV	293F cell-derived EV
ABC	ATP binding cassette
ANOVA	Analysis of variance
AO	Acridine Orange
BBB	Blood-brain barrier
CD	Cluster of differentiation
CM	Conditioned medium
CSC	Cancer stem cell
CTGF	Connective tissue growth factor
Cyr61	Cysteine-rich angiogenic protein 61
DiR	1,1'-Dioctadecyl-3,3,3',3'-Tetramethylindotricarbocyanine Iodide
DMEM	Dulbecco's Modified Eagle Medium
$DPBS^{-/-}$	Dulbecco's phosphate-buffered saline without Ca^{2+}/Mg^{2+}
EC_{50}	Half maximal effective concentration
ECS	Extracellular capillary space
EMT	Epithelial-mesenchymal transition
ER	Estrogen receptor
EV	Extracellular vesicle
FACS	Fluorescence-activated cell sorting
FBS	Fetal bovine serum
GAPDH	Glyceraldehyde 3-phosphate dehydrogenase
HER2	Human epidermal growth factor receptor 2
HI-FBS	Heat Inactivated Fetal Bovine Serum
HFB	Hollow-fibre bioreactor
IDC	Invasive ductal carcinoma
IV	Intravenous
IL	Interleukin
IT	Intratumoral
MoA	Mechanism of action

MET	Mesenchymal-epithelial transition
MISEV	Minimal information for studies of extracellular vesicles
NK	Natural killer
NK-EV	NK cell-derived EV
NOD-SCID	Non-obese diabetic/severe combined immunodeficiency
NSG	NOD-SCID gamma
PD-1	Programmed cell death protein 1
PD-L1	Programmed death ligand-1
PDX	Patient-derived xenograft
PI	Propidium Iodide
PR	Progesterone receptor
PTX	Paclitaxel
RFP	Red fluorescent protein
RT-qPCR	Quantitative reverse transcriptase polymerase chain reaction
SEM	Standard error of the mean
TAZ	Tafazzin
TEAD	Transcriptional enhanced associate domain
TME	Tumour microenvironment
TNBC	Triple-negative breast cancer
YAP	Yes-associated protein

1. Introduction

1.1. Breast cancer overview

Breast cancer is the most commonly diagnosed form of cancer and the leading cause of cancer-related mortality in women worldwide [1]. Over the last ten years, the incidence of breast cancer has gradually risen, particularly in women under the age of 50 [2]. Now, it is estimated that approximately one in four women diagnosed with cancer are found to have breast cancer.

As breast cancer is a heterogeneous disease, its molecular subtypes are defined by their unique genetic profile and the presence or absence of various receptors, specifically the estrogen receptor (ER), progesterone receptor (PR), and the human epidermal growth factor receptor 2 (HER2). These subtypes greatly influence the predicted disease outcome for individual breast cancer patients, as well as their response to treatment (**Table 1**).

Table 1. Patient prognosis for each breast cancer molecular subtype.

Breast cancer subtype	Incidence rate [3]	Overall recurrence rate [4]	Five-year overall survival [5]	Common sites of metastasis and their prevalence*
Luminal-A (ER^+, $PR^{+/-}$, and $HER2^-$)	50-60%	5.0%	95%	Bone (51 - 73%), liver (19.8 – 60.3%) [6, 7]
Luminal-B (ER^+, $PR^{+/-}$, and $HER2^-$)	15-20%	7.9%	91%	Bone (44.7 – 77.6%), liver (26.2 - 57.1%) [6, 7]
HER2-positive (ER^-, PR^-, and $HER2^+$)	15-20%	13.1%	86%	Lung (36.1 - 50.0%), liver (29.1 - 46.2%), brain (30.6 – 55.0%) [6-8]
TNBC (ER^-, PR^-, and $HER2^-$)	10-20%	16.7%	78%	Lung (30.6 - 64.0%), liver (16.6 – 50.0%), brain (29 - 46%) [6, 7, 9, 10]

*Prevalence in patients who are diagnosed with metastatic breast cancer. TNBC: Triple-negative breast cancer, ER: estrogen receptor, PR: progesterone receptor, HER2: human epidermal growth factor receptor 2.

The most common breast cancer subtype is Luminal-A (ER^+, $PR^{+/-}$, and $HER2^-$), accounting for 50-60% of breast cancer cases [3]. Luminal-A presents with low expression of proliferation-related markers, including Ki-67, translating to a low-grade, slow-growing tumour. Due to the presence of hormone receptors on these cells, Luminal-A tumours are receptive to hormonal therapies such as tamoxifen and toremifene, alongside chemotherapy. Patients diagnosed with Luminal-A tumours tend to have a good clinical outcome with better responses to treatment and a low risk of recurrence [4].

Luminal-B (ER^+, $PR^{+/-}$, and $HER2^-$) accounts for 15-20% of all breast cancer cases. Although phenotypically similar to Luminal-A, Luminal-B tumours express high levels of Ki-67 and other proliferation markers. As such, luminal-B tumours are considered higher grade and more aggressive [11, 12]. Clinical outcomes for Luminal-B are worse than Luminal-A, with a recurrence rate of 7.9% [4]; however, Luminal-B tumours are responsive to hormonal therapy and chemotherapy.

HER2-positive breast cancer (ER^-, PR^-, and $HER2^+$) accounts for 15-20% of breast cancer cases. HER2-positive tumours are typically aggressive, being associated with poorer patient outcomes and survival times relative to the luminal subtypes. However, HER2-positive tumours are dependent on HER2 functioning for survival. As a result, patients have shown a favourable response to HER2-targeted therapies, such as the use of trastuzumab, alongside chemotherapy.

Approximately 10-20% of breast cancer patients are diagnosed with triple-negative breast cancer (TNBC) (ER^-, PR^-, and $HER2^-$). TNBC is widely considered the most aggressive breast cancer subtype, characterized by a worse overall survival rate and the highest risk of recurrence [13, 14]. It is estimated that TNBC disproportionately accounts for 30% of all breast cancer-related deaths [15].

1.2. Treatment Options for TNBC

Treatment options for TNBC patients are fairly limited. The absence of ER and PR on TNBC cells translates to patients being largely unresponsive to all currently approved hormone-based therapies [16]. Furthermore, due to their negligible expression on TNBC cells, all therapies targeting HER2 are ineffective as well. As a result, TNBC patients must largely rely on conventional treatment options. For stages I – III, surgery and chemotherapy are considered the main forms of treatment and may be followed by radiation. For stage IV patients, chemotherapy is the primary, and sometimes only, treatment offered. Although chemotherapy is the mainstay form of treatment for the majority of TNBC patients, it is associated with severe side effects and limitations. For example, chemotherapy is effective against the bulk tumour cells, but it enriches cancer stem cell (CSC) populations, increasing the risk of tumour recurrence and distant metastasis [17, 18]. Furthermore, TNBC is a highly heterogeneous disease. To date, four distinct TNBC subtypes have been identified based on their gene expression: basal-like 1, basal-like 2, mesenchymal, and luminal androgen receptor [19, 20]. As a result, chemotherapy is not universally effective for TNBC, with each subtype exhibiting a varied response to treatment [16, 20, 21].

For some advanced TNBC patients, chemotherapy combined with pembrolizumab (Keytruda) has been approved. Pembrolizumab is an immunotherapy that targets the immune checkpoint molecule programmed cell death protein 1 (PD-1). PD-1 is a receptor highly expressed on T cells that interacts with programmed cell death ligand-1 (PD-L1) on cancer cells, resulting in a suppression of the anti-tumour immune response. Pembrolizumab works by blocking PD-1, preventing the interaction between PD-L1 and PD-1, to restore the immune response against cancer cells. The results from a phase III clinical trial reported that the addition of pembrolizumab

to chemotherapy raised the median overall survival from 16.1 months to 23.0 months when compared with chemotherapy alone [22]. Unfortunately, pembrolizumab is only effective against cells expressing PD-L1, amounting to only 20% of all TNBC patients [23].

In patients with recurrent metastatic TNBC, the antibody-drug conjugate sacituzumab govitecan (Trodelvy) may be considered for the targeted delivery of chemotherapy to the tumour site. In a phase III clinical trial, sacituzumab govitecan raised the median overall survival of metastatic TNBC patients to 5.6 months relative to 1.6 months for patients treated with chemotherapy alone [24]. Beyond this, no other viable treatment options have been approved for TNBC patients, demonstrating a critical need for the development of novel therapeutic options.

1.3. Cancer stem cells in TNBC

1.3.1. CSC characteristics

TNBC's aggressive nature is in part attributed to their CSC population, which is found to be elevated relative to the other breast cancer subtypes [25]. CSCs are a subpopulation of cancer cells with a vast potential to undergo self-renewal and differentiation, and have the capacity to initiate tumour growth. CSCs present with a higher level of ATP binding cassette (ABC) transporters, increasing the efflux of small molecules like chemotherapy out of the cell and contributing to their drug resistance [26]. The increase in ABC transporters, coupled with their natural quiescence, translates to CSCs being largely resistant to chemotherapy [27]. Additionally, advanced-stage tumours often harbour closely related subtypes of CSCs. These clonal phenotypes are largely shaped by their differential exposure to the tumour microenvironment (TME) and mutations gained over time, increasing the tumour's complexity and diversity [28]. As an example, if chemotherapy is effective against one clonal subtype, the other CSC clones may continue

proliferating unharmed, ultimately favouring the selection of chemoresistant cancer cells. Therefore, effective treatment options must be able to target a diverse array of cells, including the CSC clones, to eliminate the entire tumour population and prevent recurrence.

A key characteristic of CSCs is their ability to undergo the epithelial-mesenchymal transition (EMT). EMT is a cellular process through which epithelial-like cells acquire a mesenchymal-like phenotype; this phenomenon typically includes cytoskeleton rearrangement, dissolution of cell-cell junctions, and changes in the cell's overall morphology [29]. In the mesenchymal-like state, cells have increased migratory capabilities and are involved in embryogenesis, tissue repair, and fibrosis [30]. In the context of cancer, CSCs upregulate EMT to promote cell migration and the invasion of new tissue, implicating them in metastasis and drug resistance [29, 31]. Furthermore, CSCs exhibit plasticity and their morphology is highly reversible. Thus, CSCs can revert to their epithelial-like state through the mesenchymal-epithelial transition (MET). Epithelial-like CSCs are associated with increased tumorigenesis, allowing for tumour initiation and growth [32]. Ultimately, CSCs utilize both EMT and MET to promote their continued survival in the body.

1.3.2. Epithelial-like CSCs

Epithelial-like CSCs highly express aldehyde dehydrogenase 1 (ALDH1), a group of cytosolic enzymes involved in the oxidation of aldehydes to carboxylic acids. As a result, ALDH1 is heavily involved in cellular detoxification. ALDH1 is highly expressed in hepatocytes, but is also present in various tissues throughout the body. In stem cell populations, ALDH1 is implicated in cell differentiation through its conversion of retinaldehyde to retinoic acid [33]. Interestingly, ALDH1 is often upregulated in a variety of cancers, including breast cancer [34]. High expression of ALDH1 in CSCs is associated with drug resistance, tumour recurrence, and poorer overall

survival [32, 34]. ALDH1^{high} CSCs have demonstrated an immense potential for tumour initiation, where Ginestier *et al.* found that as few as 1500 ALDH1^{high} cells were capable of forming a tumour *in vivo* [32]. Conversely, the injection of cells lacking ALDH1 did not develop any tumours over the course of observation.

1.3.3. Mesenchymal-like CSCs

Mesenchymal-like CSCs are characterized by a high expression of cluster of differentiation (CD) 44 and a low expression of CD24, and are typically found towards the tumour's edge [35, 36]. CD44 is a non-kinase transmembrane proteoglycan expressed on several cell types, including B cells, T cells, and natural killer (NK) cells. CD44 activation promotes cell survival, motility, and drug resistance [37]. CD24 is a cell surface adhesion glycoprotein involved in cell adhesion and metastasis that is more highly expressed on differentiated cancer cells than CSCs [38]. In breast cancer, CD44 expression on CSCs has been found to promote EMT [39]. Al-Hajj *et al.* demonstrated that the injection of only 100 CD44^{high}/CD24^{low} breast cancer cells into a mouse model was sufficient for tumour development, demonstrating this subpopulation's high potential for tumorigenesis [31]. Furthermore, other studies have demonstrated that CD44 promotes metastasis and tissue invasion in a breast cancer model, making it a central component of CSC functioning [40, 41].

1.3.4. Mesenchymal-like stem cells and the YAP/TAZ pathway

The functioning of mesenchymal-like CSCs is dependent upon several signaling pathways, including the YAP (Yes-associated protein)/TAZ (tafazzin) pathway [42]. YAP/TAZ functioning is dependent upon its regulation by Hippo, a signaling pathway that, when activated, triggers a

downstream kinase cascade (**Figure 1**). Hippo signaling can be activated or inhibited through several pathways, such as changes in cell polarity or cell density, the introduction of soluble factors, cellular stress, and mechanical cues [43]. Active Hippo signaling inhibits YAP/TAZ nuclear localization, regulating its functioning in cells. When Hippo signaling is off, transcriptional coactivators YAP and TAZ bind to the transcription factor TEAD (transcriptional enhanced associate domain) in the nucleus. This promotes the expression of various genes, including *Ctgf* (connective tissue growth factor) and *Cyr61* (cysteine-rich angiogenic protein 61). YAP-associated genes promote cell proliferation, cell survival, stem cell self-renewal, and EMT [44-46]. Furthermore, CD44 regulates YAP/TAZ activity through the activation of RhoA, a GTPase [47, 48]. CD44 increased YAP/TAZ activity and translocation to the nucleus, upregulating subsequent gene expression.

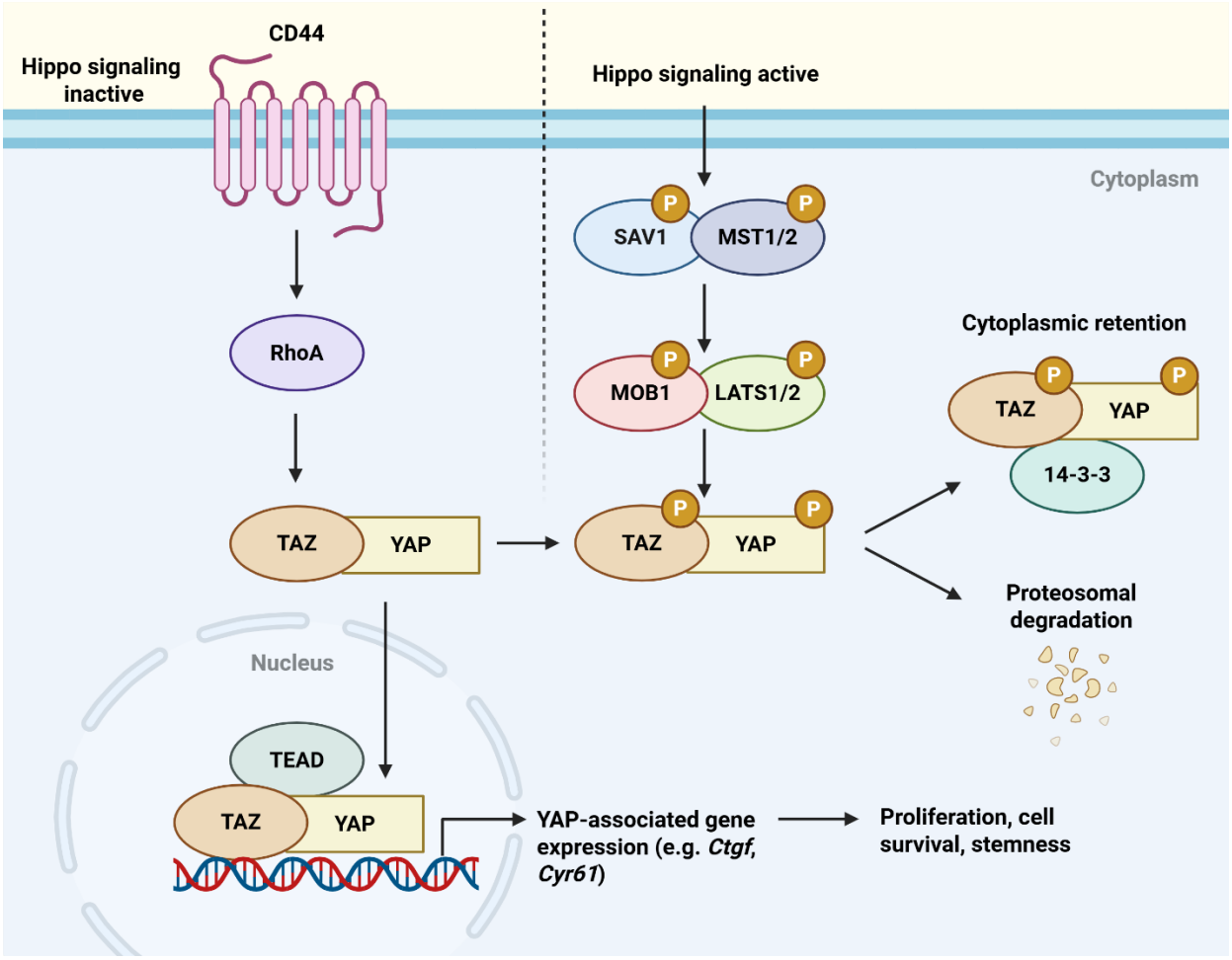

Figure 1. The YAP/TAZ signaling pathway in mammalian cells.

In the absence of Hippo signaling, YAP/TAZ complexes with TEAD in the nucleus to promote YAP-associated gene expression, leading to cell proliferation, survival, and stemness. CD44 activation can promote YAP expression and localization to the nucleus through activation of RhoA. Alternatively, when Hippo signaling is active, MST1/2 and SAV1 are phosphorylated, leading to phosphorylation of MOB1 and LATS1/2, followed by YAP/TAZ. Phosphorylated YAP/TAZ can either complex with 14-3-3 for cytoplasmic retention or be targeted for proteasomal degradation. This figure was created using BioRender.

In the context of TNBC, YAP/TAZ overexpression promotes tumorigenesis and metastasis and is associated with a shortened overall survival in patients [49-52]. Furthermore, YAP/TAZ overexpression promotes several characteristic CSC functions, including tumour initiation and EMT [44, 53]. Targeting of YAP/TAZ in a TNBC model suppressed both the bulk tumour and CSC populations, suppressing further tumour growth and tumour initiation through secondary transplantation [54, 55]. Thus, targeting both the bulk tumour cells and the CSCs, particularly through critical signaling pathways such as YAP/TAZ, is necessary to eliminate the entire tumour population and prevent tumour recurrence.

1.4. Natural killer cell-derived extracellular vesicles for cancer treatment

1.4.1. Extracellular vesicle biology

Extracellular vesicles (EVs) refer to all nano- or micro-sized particles enclosed by a lipid bilayer that are produced and secreted by cells into the extracellular environment. Depending on their biogenesis pathway, EVs are traditionally classified as exosomes, microvesicles/ectosomes, or apoptotic bodies based on the MISEV (minimal information for studies of extracellular vesicles) guidelines (**Table 2**) [56]. Several studies refer to EVs by their subclassifications (e.g. exosomes, ectosomes, microvesicles) based on their general size range. This nomenclature is generally discouraged by the current MISEV guidelines. No strict upper or lower size limits have been established for the EV subclasses, with some overlap identified in their general size range. Unless the biogenesis pathway has been clearly identified, MISEV encourages the name EV for all particles with a cellular origin. Each biogenesis pathway and subclass is enriched in different proteins, which may be used for EV classification. However, this is an understudied area of research and may be considered in the future when more research is done.

Table 2. Traditional EV classification according to the MISEV guidelines.

EV classification	Size range	Biogenesis pathway
Exosome	30 – 150 nm	Formed through inward budding of the early endosome, which matures into a multivesicular endosome and can fuse with the plasma membrane to release its content.
Microvesicle/ ectosomes	100 nm – 1 μm	Outward budding of the plasma membrane.
Apoptotic bodies	50 nm – 5 μM	Released from a cell undergoing apoptosis.

This table was adapted from Welsh *et al.* [56].

EVs are major facilitators of intercellular communication, possessing the ability to be released and taken up by every cell in the body. Conversely, the overall composition of EVs is directly influenced by their cellular origin and exposure to the extracellular environment. For example, cancer-derived EVs have been shown to promote tumorigenicity and the immunosuppressive nature of the tumour microenvironment (TME) through the transportation of anti-inflammatory cytokines, suppressing various immune cells such as the natural killer (NK) cells and dendritic cells [57]. Conversely, immune cell-derived EVs can stimulate the surrounding immune cells, boosting the anti-tumour immune response [58-60].

EV-based therapy offers numerous benefits over its cell-based counterparts. Due to their small size, inherent stability, and high biocompatibility, EVs are capable of travelling through the circulatory system to almost any site in the body. Several studies have even shown that EVs can bypass the blood-brain barrier [61-66]. Approximately 29 – 46% of TNBC patients experience brain metastasis, which is currently considered untreatable (**Table 1**) [6, 7, 9, 10]. Thus, EV treatment that can reach the brain could have major therapeutic implications for these cases. Additionally, cell therapies like CAR-T are associated with several safety issues, such as cytokine release syndrome, and are more susceptible to hijacking by the TME, leading to the unintentional promotion of tumour growth [67, 68]. Current clinical studies using EVs in humans demonstrated

that EVs were generally safe, with a low incidence of adverse events (e.g. vomiting, fever, liver dysfunction) occurring in patients [69]. Although more research is needed, EVs currently demonstrate promise as a safe treatment option in humans. Finally, EVs are unable to self-replicate (i.e. finite payload) and are thus unresponsive to the hypoxic and immunosuppressive conditions of the TME, an issue that has limited the efficacy of cell-based therapies for solid tumours relative to other hematological cancers (e.g. leukemia, lymphoma) [70, 71].

1.4.2. Natural killer cell-derived extracellular vesicles

EVs derived from immune cells, particularly NK cells, have emerged as a promising anti-cancer immunotherapeutic. NK cells are a class of lymphocytes that are released as part of the innate immune response. NK cells are enriched in cytotoxic molecules (e.g. perforin, granzyme A/B, FasL) and cytokines (e.g. TNF-α, IFN-γ) that facilitate their ability to lyse damaged, virally infected, and diseased cells upon recognition. NK cell activation is tightly regulated and dependent upon the binding of activating (e.g. NKG2D) and inhibitory (e.g. NKG2A) receptors, as well as recognition of self and non-self markers on external cells. To date, NK cell therapy has shown great promise against various hematological cancers [72, 73]. However, NK cell therapy has not been as effective against solid tumours [74]. In particular, NK cells have exhibited poor trafficking and tumour infiltration, largely due to the immunosuppressive nature of the TME [71, 75]. Additionally, the TME promotes the activity of immunosuppressive cells (e.g. regulatory T cells, M2-like tumour-associated macrophages), further impairing the NK cells' functioning.

To overcome this hurdle, more research has investigated NK cell-derived EVs (NK-EVs) as an anti-cancer therapeutic. NK-EVs possess a cytotoxic profile representative of their parental cell and are naturally capable of killing cancerous cells (**Figure 2**) [76, 77]. Several studies have

demonstrated that NK-EVs exhibit a dose-dependent and time-dependent effect on cancer cell viability, including glioblastoma [78, 79], skin cancer [80, 81], colorectal cancer [79, 81-83], leukemia [77, 84-88], and breast cancer [76, 78, 79, 81, 82, 86, 87, 89, 90]. Furthermore, NK-EVs have been tested against various breast cancer cell line-based mouse models and have demonstrated the ability to suppress and possibly reduce tumour growth [76, 79, 91, 92]. Thus, NK-EVs could be an effective treatment against more difficult-to-treat cancers like TNBC. Furthermore, McCune and Kornbluth demonstrated for the first time that NK-EVs were effective against a subpopulation of treatment-resistant leukemic cells with a CSC-like phenotype [86]. Thus, NK-EVs may be effective against both the bulk tumour cells and CSCs, allowing for a complete knockdown of the entire tumour cell population.

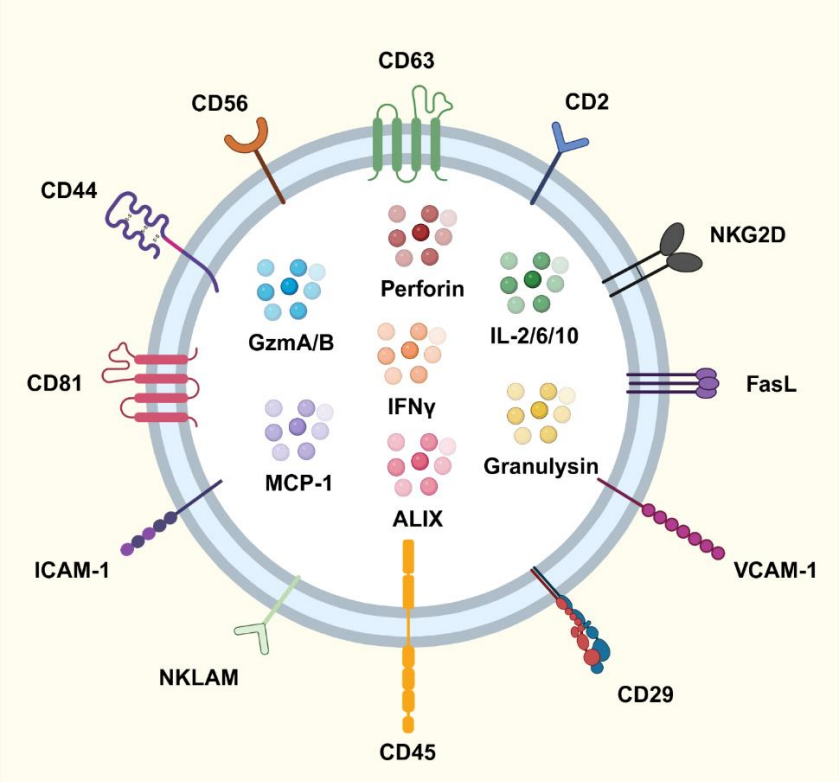

Figure 2. Representative schematic of the NK-EV's composition.
This figure was adapted from results found in [76, 77, 79]. This figure was created using BioRender.

1.5. A clinically relevant TNBC model to assess the NK-EVs' anti-cancer properties

Current studies investigating NK-EVs in a cancer model have mainly relied upon cell line-based models *in vitro* and *in vivo*. Although these models are informative, they are not entirely indicative of a therapeutic's clinical success. Cancer cell lines have several limitations, including their high mutation frequency, homogeneity, lack of tumour architecture and vasculature, lack of stromal cells and extracellular components, and a tendency to adapt to *in vitro* conditions during culturing, making them less reflective of their tumour origin over time [93]. As of 2016, the NCI has ceased testing of novel cancer therapeutics using the NCI-60, a panel of 60 human cancer cell lines, in favour of a more clinically relevant platform, patient-derived xenografts (PDX) [94].

PDX refers to tumour tissue taken from a human patient that is subsequently implanted and grown in an immunocompromised or humanized mouse model. PDX tumours preserve the original tumour's architecture, heterogeneity, organization, vasculature, and stromal/extracellular components [93, 95]. Therefore, PDX models are more reflective of human patient tumours and in-patient response to treatment [96-100].

PDX models have some limitations that must be considered for preclinical research. For example, PDX fragments can't be passaged (i.e. transplanted *in vivo* for propagation) more than 4-5 times, as the risk for mouse stromal cell infiltration increases too greatly [93]. Additionally, PDX models are primarily transplanted into mice with severe immunodeficiencies. These models are not feasible for immunotherapy studies as they lack the necessary lymphocytes for assessment. Instead, syngeneic tumour mouse models are the most commonly used preclinical model for testing immunotherapy. Humanized mouse models implanted with PDX fragments may also be used for the assessment of immunotherapies, being one of the best preclinical models for cancer research [101, 102].

1.6. Rationale, Hypothesis, and Objectives

1.6.1. Research rationale

To date, limited research has been done investigating the therapeutic efficacy of clinical-grade NK-EVs in a TNBC model and none have used a clinically relevant model such as the PDX platform, both *in vivo* and *ex vivo*. Thus, this project is focused on investigating the efficacy and cytotoxic mechanism of action (MoA) of NK-EVs against TNBC bulk tumour cells and CSCs using a variety of clinically relevant models.

1.6.2 Hypothesis

NK-EVs will suppress the growth of TNBC cells and CSCs to potentially mitigate the risk of tumour relapse (**Aim 1**), as well as inhibit the growth of *ex vivo* PDX organotypic cultures (**Aim 2**).

1.6.3. Objectives

Aim 1: Determining the cytotoxicity of NK-EVs against TNBC cells (*Aim 1.1*) and assessing their impact on the CSC populations *in vitro* (*Aim 1.2*).

Aim 2: Assessing the NK-EVs' ability to control the growth of TNBC PDX tumour fragments *ex vivo* (*Aim 2.1*) and their biodistribution following either intravenous (IV) or intratumoral (IT) administration (*Aim 2.2*).

2. Materials and Methods

2.1. Cell culture parameters

NK92-MI cells (ATCC, CRL-2408) were maintained and cultured in serum-free, xeno-free, and feeder-free ImmunoCult™-XF T Cell Expansion Medium (Stemcell Technologies, cat#10981). FreeStyle™ 293F cells (Thermo Scientific; R790-07) were cultured and maintained in FreeStyle™ 293 Expression Medium (Gibco, cat#12338018) on a shaker platform. Breast cancer HCC70 cells (ATCC, CRL-2315™) were cultured in RPMI-1640 with GlutaMAX™ (Gibco, cat#61870-036) with 10% Heat Inactivated Fetal Bovine Serum (HI-FBS, Gibco, cat#12484-028). Breast cancer MDA-MB-231 cells (ATCC, CRM-HTB-26™), breast cancer MDA-MB-468 cells (ATCC, HTB-132™) and breast cancer BT-474 cells (ATCC, HTB-20™) were cultured in Ham's F-12 Medium (Corning, cat#10-080-CV) and high glucose DMEM with GlutaMAX™ (Gibco, cat#10566-016) at a 1:1 ratio with 10% HI-FBS. Breast cancer SUM149PT cells (Asterand, 51082) were cultured in Ham's F-12 Medium with 10% HI-FBS, 10 mM HEPES (Gibco, cat#15630-080), 5 µg/mL of hR Insulin (Gibco, cat#12585-014), and 1 µg/mL hydrocortisone (Sigma, cat#H4001). Breast cancer BT-549 cells (ATCC, HTB-122™) were cultured in RPMI-1640 with 10% HI-FBS, 10 µg/mL hR Insulin (Gibco, cat#12585-014). Breast cancer MCF7 cells (ATCC, HTB-22™) were cultured in EMEM Medium (ATCC, Cat#30-2003) with 10% HI-FBS, 10 µg/mL hR Insulin (Gibco, cat#12585-014). Breast MCF10A cells (ATCC, CRL-10317™) were cultured in MEGM™ Mammary Epithelial Cell Growth Medium BulletKit™ (Lonza, cat#CC-3150) with all supplements except GA-1000. All adherent cells were passaged using TrypLe select (Gibco, cat#12563-029) after washing the cells with sterile Dulbecco's phosphate-buffered saline without Ca^{2+}/Mg^{2+} ($DPBS^{-/-}$, Gibco, cat#14190250). The E-cadherin^{+} MDA-MB-231 cell line variant was generated and maintained as detailed by Sulaiman *et al*. [54].

Cell lines were cultured at 37°C in a 5% CO_2 incubator and passaged every 2 - 3 days, except the 293F cell line, which was cultured at 37°C in an 8% CO_2 incubator. Cell counts were performed on the Cellometer Auto 2000 Viability Counter (Nexcelom BioScience LLC) using the ViaStain Acridine Orange and Propidium Iodide (AO/PI) Staining Solution (ESBE Scientific, cat#CS2-0106) with the immune cell AO/PI program (channel 1: 470/535 nm for 0.5 s of exposure and channel 2: 540/605 nm for 3 s of exposure). The PCR detection kit assessed all cell lines for mycoplasma contamination (Abcam, cat#ab289834).

2.2. NK-EV production from the NK92-MI cell line

The NK-EVs used in this study were produced from the NK92-MI cell line using a large-scale biomanufacturing workflow that adheres to Good Manufacturing Practices, as previously described by our lab [103]. Briefly, the NK-EVs were manufactured from NK cells cultured in a hollow fibre bioreactor (HFB), allowing for the generation of a large quantity of clinical-grade NK-EVs. NK cells were maintained in serum-free, xeno-free, and feeder-free ImmunoCult™-XF T Cell Expansion Medium. NK cells were expanded in the HFB cartridge and harvested once they reached confluency (~5-7 days post-seeding). EV-rich conditioned media was collected twice daily and stored at -80°C for further processing.

2.3. NK-EV isolation and characterization

The NK-EVs used in this study were isolated from the EV-rich CM and characterized as previously described by our lab [103]. Briefly, the EV-rich CM was centrifuged after thawing and then incubated for 4 h at 37°C with 50 U/mL Benzonase Nuclease (Millipore Sigma, cat#E1014-25KU) and 1.5 mM of $MgCl_2$ (Millipore Sigma, cat#M1028) while moderately shaking for nucleic

acid digestion. Size exclusion chromatography-based processing was then performed on the AKTA Fast Protein Liquid Chromatograph (GE Lifesciences, cat#29022094). The obtained solution was concentrated using a pre-equilibrated 10 kDa Centricon Plus-70 Centrifugal Filter - regenerated cellulose membrane (Millipore Sigma, cat#UFC701008). Purified NK-EV samples were then analyzed using the NanoSight NS300 (V3.4 software; Malvern, UK). For capture settings, the camera level was set to 14 and the detection threshold to 15 for analysis. The obtained concentrations were used to calculate the proper dosage for all experiments described. Protein and dsDNA levels were quantified using the Qubit 4 Fluorometer (Invitrogen, cat#Q33239) as per the manufacturer's instructions.

2.4. Potency evaluation using the PrestoBlue viability assay

A week before the cytotoxic co-culture assay, the various target cells were cultured as per the "Cell culture parameters" section. The procedure for the PrestoBlue viability assay was previously described by St. Denis-Bissonnette *et al.* with some modifications [87]. Using a 96-well Flat Clear Bottom Black Polystyrene TC-treated Microplates (Costar, cat#3603), 1500 adherent cells were seeded per well using a pipette repeater and technical triplicates. Cells were maintained in Fluorobrite DMEM (Gibco, cat#A18967-01). Adherent cells were allowed to settle into the plate for 18 - 24 hours at 37°C with 5% CO2 before adding effector EVs. Untreated cells, 1X of Triton-X 100 (Sigma, cat#T-9284) detergent-treated cells, 10 µM Paclitaxel (PTX; Caymanchem, cat#10461-25)-treated cells and 293F-EVs-treated cells were used as controls. Except for the time course experiment, the PrestoBlue™ HS Cell Viability Reagent Assay (Invitrogen, cat#P50200) was added to each well (1X) after 4 hours of treatment, where plate incubation was performed at 37°C in a 5% CO2 incubator and protected from light (60 min

incubation). Fluorescence was measured (Ex/Em 560/590 ± 9 nm) with a Microplate Reader (BioTek Synergy H1 Multimode Reader; cat#SH1M2G-SN; Gen5 software V3.14), temperature stabilized at 37°C to reduce temperature variation on fluorescence measurements. Before acquisition, the plate reader mixed the plate for 30 seconds at 350 - 500 RPM to homogenize the content in each well. Technical replicates were averaged for analysis and then corrected for background before performing a dose-response analysis using a non-linear regression for inhibition effect, showing the log(inhibitor) vs. normalized response – EC_{50} (half maximal effective concentration) curve.

2.5. Plate-based evaluation of cell death pathways following NK-EV treatment

A week before the cytotoxic co-culture assay, the various target cells were cultured as per the "Cell culture parameters" section. Using a 96-well Flat Clear Bottom Black Polystyrene TC-treated Microplates (Costar, cat#3603), 1500 adherent cells were seeded per well using a pipette repeater; technical duplicates. Cells were maintained in Fluorobrite DMEM (Gibco, cat#A18967-01) at 37°C with 5% CO_2, where the final well volume was normalized to 100 or 200 µL (assay dependent). Adherent cells were allowed to settle into the plate for 18 - 24 hours before adding effector EVs. Untreated cells, 1X of Triton-X 100 (Sigma, cat#T-9284) detergent-treated cells, and 10 uM PTX (Caymanchem, cat#10461-25)-treated cells were used as controls. For continuous measurement, we used 1X RealTime-Glo™ Annexin V Apoptosis (luminescence) and Necrosis (fluorescence; Ex/Em 485/525 ± 9 nm) Assay (Promega, cat#JA1011). Detailed caspase activity was measured after 90 minutes of treatment using the Cell Event Caspase 3/7 Green Detection Reagent, the Caspase-Glo® 8 (luminescence) Assay Systems (Promega, cat#G8201), and the Caspase-Glo® 9 (luminescence) Assay Systems (Promega, cat#G8211), where 60 µM MG-132

Inhibitor was used to reduce background for both luminescence assays. Readings were made using a prewarmed Microplate Reader (BioTek Synergy H1 Multimode Reader; cat#SH1M2G-SN; Gen5 software V3.14). Before acquisition, the plate reader mixed the plate for 30 seconds at 350 RPM to homogenize the content in each well. For analysis, technical duplicates were averaged and then corrected for background.

2.6. Tumorsphere formation assay

A week before the cytotoxic co-culture assay, the various target cells were cultured as per the "Cell culture parameters" section. The procedure for the tumorsphere formation assay was previously described by Mediratta *et al.,* with slight modifications [104]. 1500 E-cadherin$^+$ MDA-MB-231 or 2500 SUM149PT cells were seeded into a 96-well ultra-low attachment plate and maintained in 1:1 DMEM and Ham's F-12 (Wisent, cat#318-010-CL) supplemented with 2% B27 (Gibco, cat#17504044), 1% sodium pyruvate (Gibco, cat#11360070), 1% penicillin/streptomycin (cat#SV30010), 20 ng/mL basic fibroblast growth factor (R&D Systems, cat#234-FSE), and 20 ng/mL epidermal growth factor (R&D Systems, cat#236-EG). Effector EVs were added to the plate and allowed to co-incubate with their treatment for 72 hours. Tumorsphere viability was determined using the PrestoBlue viability assay as described in the "Potency evaluation using the PrestoBlue viability assay" section.

2.7. Quantitative reverse transcriptase polymerase chain reaction (RT-qPCR)

A week before treatment began, the MDA-MB-231 cells were cultured as per the "Cell culture parameters" section. 3 x 10^5 cells were seeded into 6-well plates and allowed to settle in the plate for 18 – 24 hours prior to treatment. Total RNA was extracted using the RNeasy Mini kit

(Qiagen, cat#74106). cDNA was obtained from RNA using the iScript cDNA Synthesis Kit (Bio-Rad, cat#1708891) as per the manufacturer's instructions. Gene expression was measured using the CFX Opus 96 Real-Time PCR System (Bio-Rad, cat#12011319) in a reaction mixture consisting of 50% SyBr Green Supermix (Bio-Rad, cat#1708882), 37.5% RNAse-free water (Qiagen, lot#166033558), 5% forward and reverse primers (all primers were purchased from Eurofin Genomics), and 2.5% cDNA. The RT-qPCR script followed was: 1) 1 minute and 30 seconds at 95°C, 2) 10 seconds at 95°C, 3) 30 seconds at 60°C and plate read, 4) 30 seconds at 72°C, 5) return to step 2 45X. Specific forward and reverse primers are listed in **Supplemental Table 1**. The results were normalized to the GAPDH (Glyceraldehyde 3-phosphate dehydrogenase) housekeeping gene, and the relative fold changes in gene expression were calculated using the $^{2\Delta\Delta}$CT method.

2.8. Live-cell imaging

MDA-MB-231 cells were tagged with red fluorescent protein (RFP) by lentiviral transduction of Incucyte Nuclight Red (Sartorius, cat#BA-04887), followed by puromycin (Tocris Bioscience, cat#4089) selection. A week before treatment began, RFP^+ MDA-MB-231 cells were cultured as per the "Cell culture parameters" section for the MDA-MB-231 cell line. Cells were dissociated, filtered through a 40 µM strainer (Bio Basic, cat#SP104151), and resuspended in $DPBS^{-/-}$ supplemented with 2% FBS and 2mM EDTA. To reduce non-specific binding, mouse anti-human IgG Fc (Thermo Fisher, cat#05-4220) was added at 4°C for 10 minutes. Cells were incubated with BV-650 mouse anti-human CD44 (BD Biosciences, cat#743665) and PE mouse anti-human CD24 (BD Biosciences, cat#555428) according to the manufacturer's instructions. Fluorescence-activated cell sorting (FACS) into the $CD44^{high}/CD24^{low}$ and non-$CD44^{high}/CD24^{low}$

cells was conducted using the SH800 Cell Sorter (Sony, San Jose, USA). Sorted cells were seeded back and cultured for 24 hours before live cell imaging began. Cells were seeded into a TC-treated 96-well plate (1.5×10^3 cells/well) and incubated with green Annexin-V (Sartorius, cat#4642) for live cell imaging in the Sartorius Incucyte S3 for 96 hours. Treatment occurred immediately after the first images were captured at the 0 h time point.

2.9. Evaluation of NK-EVs against TNBC PDX organotypic slice cultures

HCI-001, HCI-002, HCI-010, and HCI-15 tumour fragments were obtained from the University of Utah, where they were previously characterized (**Table 3**) [105]. 2 x 2 mm PDX fragments were incubated in 24-well plates (i.e. organotypic slice culture) and allowed to settle in the plate for 18 – 24 hours before beginning treatment. Over a five-day period, PDX fragments were treated every 24 hours with NK-EVs (1×10^{11} EVs/mL), 10 nM PTX, a combination of NK-EVs and PTX, or left untreated. Viability assessment was performed daily using the PrestoBlue viability assay as detailed in the "Potency evaluation using the PrestoBlue viability assay" 3 hours after the reagent was added.

Table 3. Summary of tested TNBC PDX lines.

Sample ID	Patient demographic	Collection source	Pre-collection systemic treatment	Clinical metastasis
HCI-001	40-year-old Caucasian; IDC (stage IV)	Primary breast tumour	Paclitaxel 2007	Lung
HCI-002	61-year-old Caucasian; IDC	Primary breast tumour	None	Bone, lymph node, lung
HCI-010	49-year-old Caucasian; IDC	Pleural effusion	Cyclophosphamide; doxorubicin; paclitaxel 2007; liposomal doxorubicin 2008; zolendronic acid 2008; Capecitibine 2008-2009; docetaxel 2008	Lung
HCI-015	49-year-old Caucasian; IDC	Brain metastasis	doxorubicin, cyclophosphamide, paclitaxel 2010	Brain

This table was adapted from Guillen *et al.* [105]. IDC: Invasive ductal carcinoma

To evaluate caspase 3/7 activation, 2 x 2 mm PDX fragments were seeded in 24-well plates and allowed to settle for 18 – 24 hours before beginning treatment. The caspase 3/7 detection assay was performed as per the "Plate-based evaluation of cell death pathways following NK-EV treatment".

2.10. *In vivo* investigation of NK-EVs in a TNBC PDX mouse model

Non-obese diabetic/severe combined immunodeficiency (NOD-SCID) gamma (NSG) mice were purchased from the Jackson Laboratory (strain #005557). All experimental and breeding work was performed in pathogen-free conditions according to guidelines set by the Animal Care Committee at the University of Ottawa (BMIb-4265 and BMIe-4035). HCI-002 tumour fragments (2 x 2 mm) were surgically implanted onto the mammary fat pad of NSG mice. Over the course of development, body weight was measured, and tumour growth was monitored three times a week using calipers.

For the biodistribution study, once tumours reached a mean diameter of 1 cm, the mice were injected IV or IT. All injected compounds were labelled with DiR (1,1'-Dioctadecyl-3,3,3',3'-Tetramethylindotricarbocyanine Iodide; Invitrogen, cat#D12731). Briefly, following SEC-based fractionation, DiR was combined with the collected EV aliquots and incubated for 15 – 20 minutes at room temperature, followed by ultrafiltration as described in the "NK-EV isolation and characterization" section.

Post-injection, live fluorescent imaging of the mice in the supine position was conducted using the DiR channel (filter position: F-800, lighting: 740 nm, aperture: 5.6, exposure time: 0.1 seconds) on the Newton 7.0 FT500 (Vilber, Marne-la-Vallée, France) at the following timepoints: 0 hours, 1 hour, 6 hours, and 24 hours. Before imaging, the mice were anesthetized with 2-3% isoflurane. At the 24-hour timepoint, the mice were humanely euthanized, and the tumours and major organs (heart, lungs, liver, spleen, kidneys, and brain) were harvested and underwent fluorescent imaging using the DiR channel.

2.11. Statistical analysis

Data were expressed as the means ± the standard error of the mean (SEM). The number of experimental and technical replicates used is indicated in the figure legends. Statistical analyses were performed using GraphPad Prism version 7.0 (GraphPad Software Inc., LaJolla, CA, USA), where a p-value of < 0.05 was considered statistically significant and significance differences were marked with a single ($p< 0.05$), double ($p< 0.01$), triple ($p< 0.001$), or quadruple ($p< 0.0001$) asterisk. One-way or two-way analysis of variance (ANOVA) was conducted, followed by post hoc tests (Tukey's or Sidak's multiple comparisons).

3. Results

3.1. NK-EV Production and characterization

In this study, NK-EVs were produced from the NK92-MI cell line using a previously characterized hollow-fibre bioreactor (HFB)-based workflow (**Figure 3**) [77, 103]. The HFB's three-dimensional design allows for the continuous production of billions of cells in a closed-loop system, increasing the total EV yield obtained over time. Quality assessment was regularly conducted to ensure that cells in culture were healthy. NK-EVs were isolated and purified from the collected CM using size-exclusion chromatography and ultrafiltration. Following the same protocol, our group has previously reported obtaining 1.0 – 1.5 mL of NK-EV product with a final concentration of at least 1×10^{12} EVs/mL, quantities that are more than sufficient for preclinical research [103]. Before any further experimentation, nanoparticle tracking analysis as well as dsDNA and protein quantification were performed to characterize the NK-EV product.

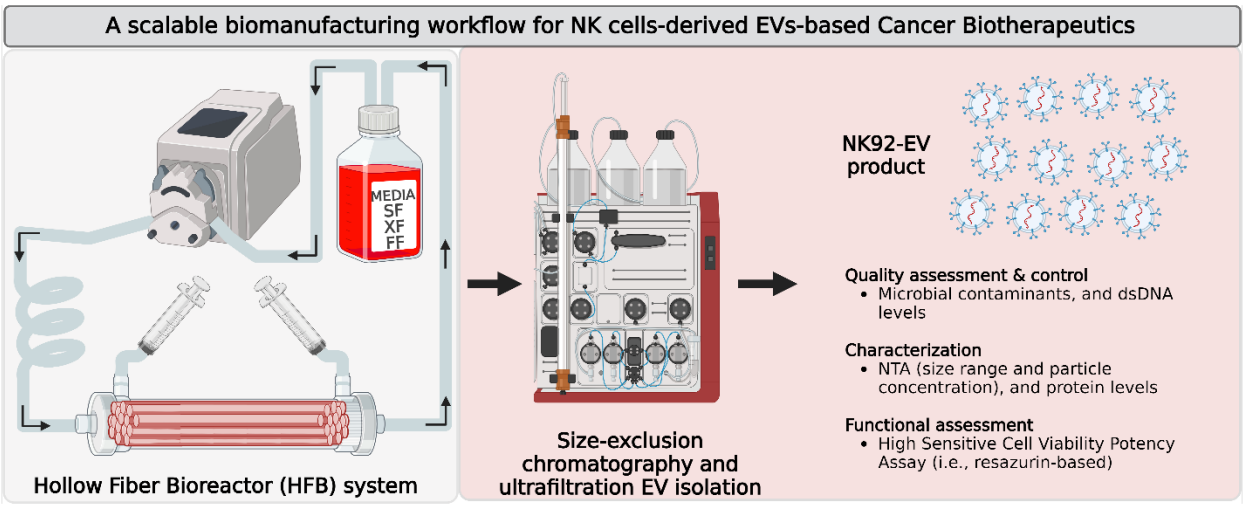

Figure 3. Biomanufacturing of NK-EVs in a closed-loop HFB with scalable isolation workflow.
SF: serum-free, XF: xeno-free, FF: feeder-free. This figure was reused from St-Denis-Bissonnette *et al.,* with permission from the Journal of Visualized Experiments [103].

3.2. NK-EVs exhibit cytotoxicity against multiple TNBC cell lines

3.2.1. Dose-dependent effect of NK-EVs on TNBC cells.

To investigate the dose-dependent effect of NK-EVs, a cytotoxic co-culture assay using the previously validated PrestoBlue HS cell viability assay was employed (**Figure 4A**) [87]. Several TNBC cells representing different morphologies (basal-like 1: MDA-MB-468; basal-like 2: SUM149-PT, HCC70; mesenchymal-like: BT-549; mesenchymal-like stem cells: MDA-MB-231) were included for analysis. Additionally, non-TNBC cell lines (luminal A: MCF7, HER2-positive: BT-474, healthy epithelial breast cells: MCF10A) were included for comparison. Paclitaxel (PTX), an approved chemotherapy for TNBC, and 293F cell-derived extracellular vesicles (293F-EVs), which lack cytotoxic granules, were included as a positive and negative control, respectively. Untreated and 1% Triton-X-treated cells were included as live and dead controls, respectively.

Following five hours of co-incubation, NK-EV treatment of all TNBC cell lines exhibited a dose-dependent effect on cell viability, achieving an average $\log(EC_{50})$ of 9.77 ± 0.14 particles/mL (**Figure 4B-J**). Conversely, the dose-escalation of 293F-EVs did not significantly impact cell viability, suggesting that the NK-EV's specific composition is responsible for its cytotoxic functionality. PTX treatment after five hours also did not significantly decrease cell viability, which is consistent with previous studies where its therapeutic effect was found to be highly time-dependent [106, 107]. The highest doses of NK-EVs killed almost 100% of the cell population, suggesting the NK-EVs' cytotoxic mechanism of action (MoA) occurs over a shorter timeframe.

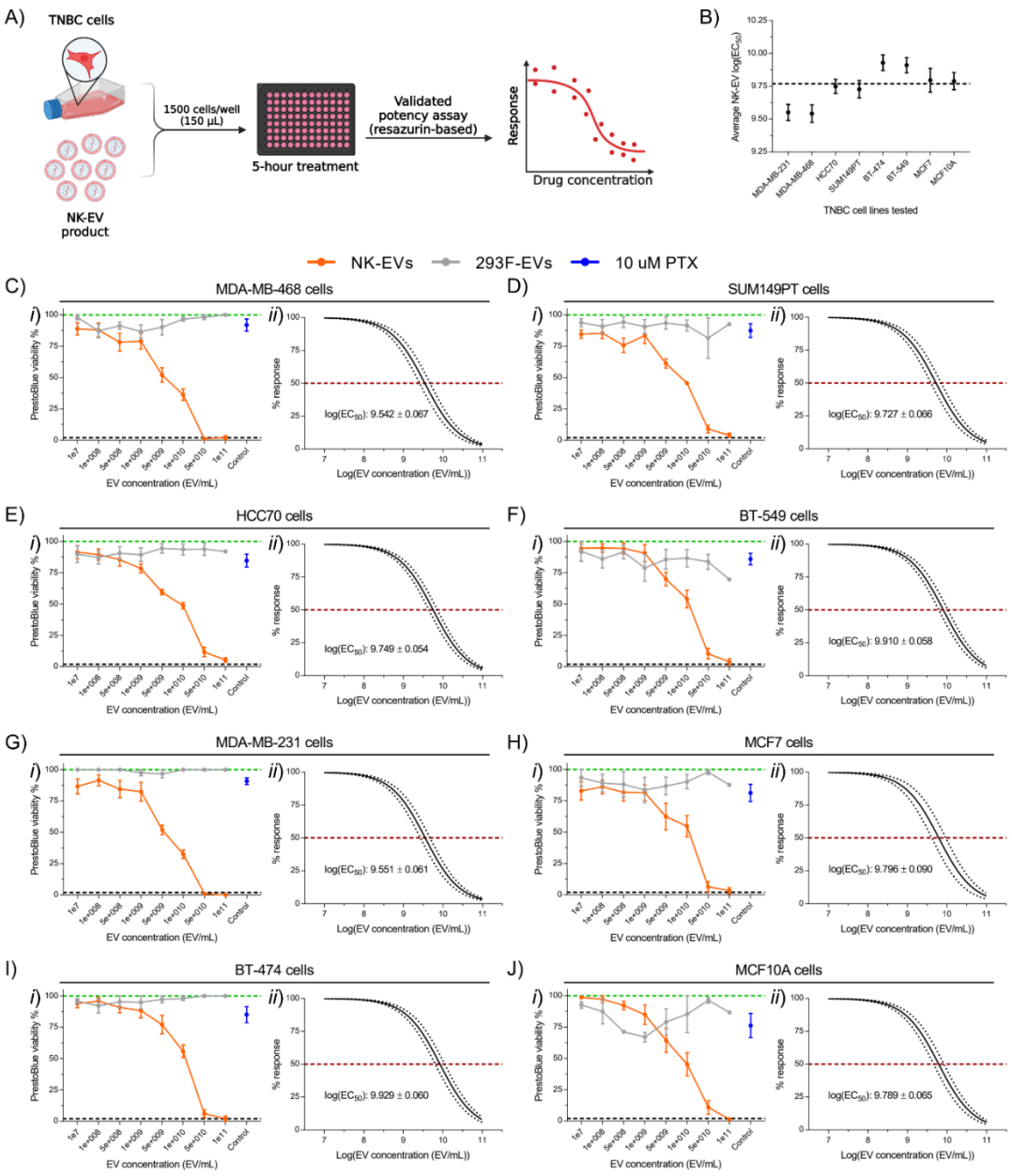

Figure 4. Cell viability of various TNBC cell lines following NK-EV treatment.
A) Schematic representation where TNBC cells were treated for 5 hours with various E:T ratios of NK-EVs (orange), 293F-EVs negative control (gray), and paclitaxel (10 uM PTX; blue), followed by endpoint resazurin-based cell viability assay. This figure was created using BioRender. B) The average NK-EV EC50 value across all TNBC cell lines. The results for C) MDA-MB-468 cells, D) SUM149PT cells, E) HCC70 cells, F) BT-549 cells, G) MDA-MB-231 cells, H) MCF7 cells, I) BT-474 cells, and J) MCF10A cells are presented in (i) RFU (green dashed line represents untreated cells, black dashed line represents lysed cell control using Triton-X) and (ii) EC_{50} curve analysis for NK-EV treatment with 95% confidence interval/prediction bands (red dashed line represents 50% response). Data are shown as mean ± SEM from six independent experiments, each with technical triplicates.

3.2.2. Time-dependent effect of NK-EVs on TNBC cells

As the NK-EVs' cytotoxicity was dose-dependent, the next point of investigation was to determine if their MoA was also time-dependent. To achieve this, MDA-MB-231 cells were co-incubated with a low (1.0 x 10^7 EVs/mL), medium (5.0 x 10^8 EVs/mL), or high (1.0 x 10^{10} EVs/mL) dose of NK-EVs and evaluated using the PrestoBlue HS cell viability assay at four timepoints: 5, 24, 48, and 72 hours. PTX- and 1% Triton-X-treated cells were included as positive and dead controls, respectively.

Across all three concentrations, the NK-EVs' anti-proliferative effect was most significant at the 24-hour mark, after which cell viability was restored at 72 hours of co-incubation (**Figure 5, Supplemental Figure 1**). As expected, PTX treatment resulted in a gradual decline of cell viability over the 72 hours. This result suggests that the NK-EVs only exert a short-term anti-proliferative effect on TNBC cells.

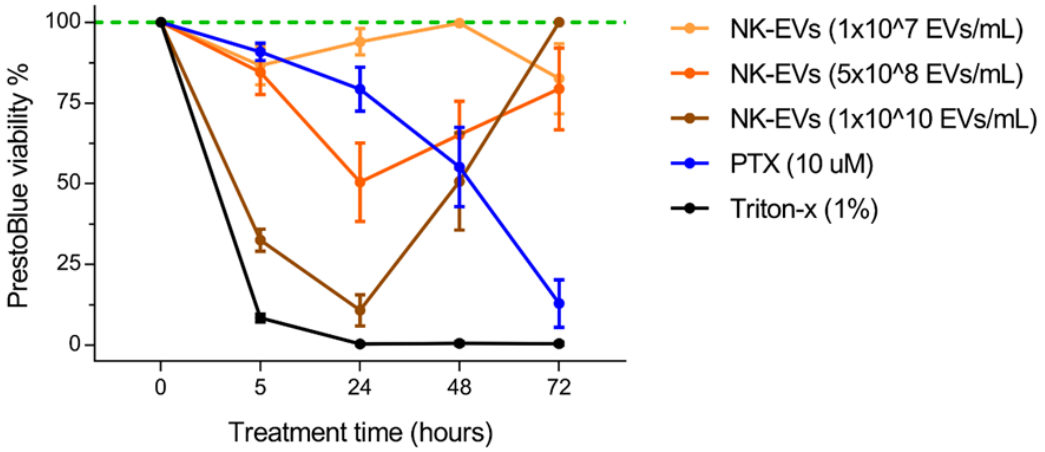

Figure 5. TNBC cell viability following NK-EV treatment over a 72-hour time course. MDA-MB-231 cells were treated for 5, 24, 48 and 72 hours with various E:T ratios (1 x 10^7 EVs/mL (or 2.0 x 10^6 EVs) dose (yellow), 5 x 10^8 (or 1.0 × 10^8 EVs) dose (orange), and 1 x 10^{10} (or 2.0 × 10^9 EVs) dose (brown); as EVs/mL) of NK-EVs and paclitaxel (10 uM PTX; blue). The results are presented as the normalized RFU values (green dashed line representing untreated cells, black dashed line represents lysed cell control using Triton-X). Data are shown as mean ± SEM from six independent experiments, each with technical triplicates.

3.3. NK-EVs induce apoptosis and necrosis as part of their mechanism of action.

To investigate the NK-EVs' MoA, we evaluated the activation of apoptosis and necrosis across various TNBC cell lines over a 72-hour period. Additionally, the activation of caspase 8/9 (initiator caspases) and caspase 3/7 (executioner caspases) was evaluated after 90 minutes of treatment to further explore their impact upon the apoptosis pathway (**Figure 6A**). NK-EVs were delivered at a low (1 x 10^9 EV/mL) or high (1 x 10^{10} EV/mL) concentration. Untreated and PTX-treated cells were included as live and dead controls, respectively. The high concentration of NK-EVs resulted in a rapid increase of apoptosis and necrosis that was sustained over 72 hours of observation (**Figure 6B-C**). This trend was observed in the low NK-EV concentration group to a much lesser degree, again indicating that the NK-EVs' MoA is largely dose-dependent. Similarly, both the high and, to a lesser extent, low concentrations of NK-EVs increased caspase activation (3/7/8/9) after only 1.5 hours across all cell lines tested (**Figure 6D-F**). Thus, it appears that a component of the NK-EVs' cytotoxic MoA involves increasing caspase activation to induce apoptosis of cancer cells.

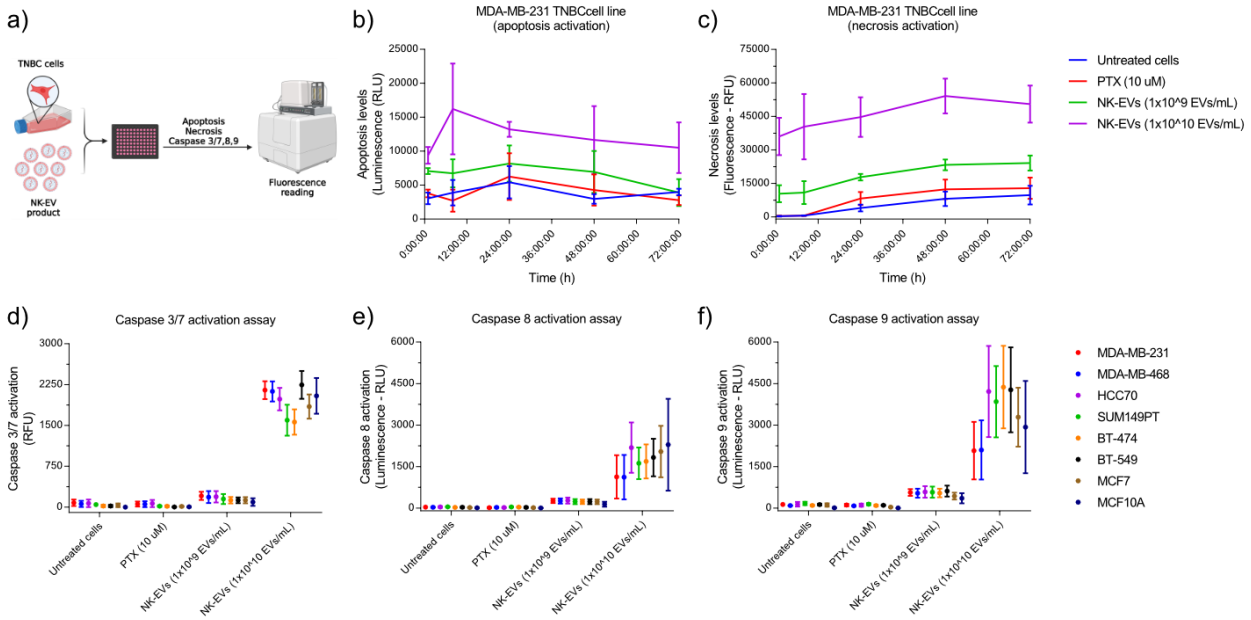

Figure 6. NK-EVs activate cell-death pathways via an *in vitro* assay against triple-negative breast cancer cell lines.

A) Schematic representation where various TNBC cell lines were treated with NK-EVs (1 x 10^9 (or 2.0 × 10^8 EVs) dose and 1 x 10^{10} (or 2.0 × 10^8 EVs) dose; as EVs/mL), where cell-death pathways were assessed. Paclitaxel (PTX; 10uM) was used as a control. B) Representative apoptosis readings (Annexin V binding - RLU) over time using the MDA-MB-231 cell line. Data is shown as mean ± S.E.M., n=3 from independent experimental replicates with technical duplicates. C) Representative necrosis readings (DNA binding - RFU) over time using the MDA-MB-231 cell line. Data is shown as mean ± S.E.M., n=3 from independent experimental replicates with technical duplicates. Caspase activation after 90 minutes of treatment of (D) Caspase 3/7 (RFU), (E) Caspase 8 (RLU) and (F) Caspase 9 (RLU) in various TNBC and breast cell lines. Data is shown as mean ± S.E.M., n=4 from independent experimental replicates with technical duplicates.

3.4. Investigating the effect of NK-EVs on CSCs

3.4.1. NK-EVs disrupt CSC functionality

As NK-EVs have demonstrated cytotoxicity against the bulk tumour cells, we wanted to investigate their impact on the CSCs. First, the dose-dependent effect of NK-EVs on tumorsphere formation, a characteristic typically reflective of CSC functionality, was assessed. In this assay, the tumour-initiating cell populations, including the CSCs, were treated with various doses of NK-EVs. Untreated and PTX-treated cells were included as a control. The SUM149-PT cells were co-incubated with the NK-EVs for 72 hours. Similar to the bulk tumour cells, there was a dose-dependent effect observed on tumorsphere viability, where the obtained EC_{50} was 6.59×10^8 EV/mL (**Figure 7A**). This experiment was repeated on the E-cadherin$^+$ MDA-MB-231 cell line, an epithelial-like MDA-MB-231 cell line variant. E-cadherin$^+$ MDA-MB-231 demonstrated a similar trend, with the NK-EVs significantly decreasing tumorsphere viability to a higher degree than PTX treatment (**Figure 7B**). The E-cadherin$^+$ MDA-MB-231 cells achieved an EC_{50} of 4.49×10^9 EV/mL. The ability of NK-EV treatment to impair tumorsphere formation suggests an impact on CSC functionality.

As previously mentioned, the YAP/TAZ signaling pathway has been implicated in several characteristic CSC traits, including tumour initiation [44, 53]. Thus, to further assess the MoA of NK-EVs on CSCs, RT-qPCR was used to investigate the expression of two genes involved in mesenchymal-like CSCs and the YAP/TAZ signaling pathway: *Ctgf* and *Cyr61*. Here, MDA-MB-231 cells were co-incubated with their treatment group for a total of 72 hours. The treatment groups included NK-EVs (1×10^9 EVs/mL), PTX (10 nM), and PTX combined with NK-EVs added 72 or 24 hours prior to investigation. Untreated cells were included as a control. For both *Ctgf* and *Cyr61*, NK-EV treatment suppressed gene expression relative to PTX treatment, which instead

enriched their expression (**Figure 7C**). Furthermore, NK-EV treatment reduced the expression of *Ctgf* relative to the untreated group, suggesting that NK-EVs can decrease YAP signaling to impair CSC survival. However, the combination of PTX and NK-EVs was insufficient to decrease PTX-mediated upregulation of both *Ctgf* and *Cyr61*. Nonetheless, NK-EV treatment did not further promote the YAP/TAZ signaling pathway in cancer cells.

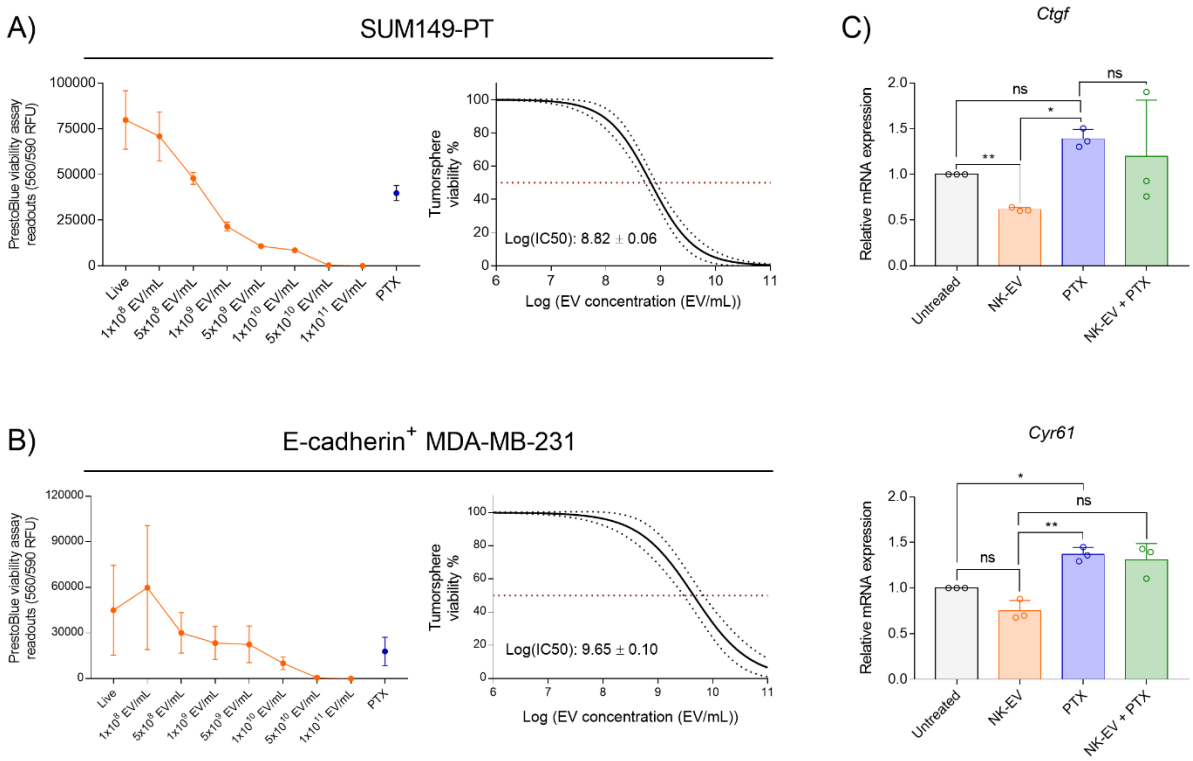

Figure 7. NK-EV treatment impacted TNBC CSC functionality.

The tumorsphere formation assay was conducted on A) 2000 SUM149-PT cells after seven days of treatment and B) 1500 E-cadherin^{+} MDA-MB-231 cells after four days of treatment with the results presented as the (i) RFU and (ii) EC50 curve analysis for NK-EV treatment with 95% confidence interval/prediction bands (red dashed line represents 50% response). C) RT-qPCR was conducted to assess gene expression of MDA-MB-231 cells after 72 hours of treatment. Treatment groups include untreated (grey), 1.0×10^{9} EVs/mL (or 5.0×10^{8} EVs) NK-EVs (orange), 10nM paclitaxel (PTX; blue), a combination of 1.0×10^{9} EVs/mL NK-EVs (72 hours) and paclitaxel (green), and a combination of 1.0×10^{9} EVs/mL NK-EVs (24 hours) and paclitaxel (purple). Data are shown as the mean ± SEM, n=3 from independent experimental replicates with technical duplicates, ns: non-significant, *: $p < 0.05$, **: $p < 0.01$.

3.4.2. Assessment of NK-EVs on CSC viability

Live-cell Incucyte analysis was used to assess CSC viability following NK-EV treatment. Briefly, FACS was used to sort MDA-MB-231 cells into the $CD44^{high}/CD24^{low}$ CSCs and non-CSCs (i.e. any cell that was not $CD44^{high}/CD24^{low}$). The sorted cells were then treated with a low (1.0×10^8 EV/mL), medium (1.0×10^9 EV/mL), or high (1.0×10^{10} EV/mL) concentration of NK-EVs and co-incubated for 96 hours. Untreated and 293F-EV-treated cells were included as controls.

The medium and high NK-EV concentration significantly increased Annexin V expression on both CSC and non-CSC cell populations, but did not significantly decrease cell viability over time (**Figure 8A - B**). Annexin V is a marker for early apoptosis, suggesting that NK-EV treatment primes CSCs towards apoptosis-mediated death. Interestingly, a comparison of Annexin V expression alone or merged with the signal from RFP^+ cell viability revealed that NK-EV treatment was more effective at inducing apoptosis in the CSCs compared to the non-CSCs (**Figure 8C - D**). 293F-EV treatment did not induce a significant level of cell killing or Annexin V expression, indicating that the NK-EVs' specific composition is primarily responsible for the observed effect on CSCs (**Figure 8A - B, 8E**). Overall, these findings suggest that NK-EVs are capable of targeting both bulk tumour cells and CSCs, with an increased capacity against the CSCs.

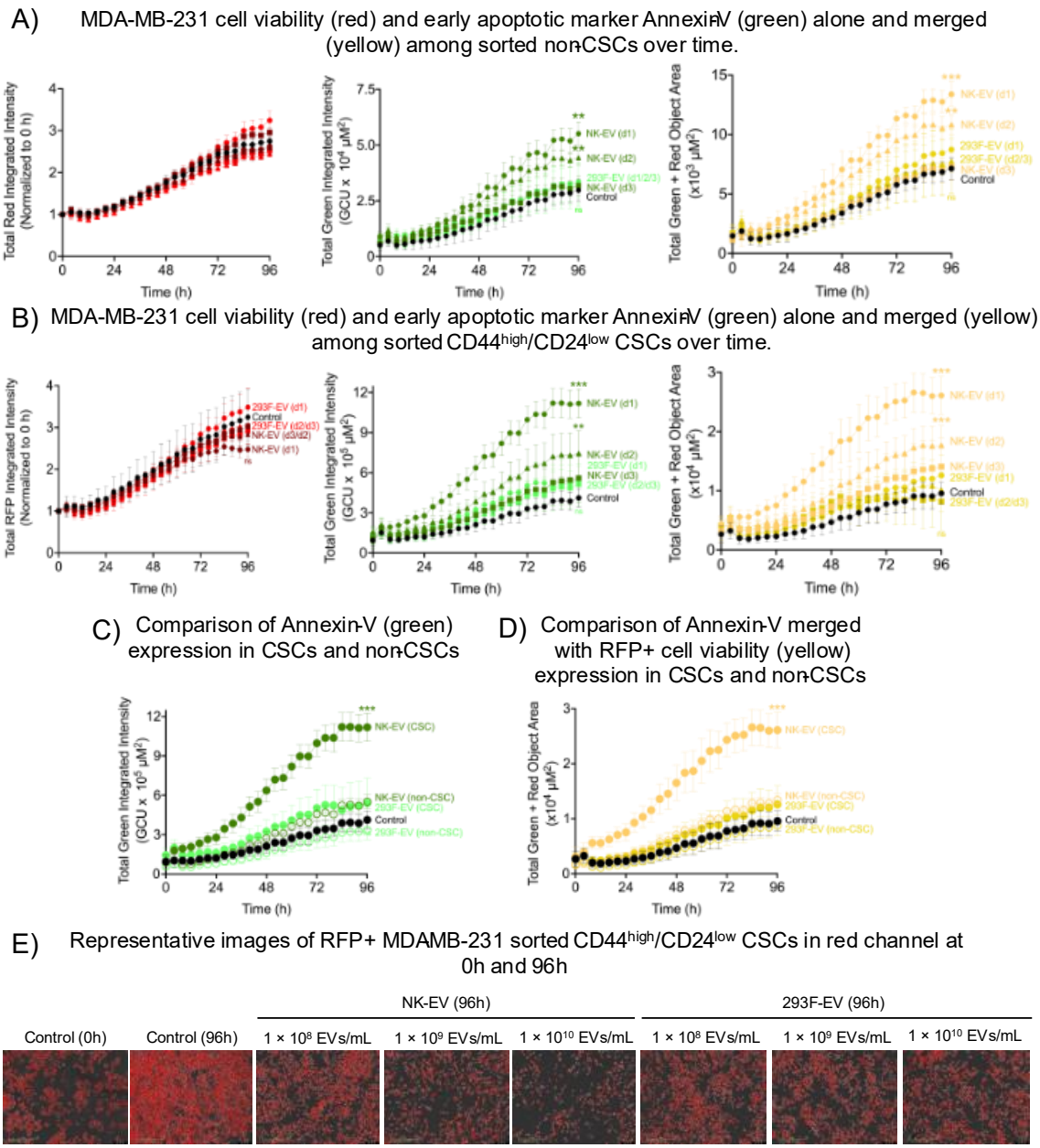

Figure 8. Live cell analysis of NK-EVs and 293F-EVs against CSC and non-CSC populations. RFP$^+$ MDA-MB-231 cells were sorted by A) non-cancer stem cells (CSCs) and B) CD44^{high}/CD24^{low} CSCs. Sorted cells were treated with either NK-EVs or 293F-EVs in the following dosage: 1×10^{10} EV/mL (2.0×10^9 EVs; d1), 1×10^9 EV/mL (2.0×10^8 EVs; d2) and 1×10^8 EV/mL (2.0×10^7 EVs; d3). Treated cells were incubated with Annexin-V and monitored by Incucyte S3 live cell imaging over time (red: RFP cell viability, green: Annexin V expression, yellow: Annexin V expression merged with RFP$^+$ cell viability). Expressions of C) Annexin V alone and D) merged with RFP$^+$ cell viability were compared between CSCs and non-CSCs. E) Representative images of the untreated control cells at 0h and 96h, as well as NK-EV and 293F-EV treatment at the 96h timepoints. Data are shown as the mean ± SEM, n=3 with technical triplicates, *: $p < 0.05$, **: $p < 0.01$, ***: $p < 0.001$.

3.5. NK-EVs demonstrate *ex vivo* cytotoxicity against clinically relevant PDX samples.

To further validate the efficacy and cytotoxicity of the NK-EVs, we investigated their effect on various clinically relevant TNBC PDX cultures. All PDXs tested were obtained from and previously characterized by the Huntsman Cancer Institute at the University of Utah (**Table 3)**. To assess cytotoxicity, PDX organotypic slice cultures were treated with a high concentration of NK-EVs (1.0×10^{11} EV/mL) and assessed using the PrestoBlue HS cell viability assay every 24 hours over a five-day period (**Figure 9A**). Untreated and PTX-treated PDX cultures were included as a control. Additionally, the combination of PTX and NK-EVs was included to observe a possible synergistic effect on cell viability. Across all PDX organotypic cultures, NK-EV treatment resulted in a significant decrease in cell viability after only 24 hours of co-incubation (**Figure 9B-E**). Continuous treatment of PDX cultures with the NK-EVs maintained a low tumour fragment viability throughout the investigation. There was no significant difference in viability between NK-EVs used on their own or in combination with PTX, suggesting that NK-EV treatment alone was effective at inducing cell death of heterogeneous TNBC PDX organotypic cultures.

To validate the NK-EVs' MoA in the *ex vivo* PDX model, apoptotic activity was measured through caspase 3/7 activation after 90 minutes of treatment. In stark contrast to the untreated and PTX-treated PDX slice cultures, NK-EV treatment resulted in a rapid increase in caspase 3/7 activation (**Figure 9F-I**). Again, no significant differences in caspase 3/7 activation were observed between NK-EVs used alone or in combination with PTX. Overall, solely NK-EV treatment is sufficient to rapidly facilitate apoptosis-mediated cell death.

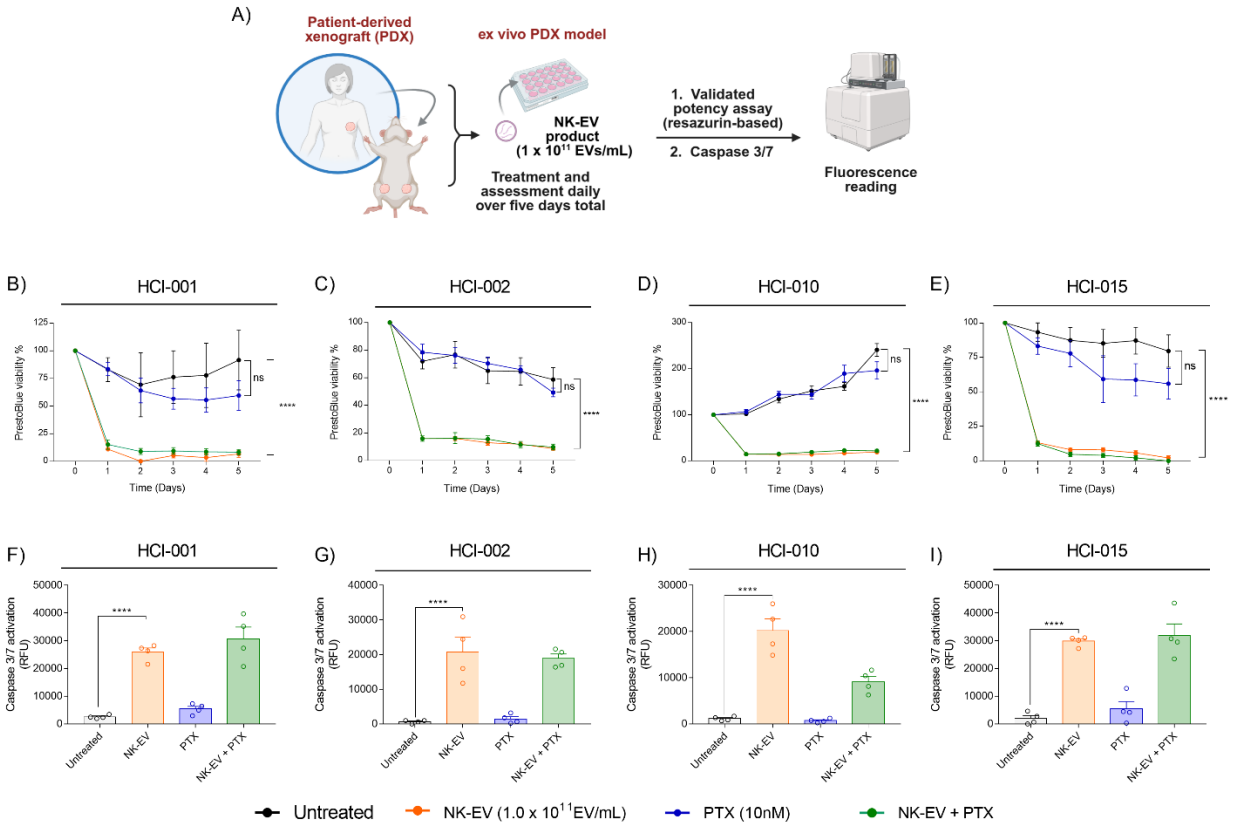

Figure 9. NK-EV treatment induces apoptosis-mediated cell death in human TNBC-PDX organotypic slice cultures.

A) Schematic representation of the cytotoxic co-culture assay where TNBC PDX fragments were assessed using the resazurin-based cell viability assay and treated with NK-EVs daily for five days in total. TNBC PDX cultures were treated with 1.0×10^{11} EVs/mL (or 5.0×10^{10} EVs) NK-EVs (orange), paclitaxel (10nM PTX; blue), a combination of 10nM paclitaxel and 1.0×10^{11} EVs/mL NK-EVs (green), or left untreated (black) for five days. The resazurin-based cell viability was determined for B) HCI-001; C) HCI-002; D) HCI-010; and E) HCI-015 PDX fragments. Data are shown as mean ± S.E.M., n=5 from five independent experiments. Caspase3/7 activation (RFU) after 90 minutes of treatment was investigated for F) HCI-001; G) HCI-002; H) HCI-010; and I) HCI-015 PDX fragments. Data are shown as mean ± S.E.M., n=4 from four independent experiments, ns: nonsignificant, ****: $p<0.0001$.

3.6. Biodistribution of NK-EVs in a TNBC PDX *in vivo* model

3.6.1. Live imaging of TNBC PDX mice following NK-EV administration

Using a TNBC PDX model, the *in vivo* biodistribution of NK-EVs was observed. To accomplish this, NSG mice were surgically implanted with PDX fragment HCI-002 on their mammary fat pads to generate a TNBC PDX model (**Table 3**). Once tumours reached a mean diameter of 1 cm, the mice were administered a high dose of DiR-labelled NK-EVs (5.0×10^{10} EVs) either IV or IT, administration routes that are both used in the clinical setting. IV administration of DiR-labelled 293F-EVs or DiR-labelled PBS was included as a control. Live imaging of the IT-administered NK-EVs revealed that the signal remained localized to the site of injection: directly in the tumour (**Figure 10A**). In contrast, IV administration of the NK-EVs resulted in rapid uptake by the liver, with signal spreading more readily towards the tumours and the rest of the body towards the 24-hour timepoint (**Figure 10B**). No significant differences were observed between the distribution of NK-EVs and the non-cytotoxic 293F-EVs (**Figure 10C**). This suggests that the distribution pattern of the NK-EVs is not specific to their cellular origin.

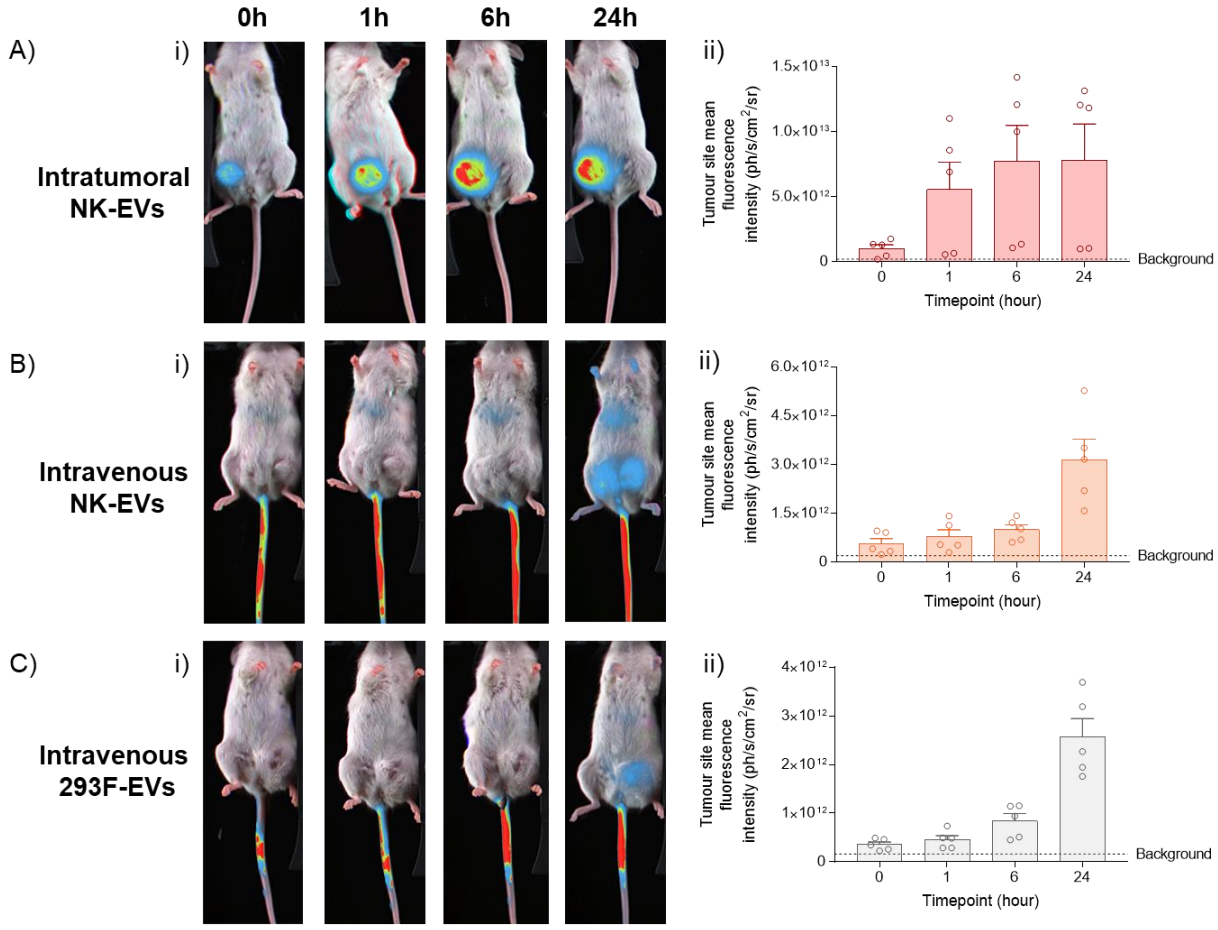

Figure 10. Biodistribution of NK-EVs in a TNBC PDX mouse model over a 24-hour period. PDX HCI-002 fragments were implanted onto the mammary fat pad of NSG mice to generate a TNBC PDX model. Post-treatment, fluorescent imaging of the mice was conducted using the Newton 7.0 FT500 at the 0h, 1h, 6h, and 24h timepoints. TNBC PDX mice were injected with A) DiR-labelled NK-EVs intratumorally (red), B) DiR-labelled NK-EVs intravenously (orange), or C) DiR-labelled 293F-EVs intravenously (grey) (all administered at a dose of 5.0×10^{10} EVs). Data presented as i) representative photos of the mice with the DiR signal overlayed, and ii) the mean fluorescent intensity around the tumour site in live animals (the black dashed line represents the background signal). Data are presented as the mean ± SEM, n=5.

3.6.2. Biodistribution of NK-EVs in the tumours and organs at the 24-hour timepoint.

As a follow-up to live imaging, the tumours and major organs (heart, lungs, liver, spleen, kidney, brain) were harvested for *ex vivo* fluorescent imaging to directly image the DiR signal that had accumulated in the tumours and peripheral organs (heart, lungs, liver, spleen, kidneys, brain). Similar to what was observed during live imaging, IT-administered NK-EVs accumulated primarily in the tumour, with minimal signal being detected in all other organs analyzed (**Figure 11A**). IV administration of NK-EVs primarily accumulated in the liver and spleen, with high signal also being detected in both the tumours and the lungs (**Figure 11B**). A small but significant amount of signal was also detected in the heart, kidneys, and brain. No significant differences were observed between the distribution of 293F-EVs and NK-EVs (**Figure 11C**), suggesting that EVs from multiple sources are naturally capable of travelling throughout the entire body, including into the difficult-to-reach regions such as the brain. DiR-labelled PBS (i.e. free DiR) did not contribute greatly to the signal observed in the tumours or organs (**Supplemental Figure 2**).

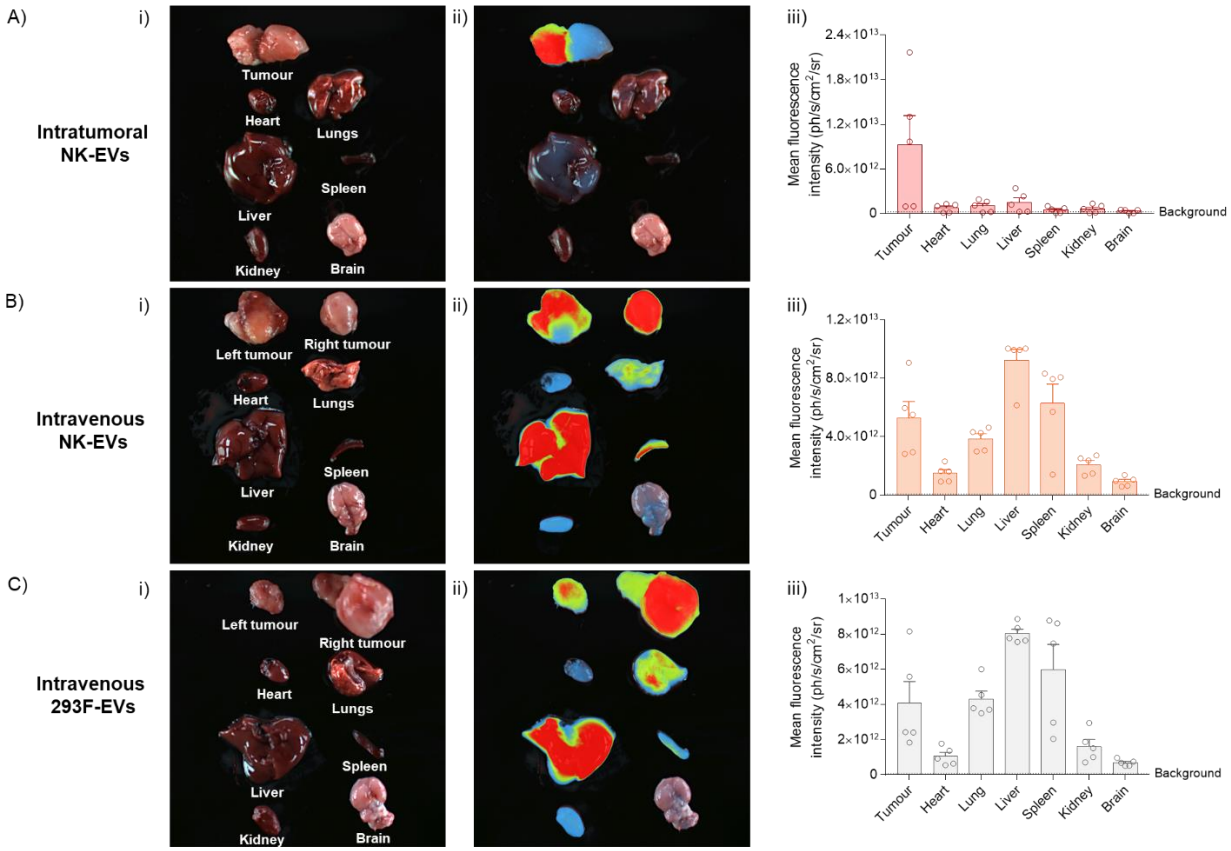

Figure 11. NK-EVs' signal following 24 hours of treatment in a TNBC mouse model.
The Newton 7.0 FT500 was used to collect fluorescent images of the tumours and major organs (heart, lung, liver, spleen, kidney, brain) 24 hours post-treatment. TNBC mice were injected with A) DiR-labelled NK-EVs intratumorally, B) DiR-labelled NK-EVs intravenously, or C) DiR-labelled 293F-EVs intravenously (all administered at a dose of 5.0×10^{10} EVs). Representative images of tumours and organs, both i) without fluorescence and ii) with the fluorescent signal overlayed, are presented, and iii) their mean fluorescence intensity is presented for each treatment group (the black dashed line represents the background signal). Data are presented as the mean ± SEM, n=5.

4. Discussion

Breast cancer is the leading form of cancer and cancer-related mortality in women worldwide. TNBC is considered the most aggressive form of breast cancer. Due to a lack of targetable receptors, TNBC is characterized by a lack of viable treatment options, contributing to poor patient prognosis. Chemotherapy is the primary form of treatment for many TNBC patients, but it is associated with several drawbacks. This includes its adverse effect of enriching CSC populations. Thus, there is a dire need to develop novel treatment options that are effective against both the bulk TNBC cells as well as the treatment-resistant CSCs.

4.1. Elucidation of the NK-EVs' mechanism of action against TNBC

NK-EVs have arisen as a promising therapeutic for several diseases, including difficult-to-treat cancers like TNBC. Similar to NK cells, NK-EVs are enriched in cytotoxic molecules (e.g. perforin, granzyme A/B, IFNγ) that facilitate their ability to recognize and lyse cancerous cells [76, 77, 79, 84, 85]. Thus, we sought to investigate the efficacy and cytotoxic MoA of NK-EVs using various clinically relevant TNBC models.

In this study, we determined that the NK-EVs exhibit a dose-dependent cytotoxic effect on TNBC cell viability. Several TNBC cell lines of varying morphologies were included in this study, demonstrating the broad effectiveness of the NK-EVs against all identified TNBC subtypes. The dose-dependent effect of NK-EVs is heavily supported by other researchers, where higher doses of NK-EVs were inversely correlated with cell viability, while other non-cytotoxic EVs had no impact on cell viability [76, 78, 82, 87]. This demonstrates that EV cytotoxicity is largely dependent upon its parental cell's composition.

In this study, we found that the NK-EVs were highly cytotoxic over the first 24 hours of incubation. Other studies have also suggested that NK-EVs exhibit a time-dependent cytotoxic effect over the first 24 hours of incubation [80, 82], but few studies have reported their observations in a TNBC or breast cancer model beyond this time point. Cecchetti *et al.* investigated NK-EVs against various hematological cancer lines and observed that the percentage of dead cells was elevated after both 24 and 48 hours of co-incubation [108]. Another study by Jiang *et al.* investigated the effects of hypoxia on NK-EV cytotoxicity over 120 hours [90]. NK-EVs exposed to hypoxia were more effective at controlling cell proliferation over time relative to the unaltered NK-EVs, suggesting that hypoxic conditions may be more beneficial to the long-term cytotoxic functioning of NK-EVs; however, cancer cells treated with unaltered NK-EVs (i.e. not exposed to hypoxia) had a gradual restoration of cell viability after their initial exposure, irrespective of their dosage. Altogether, these findings suggest that unaltered NK-EV-mediated cytotoxicity is confined to a short-term timeframe. In a clinical setting, this would translate to the need for multiple administrations of NK-EVs or some form of stimulation/priming to benefit from their cytotoxicity long-term.

To confirm their cytotoxic MoA, activation of apoptosis and necrosis was observed over 72 hours. Additionally, caspase 3/7, caspase 8, and caspase 9 activation were assessed following 90 minutes of co-incubation. Previous studies have determined that NK-EVs increase apoptosis and, to a lesser extent, necrosis of cancer cells, facilitating direct cell death [76, 82, 84, 90, 109]. Similarly, in this study, NK-EV treatment upon various TNBC cell lines increased the activation of each tested caspase in a dose-dependent manner. This finding suggests that NK-EVs use caspase-dependent apoptotic pathways to facilitate cell death. Similarly, NK-EV-treated cells

presented with elevated levels of apoptosis and necrosis over a 72-hour time period. Thus, the cytotoxic MoA of NK-EVs involves the induction of cell death through multiple pathways.

To complement the results obtained against TNBC cell lines, various TNBC PDX organotypic cultures were used to assess both cell viability and MoA. As PDX models are obtained from a patient following surgery, they maintain the heterogeneity, architecture, and characteristics of the original tumour. This makes PDX a clinically relevant model that tends to closely reflect the patient response to treatment. Additionally, as each PDX line is obtained from a different patient, using multiple PDX lines allows for a better understanding of the tested therapy's universal applicability.

In this study, the NK-EVs induced a rapid *ex vivo* cytotoxic effect on PDX organotypic cultures, where viability was reduced by at least 80% after the first 24 hours. To our knowledge, this is one of the first studies to investigate NK-EVs using a PDX model. Another study by Nathani *et al.* utilized an Osimertinib-resistant PDX lung cancer (TM0019) mouse model, where NK-EVs (empty or loaded with miR-5193/miR-149-5p) significantly reduced cell viability *in vitro* and reduced tumour growth *in vivo* [110]. Similarly, three-dimensional cancer cell cultures (i.e. generated from a cancer cell line) had an increased capacity of taking up NK-EVs relative to non-cancerous cell lines, leading to an increased frequency of dead cells over time [86, 111, 112]. Overall, NK-EVs have demonstrated effectiveness against a three-dimensional tumour model, indicating their potential benefit in a clinical setting against various cancer types, including TNBC.

4.2. The relationship between NK-EVs and CSC populations

CSCs are a subpopulation of cancer cells with an immense capacity for self-renewal and cell proliferation. CSCs are largely unaffected by conventional chemotherapy and can contribute to

treatment resistance, tumour recurrence, and metastasis. As a result, the development of novel treatment options that can target and eliminate CSCs is crucial.

Increasing research has highlighted the capability of NK cells to target CSCs. Although CSCs tend to downregulate MHC expression to avoid immune recognition, CSCs upregulate various ligands (e.g. MICA, ULBP) that can be recognized by the NK cells' activating receptor NKG2D, a receptor that is also found on the NK-EVs [113-115]. Interestingly, NK cells were more cytotoxic against $CD44^{high}/CD24^{low}$ and $ALDH^{high}$ CSCs relative to non-CSCs [113, 115]. To date, NK cells have demonstrated the ability to target the CSCs of various cancer types, including breast cancer, colorectal cancer, pancreatic cancer, melanoma, and glioblastoma [113, 115-118]. Unfortunately, poor infiltration of solid tumours following NK cell therapy could not effectively target CSCs in human patients, suggesting that alternative treatment options are required.

As NK-EVs possess high biocompatibility and are capable of infiltrating solid tumours, they may be capable of uptake by the CSCs. For the first time, McCune and Kornbluth reported that NK-EVs were particularly cytotoxic against a subpopulation of treatment-resistant leukemic cells with a CSC-like ($CD34^{high}/CD38^{low}$) phenotype [86]. Similar to their parental cell, NK-EVs seem to possess a heightened cytotoxicity against CSCs.

To the best of our knowledge, this study demonstrates for the first time that NK-EVs are effective against CSCs in breast cancer. Live cell analysis revealed that NK-EVs were more cytotoxic against CSCs compared to non-CSCs over a 72-hour period. Furthermore, *Ctgf* and *Cyr61* gene expression, both of which are involved in the stem cell-promoting YAP/TAZ pathway, was suppressed. Finally, tumorsphere formation, a defining characteristic of CSC functionality, was impaired. Further validation in an *in vivo* biological system is required; however, this finding

could have major implications for the NK-EVs' ability to inhibit tumour recurrence and distant metastasis, major issues that affect TNBC patients' survival worldwide.

4.3. NK-EV's biodistribution in a TNBC PDX mouse model

A critical step in evaluating a therapeutic's clinical applicability is to test its efficacy in a clinically relevant biological system. To date, the majority of experiments in the nanomedicine field have been conducted in a cancer cell line-based mouse tumour model, which does not accurately reflect the three-dimensional structure, architecture, and heterogeneity of an actual tumour [93, 94]. In this study, TNBC PDX fragments originating from breast cancer patients were transplanted onto the mammary fat pad of NSG mice to generate a clinically relevant TNBC mouse model. The TNBC PDX mouse model provides a more accurate platform to investigate NK-EV efficacy, as well as to understand how the enhanced permeability and retention mechanisms affect NK-EV biodistribution and tumour entry [96, 99, 100].

In this study, we injected a high dose of DiR-labelled NK-EVs (5.0×10^{10} EVs) either IT or IV and assessed their biodistribution in a TNBC PDX mouse model over a 24-hour period. IT-administered NK-EVs remained largely localized to their site of injection over the course of the investigation. In contrast, IV-administered NK-EVs primarily accumulated at the site of injection (i.e. the tail) or around the liver. More signal was detected throughout the entire body at the 24-hour timepoint, particularly at the tumour site. *Ex vivo* imaging of the tumours and organs was also conducted at the 24-hour timepoint to confirm NK-EV accumulation within the body. In the IT mice, the highest amount of signal was detected in the tumours, with significantly lower amounts of signal found in the peripheral organs like the liver, lungs, and spleen. This observation aligns with a previous study by Smyth *et al.* that compared the uptake of IT-administered tumour-derived

EVs against liposomes, which revealed that the EVs accumulated in the tumour to a far greater extent than the liposomes [119]. This suggests that the EVs' specific composition is more efficient for uptake by the tumour cells. Conversely, IV administration of NK-EVs resulted in a broader distribution pattern. The highest amount of signal was detected in the liver and spleen, the major organs involved in detoxification and blood filtration. High amounts of signal were also detected in the tumours and lungs. The EVs' biodistribution does not appear to be dependent upon cell source, as the patterns observed for both NK-EVs and 293F-EVs were very similar. Other studies using a breast cancer cell line-based model have reported a similar biodistribution pattern, with the liver, spleen, and lungs being the major accumulation sites for IV-administered tumour-derived EVs [119-122]. These findings suggest that the biodistribution pattern of EVs is largely a result of their inherent biocompatibility.

In the literature, some studies have engineered their NK-EVs to target specific receptors on the cancer cells' surfaces. For example, in a TNBC mouse model, Si *et al.* engineered 293F-EVs for the dual targeting of EGFR and CD47, two markers highly expressed on TNBC cells, which resulted in EV accumulation exclusively in the tumour, liver, and kidneys, with no detectable off-target uptake in the other peripheral organs [123]. In a neuroblastoma mouse model, Wang *et al.* found that NK-EVs fused with the let-7a-loaded dendrimers were more effective at specifically targeting the tumours compared to the unmodified NK-EVs [89]. Thus, engineering the NK-EVs to target cancer cell-specific markers could be a potential strategy to increase EV accumulation in the tumours and reduce the risk of off-target cytotoxicity.

One of the major obstacles in the treatment of TNBC is the occurrence of metastasis in late-stage patients. In metastatic TNBC patients, the primary sites of metastasis are the lungs, liver, and brain (**Table 1**). The prognosis for metastatic TNBC patients is very poor, where available

treatment options are increasingly limited and, in many cases, unsuccessful. Particularly, in patients with brain metastases, no approved TNBC treatments can bypass the blood-brain barrier (BBB), rendering them ineffective. As a result, the median survival following a diagnosis of brain metastases is only 5-7 months, highlighting a dire need to develop novel therapies that are effective against distant metastases. To this end, several studies report that EVs possess the inherent ability to traverse the entire body and bypass the BBB [61-66, 124]. In a study by Alvarez-Erviti *et al.*, they successfully delivered engineered dendritic cell-derived EVs loaded with siRNA targeting GAPDH to the brain without any notable side effects being observed [64]. In our study, *ex vivo* imaging of the organs following IV administration revealed that low levels of unaltered NK-EVs and 293F-EVs accumulated in all organs analyzed, including the brain of a TNBC mouse model. Altogether, these finding suggests that NK-EVs could potentially target distant metastases; however, further research in a metastatic TNBC model is required. Additionally, to increase the abundance of EVs travelling to sites of metastasis, EV engineering could be considered. For example, to increase the abundance of EVs crossing the BBB, they could be modified to target markers specifically upregulated on brain metastases.

4.4. Future directions: *In vivo* models to assess NK-EV efficacy and immunoregulation

A major limitation for the use of TNBC PDX models is the absence of an immune system. In this study, NSG mice were selected for the transplantation of PDX tissue. NSG mice lack T and B cells, eliminating their adaptive immune system. Furthermore, NSG mice do not possess functional NK cells, and the dendritic cells and macrophages are defective, greatly impairing their innate immunity. Severe immunodeficiency in these mice is necessary for the successful implantation of human PDX lines, but does not allow for the investigation of immune cell

recruitment following treatment or assessment of the NK-EVs' immunomodulation, an emerging area of research.

Despite the efficacy of NK-EVs *in vitro* and *ex vivo*, NK-EVs administered *in vivo* into NSG TNBC mouse model alone were not effective at controlling tumour growth relative to the PBS control group (**Appendix A: Figure 1B – C, Figure 2**). However, NK-EV treatment was more effective at controlling tumour growth relative to the PTX and PTX + NK-EV combination group (**Appendix A: Figure 1B - C**). NK-EV treatment did result in a lower but non-statistically significant difference in tumour weight relative to all other treatment groups (**Appendix A: Figure 1E, Figure 2D**). This can be partially explained by the hollow tumour core observed in several of the NK-EV-treated tumours (**Appendix A: Figure 1F**), meaning the NK-EVs may have affected the tumour's final morphology. Additionally, NK-EV treatment suppressed CSC frequencies relative to PTX alone; however, this had no significant impact upon subsequent tumour growth following secondary transplantation of the treated tumours (**Appendix A: Figure 1G, Figure 2E, Figure 3**). This may be partially associated with the heterogeneity of the PDX model used in this study, where increasing sample size may help achieve statistical significance. The results presented are preliminary, but will serve to inform the experimental design of our future animal studies investigating NK-EVs.

It's noteworthy that our results stand in contrast to other studies that have investigated NK-EVs in a breast cancer cell line-based mouse model, which have all reported a reduction in tumour growth and improved survival times [76, 79, 91, 92]. In contrast to this study, less severely immunocompromised mouse models were used in other reports for the engraftment of human cancer cell lines. This includes athymic nude mice, which possess functional B cells and NK cells,

as well as NOD-SCID mice, which have functional NK cells. Thus, it is possible that the selected NSG mouse model in this study may not be suitable for investigating NK-EV efficacy.

Indeed, increasing studies have demonstrated that NK-EVs are capable of stimulating the anti-tumour immune response. Studies in support of this hypothesis include proteomic analysis of NK-EVs, which revealed a high abundance of proteins related to the immune system (granzyme A/B, granulysin, human leukocyte antigen class II, inducible T cell costimulator, etc.) [59]. Further analysis of NK-EVs co-cultured with peripheral blood mononuclear cells revealed that NK-EVs promoted Th1 polarization, T cell activation, monocyte and monocyte-derived dendritic cell activation, and NK cell activation, suggesting a large impact on immune regulation *in vitro* [59, 125]. A study by Shoae-Hassani *et al.* determined that NK-EVs derived from NK cells co-cultured with neuroblastoma cells educated the naïve NK cell populations, making them more cytotoxic against neuroblastoma cells [58]. Furthermore, in a Lewis lung carcinoma model, Zhou *et al.* found that artificial NK-EV treatment reduced immunosuppressive macrophages and myeloid-derived suppressor cells in the spleen, and increased CD8+ T cell, NK cell, and macrophage frequencies at the tumour site [60]. These findings highlight the role of NK-EVs as an immunotherapy. Thus, although NK-EVs can induce rapid cytotoxicity in cancer cells, this alone is unlikely to achieve sustained control of tumour growth. Instead, their long-term regulation of tumour growth may rely on promoting the anti-tumour immune response, an effect that's not observable in the immunodeficient NSG mouse used in this study.

To further investigate the effects of NK-EVs on the anti-tumour immune response, an alternative animal model should be considered. As previously discussed, mouse models with a decreased severity of immunodeficiency have demonstrated positive results regarding NK-EV efficacy. Additionally, immunocompetent mouse models bearing tumours derived from a murine

cell line could be considered; however, all these models retain components of the mouse's immune system. An ideal model for investigating the effects of NK-EVs on the human immune response would be a humanized mouse model. Humanized mouse models allow for the transplantation of human PDX fragments while partially recapitulating the TME, including the human tumour-associated and circulating immune cells, as well as cytokine/chemokine signaling and production [101, 102]. To date, several studies have successfully developed and used humanized mouse models transplanted with breast cancer-derived PDX tumours to investigate novel cancer immunotherapies, including anti-PD-L1 antibody pembrolizumab [126-130]. Thus, this model provides a robust platform for the assessment of NK-EVs as a potential immunotherapy for TNBC for future studies.

5. Conclusion

In conclusion, this study demonstrated that NK-EVs exhibited a short-term, dose-dependent cytotoxic effect on TNBC cell viability. NK-EVs induce cell death through the activation of apoptosis and necrosis pathways. These findings were validated using clinically relevant PDX organotypic cultures. NK-EVs also effectively inhibit the viability and functionality of TNBC CSCs, suggesting their potential to suppress tumour recurrence and metastatic progression. Finally, using a TNBC PDX mouse model, NK-EVs accumulated in the tumours following both IV and IT administration.

Although NK-EVs were effective *in vitro* and *ex vivo*, further validation in a humanized mouse model is necessary to assess their long-term impact on tumour control. Future studies should also consider investigating NK-EVs in a metastatic TNBC model, an aspect that has not been explored in the literature. Finally, the use of engineered or cargo-loaded NK-EVs may further improve their tumour-targeting and efficacy against both the bulk tumour cells and CSCs. Given their versatility and multi-faceted mechanisms of action, NK-EVs hold significant promise for clinical application in managing tumour growth, preventing recurrence, and suppressing distant metastasis.

6. References

1. Bray, F.; Laversanne, M.; Sung, H.; Ferlay, J.; Siegel, R. L.; Soerjomataram, I.; Jemal, A. Global cancer statistics 2022: GLOBOCAN estimates of incidence and mortality worldwide for 36 cancers in 185 countries. *CA: A Cancer Journal for Clinicians* **2024**, *74* (3), 229-263. DOI: 10.3322/caac.21834.

2. Kim, J.; Harper, A.; McCormack, V.; Sung, H.; Houssami, N.; Morgan, E.; Mutebi, M.; Garvey, G.; Soerjomataram, I.; Fidler-Benaoudia, M. M. Global patterns and trends in breast cancer incidence and mortality across 185 countries. *Nature Medicine* **2025**, *31* (4), 1154–1162. DOI: 10.1038/s41591-025-03502-3.

3. Yersal, O.; Barutca, S. Biological subtypes of breast cancer: Prognostic and therapeutic implications. *World Journal of Clinical Oncology* **2014**, *5* (3), 412-424. DOI: 10.5306/wjco.v5.i3.412.

4. Shim, H. J.; Kim, S. H.; Kang, B. J.; Choi, B. G.; Kim, H. S.; Cha, E. S.; Song, B. J. Breast Cancer Recurrence According to Molecular Subtype. *Asian Pacific Journal of Cancer Prevention* **2014**, *15* (14), 5539-5544. DOI: 10.7314/APJCP.2014.15.14.5539.

5. Giaquinto, A. N.; Sung, H.; Newman, L. A.; Freedman, R. A.; Smith, R. A.; Star, J.; Jemal, A.; Siegel, R. L. Breast cancer statistics 2024. *CA: A Cancer Journal for Clinicians* **2024**, *74* (6), 477-495. DOI: 10.3322/caac.21863.

6. Courtney, D.; Davey, M. G.; Moloney, B. M.; Barry, M. K.; Sweeney, K.; McLaughlin, R. P.; Malone, C. M.; Lowery, A. J.; Kerin, M. J. Breast cancer recurrence: factors impacting occurrence and survival. *Irish Journal of Medical Science* **2022**, *191* (6), 2501–2510. DOI: 10.1007/s11845-022-02926-x.

7. Fan, J.-H.; Zhang, S.; Yang, H.; Yi, Z.-B.; Ouyang, Q.-C.; Yan, M.; Wang, X.-J.; Hu, X.-C.; Jiang, Z.-F.; Huang, T.; et al. Molecular subtypes predict the preferential site of distant metastasis in advanced breast cancer: a nationwide retrospective study. *Frontiers in Oncology* **2023**, *13*, 978985. DOI: 10.3389/fonc.2023.978985.

8. Liu, N. U.; Amiri-Kordestani, L.; Palmieri, D.; Liewehr, D. J.; Steeg, P. A. CNS Metastases in Breast Cancer: Old Challenge, New Frontiers. *Clinical Cancer Research* **2013**, *19* (23), 6404-6418. DOI: 10.1158/1078-0432.CCR-13-0790.

9. Lin, N. U.; Claus, E.; Sohl, J.; Razzak, A. R.; Arnaout, A.; Winer, E. P. Sites of distant recurrence and clinical outcomes in patients with metastatic triple-negative breast cancer. *Cancer* **2008**, *113* (10), 2638-2645. DOI: 10.1002/cncr.23930.

10. Jin, J.; Gao, Y.; Zhang, J.; Wang, L.; Wang, B.; Cao, J.; Shao, Z.; Wang, Z. Incidence, pattern and prognosis of brain metastases in patients with metastatic triple negative breast cancer. *BMC Cancer* **2018**, *18* (1), 446. DOI: 10.1186/s12885-018-4371-0.

11. Creighton, C. J. The molecular profile of luminal B breast cancer. *Biologics* **2012**, *6*, 289-297. DOI: 10.2147/BTT.S29923.

12. Inic, Z.; Zegarac, M.; Inic, M.; Markovic, I.; Kozomara, Z.; Djurisic, I.; Inic, I.; Pupic, G.; Jancic, S. Difference between Luminal A and Luminal B Subtypes According to Ki-67, Tumor Size, and Progesterone Receptor Negativity Providing Prognostic Information. *Clinical Medicine Insights: Oncology* **2014**, *8*, 107-111. DOI: 10.4137/CMO.S18006.

13. Li, X.; Yang, J.; Peng, L.; Sahin, A. A.; Huo, L.; Ward, K. C.; O'Regan, R.; Torres, M. A.; Meisel, J. L. Triple-negative breast cancer has worse overall survival and cause-specific survival than non-triple-negative breast cancer - PubMed. *Breast cancer research and treatment* **2017**, *161* (2), 279-287. DOI: 10.1007/s10549-016-4059-6.

14. Xiao, W.; Zheng, S.; Yang, A.; Zhang, X.; Zou, Y.; Tang, H.; Xie, X. Breast cancer subtypes and the risk of distant metastasis at initial diagnosis: a population-based study. *Cancer Management and Research* **2018**, *10*, 5329—5338. DOI: 10.2147/CMAR.S176763.

15. Saraiva, D. P.; Cabral, M. G.; Jacinto, A.; Braga, S. How many diseases is triple negative breast cancer: the protagonism of the immune microenvironment. *ESMO Open* **2017**, *2* (4), e000208. DOI: 10.1136/esmoopen-2017-000208.

16. Kirkby, M.; Popatia, A. M.; Lavoie, J. R.; Wang, L. The Potential of Hormonal Therapies for Treatment of Triple-Negative Breast Cancer. *Cancers* **2023**, *15* (19), 4702. DOI: 10.3390/cancers15194702.

17. Jia, D.; Li, L.; Sulaiman, A.; Allen, D.; Li, X.; Lee, J.; Ji, G.; Yao, Z.; Gadde, S.; Figeys, D.; Wang, L. An autocrine inflammatory forward-feedback loop after chemotherapy withdrawal facilitates the repopulation of drug-resistant breast cancer cells. *Cell Death & Disease* **2017**, *8* (7), e2932. DOI: 10.1038/cddis.2017.319.

18. He, J.; Lee, H.-J.; Saha, S.; Ruan, D.; Guo, H.; Chan, C.-H. Inhibition of USP2 eliminates cancer stem cells and enhances TNBC responsiveness to chemotherapy. *Cell Death & Disease* **2019**, *10* (4), 285. DOI: 10.1038/s41419-019-1512-6.

19. Lehmann, B. D.; Bauer, J. A.; Chen, X.; Sanders, M. E.; Chakravarthy, A. B.; Shyr, Y.; Pietenpol, J. A. Identification of human triple-negative breast cancer subtypes and preclinical models for selection of targeted therapies. *The Journal of Clinical Investigation* **2011**, *121* (7), 2750-2767. DOI: 10.1172/JCI45014.

20. Lehmann, B. D.; Jovanović, B.; Chen, X.; Estrada, M. V.; Johnson, K. N.; Shyr, Y.; Moses, H. L.; Sanders, M. E.; Pietenpol, J. A. Refinement of Triple-Negative Breast Cancer Molecular Subtypes: Implications for Neoadjuvant Chemotherapy Selection. *PloS one* **2016**, *11* (6). DOI: 10.1371/journal.pone.0157368.

21. Santonja, A.; Sánchez-Muñoz, A.; Lluch, A.; Chica-Parrado, M. R.; Albanell, J.; Chacón, J. I.; Antolín, S.; Jerez, J. M.; Haba, J. d. l.; Luque, V. d.; et al. Triple negative breast cancer subtypes and pathologic complete response rate to neoadjuvant chemotherapy. *Oncotarget* **2018**, *9* (41), 26406-26416. DOI: 10.18632/oncotarget.25413.

22. Cortes, J.; Rugo, H. S.; Cescon, D. W.; Im, S.-A.; Yusof, M. M.; Gallardo, C.; Lipatov, O.; Barrios, C. H.; Perez-Garcia, J.; Iwata, H.; et al. Pembrolizumab plus Chemotherapy in Advanced Triple-Negative Breast Cancer. *The New England Journal of Medicine* **2022**, *387* (3), 217-226. DOI: 10.1056/NEJMoa2202809.

23. Mittendorf, E. A.; Philips, A. V.; Meric-Bernstam, F.; Qiao, N.; Wu, Y.; Harrington, S.; Su, X.; Wang, Y.; Gonzalez-Angulo, A. M.; Akcakanat, A.; et al. PD-L1 Expression in Triple-Negative Breast Cancer. *Cancer Immunology Research* **2014**, *2* (4), 361-370. DOI: 10.1158/2326-6066.CIR-13-0127.

24. Bardia, A.; Hurvitz, S. A.; Tolaney, S. M.; Loirat, D.; Punie, K.; Oliveira, M.; Brufsky, A.; Sardesai, S. D.; Kalinsky, K.; Zelnak, A. B.; et al. Sacituzumab Govitecan in Metastatic Triple-Negative Breast Cancer. *New England Journal of Medicine* **2021**, *384* (16), 1529-1541. DOI: 10.1056/NEJMoa2028485.

25. Fultang, N.; Chakraborty, M.; Peethambaran, B. Regulation of cancer stem cells in triple negative breast cancer. *Cancer Drug Resistance* **2021**, *4* (2), 321–342. DOI: 10.20517/cdr.2020.106.

26. Hirschmann-Jax, C.; Foster, A. E.; Wulf, G. G.; Nuchtern, J. G.; Jax, T. W.; Gobel, U.; Goodell, M. A.; Brenner, M. K. A distinct “side population” of cells with high drug efflux capacity in human tumor cells. *Proceedings of the National Academy of Sciences* **2004**, *101* (39), 14228-14233. DOI: 10.1073/pnas.0400067101.

27. Dean, M.; Fojo, T.; Bates, S. Tumour stem cells and drug resistance. *Nature Reviews Cancer* **2005**, *5* (4), 275-284. DOI: 10.1038/nrc1590.

28. Baccelli, I.; Trumpp, A. The evolving concept of cancer and metastasis stem cells. *Journal of Cell Biology* **2012**, *198* (3), 281-293. DOI: 10.1083/jcb.201202014.

29. Shibue, T.; Weinberg, R. A. EMT, CSCs, and drug resistance: the mechanistic link and clinical implications. *Nature Reviews Clinical Oncology* **2017**, *14* (10), 611-629. DOI: 10.1038/nrclinonc.2017.44.

30. Youssef, K. K.; Nieto, M. A. Epithelial–mesenchymal transition in tissue repair and degeneration. *Nature Reviews Molecular Cell Biology* **2024**, *25* (9), 720-739. DOI: 10.1038/s41580-024-00733-z.

31. Al-Hajj, M.; Wicha, M. S.; Benito-Hernandez, A.; Morrison, S. J.; Clarke, M. F. Prospective identification of tumorigenic breast cancer cells. *Proceedings of the National Academy of Sciences* **2003**, *100* (7), 3983-3988. DOI: 10.1073/pnas.0530291100.

32. Ginestier, C.; Hur, M. H.; Charafe-Jauffret, E.; Monville, F.; Dutcher, J.; Brown, M.; Jacquemier, J.; Viens, P.; Kleer, C. G.; Liu, S.; et al. ALDH1 is a marker of normal and malignant human mammary stem cells and a predictor of poor clinical outcome. *Cell Stem Cell* **2007**, *1* (5), 555-567. DOI: 10.1016/j.stem.2007.08.014.

33. Chute, J. P.; Muramoto, G. G.; Whitesides, J.; Colvin, M.; Safi, R.; Chao, N. J.; McDonnell, D. P. Inhibition of aldehyde dehydrogenase and retinoid signaling induces the expansion of human hematopoietic stem cells. *Proceedings of the National Academy of Sciences* **2006**, *103* (31), 11707-11712. DOI: 10.1073/pnas.0603806103.

34. Wei, Y.; Li, Y.; Chen, Y.; Liu, P.; Huang, S.; Zhang, Y.; Sun, Y.; Wu, Z.; Hu, M.; Wu, Q.; et al. ALDH1: A potential therapeutic target for cancer stem cells in solid tumors. *Frontiers in Oncology* **2022**, *12*, 1026278. DOI: 10.3389/fonc.2022.1026278.

35. M, A.-H.; MS, W.; A, B.-H.; SJ, M.; MF, C. Prospective identification of tumorigenic breast cancer cells - PubMed. *Proceedings of the National Academy of Sciences of the United States of America* **04/01/2003**, *100* (7). DOI: 10.1073/pnas.0530291100.

36. Lü, X.; Xu, K.; Lü, H.; Yin, Y.; Ma, C.; Liu, Y.; Li, H.; Suo, Z. CD44(+)/CD24(−) Cells Are Transit Progenitors and Do Not Determine the Molecular Subtypes and Clinical Parameters in Breast Carcinomas. *Ultrastructural Pathology* **2011**, *35* (2), 72-78. DOI: 10.3109/01913123.2010.544843.

37. Chen, C.; Zhao, S.; Karnad, A.; Freeman, J. W. The biology and role of CD44 in cancer progression: therapeutic implications. *Journal of Hematology & Oncology* **2018**, *11* (1), 64. DOI: 10.1186/s13045-018-0605-5.

38. Jaggupilli, A.; Elkord, E. Significance of CD44 and CD24 as Cancer Stem Cell Markers: An Enduring Ambiguity. *Clinical and Developmental Immunology* **2012**, *2012* (1). DOI: 10.1155/2012/708036.

39. Xu, H.; Tian, Y.; Yuan, X.; Wu, H.; Liu, Q.; Pestell, R. G.; Wu, K. The role of CD44 in epithelial–mesenchymal transition and cancer development. *OncoTargets and Therapy* **2015**, *8*, 3783-3792. DOI: 10.2147/OTT.S95470.

40. McFarlane, S.; Coulter, J. A.; Tibbits, P.; O'Grady, A.; McFarlane, C.; Montgomery, N.; Hill, A.; McCarthy, H. O.; Young, L. S.; Kay, E. W.; et al. CD44 increases the efficiency of distant metastasis of breast cancer. *Oncotarget* **2015**, *6* (13), 11465-11476. DOI: 10.18632/oncotarget.3410.

41. Leth-Larsen, R.; Terp, M. G.; Christensen, A. G.; Elias, D.; Kühlwein, T.; Jensen, O. N.; Petersen, O. W.; Ditzel, H. J. Functional Heterogeneity within the CD44 High Human Breast Cancer Stem Cell-Like Compartment Reveals a Gene Signature Predictive of Distant Metastasis. *Molecular Medicine* **2012**, *18*, 1109-1121. DOI: 10.2119/molmed.2012.00091.

42. Sulaiman, A.; McGarry, S.; Han, X.; Liu, S.; Wang, L. CSCs in Breast Cancer—One Size Does Not Fit All: Therapeutic Advances in Targeting Heterogeneous Epithelial and Mesenchymal CSCs. *Cancers* **2019**, *11* (8), 1128. DOI: 10.3390/cancers11081128.

43. Fu, M.; Hu, Y.; Lan, T.; Guan, K.-L.; Luo, T.; Luo, M. The Hippo signalling pathway and its implications in human health and diseases. *Signal Transduction and Targeted Therapy* **2022**, *7* (1), 376. DOI: 10.1038/s41392-022-01191-9.

44. Lei, Q.-Y.; Zhang, H.; Zhao, B.; Zha, Z.-Y.; Bai, F.; Pei, X.-H.; Zhao, S.; Xiong, Y.; Guan, K.-L. TAZ promotes cell proliferation and epithelial-mesenchymal transition and is inhibited by the hippo pathway. *Molecular and cellular biology* **2008**, *28* (7), 2426-2436. DOI: 10.1128/MCB.01874-07.

45. Campbell, K. N.; Wong, J. S.; Gupta, R.; Asanuma, K.; Sudol, M.; He, J. C.; Mundel, P. Yes-associated Protein (YAP) Promotes Cell Survival by Inhibiting Proapoptotic Dendrin Signaling. *Journal of Biological Chemistry* **2013**, *288* (24), 17057-17062. DOI: 10.1074/jbc.C113.457390.

46. Song, Q.; Mao, B.; Cheng, J.; Gao, Y.; Jiang, K.; Chen, J.; Yuan, Z.; Meng, S. YAP Enhances Autophagic Flux to Promote Breast Cancer Cell Survival in Response to Nutrient Deprivation. *PLoS One* **2015**, *10* (3), e0120790. DOI: 10.1371/journal.pone.0120790.

47. Yu, S.; Cai, X.; Wu, C.; Wu, L.; Wang, Y.; Liu, Y.; Yu, Z.; Qin, S.; Ma, F.; Thiery, J. P.; Chen, L. Adhesion glycoprotein CD44 functions as an upstream regulator of a network connecting ERK, AKT and Hippo-YAP pathways in cancer progression. *Oncotarget* **2014**, *6* (5), 2951-2965. DOI: 10.18632/oncotarget.3095.

48. Zhang, Y.; Xia, H.; Ge, X.; Chen, Q.; Yuan, D.; Chen, Q.; Leng, W.; Chen, L.; Tang, Q.; Bi, F. CD44 acts through RhoA to regulate YAP signaling. *Cellular Signalling* **2014**, *26* (11), 2504-2513. DOI: 10.1016/j.cellsig.2014.07.031.

49. Kim, H. M.; Jung, W. H.; Koo, J. S. Expression of Yes-associated protein (YAP) in metastatic breast cancer. *International Journal of Clinical and Experimental Pathology* **2015**, *8* (9), 11248-11257.

50. Wang, T.; Mao, B.; Cheng, C.; Zou, Z.; Gao, J.; Yang, Y.; Lei, T.; Qi, X.; Yuan, Z.; Xu, W.; Lu, Z. YAP promotes breast cancer metastasis by repressing growth differentiation factor-15. *Biochimica et Biophysica Acta (BBA) - Molecular Basis of Disease* **2018**, *1864* (5), 1744-1753. DOI: 10.1016/j.bbadis.2018.02.020.

51. Zhi, X.; Zhao, D.; Zhou, Z.; Liu, R.; Chen, C. YAP promotes breast cell proliferation and survival partially through stabilizing the KLF5 transcription factor. *The American journal of pathology* **2012**, *180* (6), 2452-2461. DOI: 10.1016/j.ajpath.2012.02.025.

52. Chen, W.; Park, S.; Patel, C.; Bai, Y.; Henary, K.; Raha, A.; Mohammadi, S.; You, L.; Geng, F. The migration of metastatic breast cancer cells is regulated by matrix stiffness via YAP signalling. *Heliyon* **2021**, *7* (2), e06252. DOI: 10.1016/j.heliyon.2021.e06252.

53. Cordenonsi, M.; Zanconato, F.; Azzolin, L.; Forcato, M.; Rosato, A.; Frasson, C.; Inui, M.; Montagner, M.; Parenti, A. R.; Poletti, A.; et al. The Hippo transducer TAZ confers cancer stem cell-related traits on breast cancer cells. *Cell* **2011**, *147* (4), 759-772. DOI: 10.1016/j.cell.2011.09.048.

54. Sulaiman, A.; McGarry, S.; Li, L.; Jia, D.; Ooi, S.; Addison, C.; Dimitroulakos, J.; Arnaout, A.; Nessim, C.; Yao, Z.; et al. Dual inhibition of Wnt and Yes-associated protein signaling retards the growth of triple-negative breast cancer in both mesenchymal and epithelial states. *Molecular Oncology* **2018**, *12* (4), 423-440. DOI: 10.1002/1878-0261.12167.

55. Quinn, H. M.; Vogel, R.; Popp, O.; Mertins, P.; Lan, L.; Messerschmidt, C.; Landshammer, A.; Lisek, K.; Château-Joubert, S.; Marangoni, E.; et al. YAP and β-Catenin Cooperate to Drive Oncogenesis in Basal Breast Cancer. *Cancer Research* **2021**, *81* (8), 2116-2127. DOI: 10.1158/0008-5472.CAN-20-2801.

56. Welsh, J. A.; Goberdhan, D. C. I.; O'Driscoll, L.; Buzas, E. I.; Blenkiron, C.; Bussolati, B.; Cai, H.; Vizio, D. D.; Driedonks, T. A. P.; Erdbrügger, U.; et al. Minimal information for studies of extracellular vesicles (MISEV2023): From basic to advanced approaches. *Journal of Extracellular Vesicles* **2024**, *13* (2), e12404. DOI: 10.1002/jev2.12404.

57. Kuang, L.; Wu, L.; Li, Y. Extracellular vesicles in tumor immunity: mechanisms and novel insights. *Molecular Cancer* **2025**, *24* (1), 45. DOI: 10.1186/s12943-025-02233-w.

58. Shoae-Hassani, A.; Hamidieh, A. A.; Behfar, M.; Mohseni, R.; Mortazavi-Tabatabaei, S. A.; Asgharzadeh, S. NK Cell–derived Exosomes From NK Cells Previously Exposed to Neuroblastoma Cells Augment the Antitumor Activity of Cytokine-activated NK Cells. *Journal of Immunotherapy* **2017**, *40* (7), 265-276. DOI: 10.1097/CJI.0000000000000179.

59. Federici, C.; Shahaj, E.; Cecchetti, S.; Camerini, S.; Casella, M.; Iessi, E.; Camisaschi, C.; Paolino, G.; Calvieri, S.; Ferro, S.; et al. Natural-Killer-Derived Extracellular Vesicles: Immune Sensors and Interactors. *Frontiers in Immunology* **2020**, *11*, 262. DOI: 10.3389/fimmu.2020.00262.

60. Zhou, X.; Yuan, H.; Zhu, X.; Liu, Y.; Xiao, J.; Xie, X.; Che, L.; Fang, C.; Yao, C.; Hu, D.; et al. NK cell-derived artificial extracellular vesicles elicit potent anti-tumor efficacy and tumor microenvironment reprogramming capability. *Cancer Nanotechnology 2025 16:1* **2025**, *16* (1). DOI: 10.1186/s12645-025-00328-z.

61. Morad, G.; Carman, C. V.; Hagedorn, E. J.; Perlin, J. R.; Zon, L. I.; Mustafaoglu, N.; Park, T.-E.; Ingber, D. E.; Daisy, C. C.; Moses, M. A. Tumor-Derived Extracellular Vesicles Breach the Intact Blood–Brain Barrier via Transcytosis. *ACS Nano* **2019**, *13* (12), 13853-13865. DOI: 10.1021/acsnano.9b04397.

62. Matsumoto, J.; Stewart, T.; Sheng, L.; Li, N.; Bullock, K.; Song, N.; Shi, M.; Banks, W. A.; Zhang, J. Transmission of α-synuclein-containing erythrocyte-derived extracellular vesicles across the blood-brain barrier via adsorptive mediated transcytosis: another mechanism for initiation and progression of Parkinson's disease? *Acta Neuropathologica Communications 2017 5:1* **2017**, *5* (1), 71. DOI: 10.1186/s40478-017-0470-4.

63. Gupta, D.; Liang, X.; Pavlova, S.; Wiklander, O. P. B.; Corso, G.; Zhao, Y.; Saher, O.; Bost, J.; Zickler, A. M.; Piffko, A.; et al. Quantification of extracellular vesicles in vitro and in vivo using sensitive bioluminescence imaging. *Journal of Extracellular Vesicles* **2020**, *9* (1), 1800222. DOI: 10.1080/20013078.2020.1800222.

64. Alvarez-Erviti, L.; Seow, Y.; Yin, H.; Betts, C.; Lakhal, S.; Wood, M. J. A. Delivery of siRNA to the mouse brain by systemic injection of targeted exosomes. *Nature Biotechnology* **2011**, *29* (4), 341-345. DOI: 10.1038/nbt.1807.

65. Zhuang, X.; Xiang, X.; Grizzle, W.; Sun, D.; Zhang, S.; Axtell, R. C.; Ju, S.; Mu, J.; Zhang, L.; Steinman, L.; et al. Treatment of Brain Inflammatory Diseases by Delivering Exosome Encapsulated Anti-inflammatory Drugs From the Nasal Region to the Brain. *Molecular Therapy* **2011**, *19* (10), 1769-1779. DOI: 10.1038/mt.2011.164.

66. Tolomeo, A. M.; Zuccolotto, G.; Malvicini, R.; Lazzari, G. D.; Penna, A.; Franco, C.; Caicci, F.; Magarotto, F.; Quarta, S.; Pozzobon, M.; et al. Biodistribution of Intratracheal, Intranasal, and Intravenous Injections of Human Mesenchymal Stromal Cell-Derived Extracellular Vesicles in a Mouse Model for Drug Delivery Studies. *Pharmaceutics* **2023**, *15* (2), 548. DOI: 10.3390/pharmaceutics15020548.

67. Li, J.-H.; Fan, W.-S.; Wang, M.-M.; Wang, Y.-H.; Ren, Z.-G. Effects of mesenchymal stem cells on solid tumor metastasis in experimental cancer models: a systematic review and meta-analysis. *Journal of Translational Medicine* **2018**, *16* (1), 113. DOI: 10.1186/s12967-018-1484-9.

68. Morris, E. C.; Neelapu, S. S.; Giavridis, T.; Sadelain, M. Cytokine release syndrome and associated neurotoxicity in cancer immunotherapy. *Nature Reviews Immunology 2021 22:2* **2021**, *22* (2), 85-96. DOI: 10.1038/s41577-021-00547-6.

69. Delen, M. V.; Derdelinckx, J.; Wouters, K.; Nelissen, I.; Cools, N. A systematic review and meta-analysis of clinical trials assessing safety and efficacy of human extracellular vesicle-based therapy. *Journal of Extracellular Vesicles* **2024**, *13* (7), e12458. DOI: 10.1002/jev2.12458.

70. St-Denis-Bissonnette, F.; Khoury, R.; Mediratta, K.; El-Sahli, S.; Wang, L.; Lavoie, J. R. Applications of Extracellular Vesicles in Triple-Negative Breast Cancer. *Cancers* **2022**, *14* (2), 451. DOI: 10.3390/cancers14020451.

71. Tong, L.; Jiménez-Cortegana, C.; Tay, A. H. M.; Wickström, S.; Galluzzi, L.; Lundqvist, A. NK cells and solid tumors: therapeutic potential and persisting obstacles. *Molecular Cancer* **2022**, *21* (1), 206. DOI: 10.1186/s12943-022-01672-z.

72. Tang, X.; Yang, L.; Li, Z.; Nalin, A. P.; Dai, H.; Xu, T.; Yin, J.; You, F.; Zhu, M.; Shen, W.; et al. First-in-man clinical trial of CAR NK-92 cells: safety test of CD33-CAR NK-92 cells in patients with relapsed and refractory acute myeloid leukemia. *American Journal of Cancer Research* **2018**, *8* (6), 1083-1089.

73. Liu, E.; Marin, D.; Banerjee, P.; Macapinlac, H. A.; Thompson, P.; Basar, R.; Kerbauy, L. N.; Overman, B.; Thall, P.; Kaplan, M.; et al. Use of CAR-Transduced Natural Killer Cells in CD19-Positive Lymphoid Tumors. *The New England Journal of Medicine* **2020**, *382* (6), 545-553. DOI: 10.1056/NEJMoa1910607.

74. Knorr, D. A.; Bachanova, V.; Verneris, M. R.; Miller, J. S. Clinical utility of natural killer cells in cancer therapy and transplantation. *Seminars in Immunology* **2014**, *26* (2), 161-172. DOI: 10.1016/j.smim.2014.02.002.

75. Vitale, M.; Cantoni, C.; Pietra, G.; Mingari, M. C.; Moretta, L. Effect of tumor cells and tumor microenvironment on NK-cell function. *European Journal of Immunology* **2014**, *44* (6), 1582-1592. DOI: 10.1002/eji.201344272.

76. Cochran, A. M.; Kornbluth, J. Extracellular Vesicles From the Human Natural Killer Cell Line NK3.3 Have Broad and Potent Anti-Tumor Activity - PubMed. *Frontiers in Cell and Developmental Biology* **2021**, *9*, 698639. DOI: 10.3389/fcell.2021.698639.

77. St-Denis-Bissonnette, F.; Cummings, S. E.; Qiu, S.; Stalker, A.; Muradia, G.; Mehic, J.; Mediratta, K.; Kaczmarek, S.; Burger, D.; Lee, S.-H.; et al. A clinically relevant large-scale biomanufacturing workflow to produce natural killer cells and natural killer cell-derived extracellular vesicles for cancer immunotherapy. *Journal of Extracellular Vesicles* **2023**, *12* (12), e12387. DOI: 10.1002/jev2.12387.

78. Zhu, L.; Kalimuthu, S.; Oh, J. M.; Gangadaran, P.; Baek, S. H.; Jeong, S. Y.; Lee, S.-W.; Lee, J.; Ahn, B.-C. Enhancement of antitumor potency of extracellular vesicles derived from natural killer cells by IL-15 priming. *Biomaterials* **2019**, *190-191*, 38-50. DOI: 10.1016/j.biomaterials.2018.10.034.

79. Choi, J.-W.; Lim, S.; Kang, J. H.; Hwang, S. H.; Hwang, K.-C.; Kim, S. W.; Lee, S. Proteome Analysis of Human Natural Killer Cell Derived Extracellular Vesicles for Identification of Anticancer Effectors. *Molecules* **2020**, *25* (21), 5216. DOI: 10.3390/molecules25215216.

80. Zhu, L.; Kalimuthu, S.; Gangadaran, P.; Oh, J. M.; Lee, H. W.; Baek, S. H.; Jeong, S. Y.; Lee, S.-W.; Lee, J.; Ahn, B.-C. Exosomes Derived From Natural Killer Cells Exert Therapeutic Effect in Melanoma. *Theranostics* **2017**, *7* (10), 2732–2745. DOI: 10.7150/thno.18752.

81. Aarsund, M.; Segers, F. M.; Wu, Y.; Inngjerdingen, M. Comparison of characteristics and tumor targeting properties of extracellular vesicles derived from primary NK cells or NK-cell lines stimulated with IL-15 or IL-12/15/18. *Cancer Immunology, Immunotherapy* **2022**, *71* (9), 2227-2238. DOI: 10.1007/s00262-022-03161-0.

82. Jong, A. Y.; Wu, C.-H.; Li, J.; Sun, J.; Fabbri, M.; Wayne, A. S.; Seeger, R. C. Large-scale isolation and cytotoxicity of extracellular vesicles derived from activated human natural killer cells. *Journal of Extracellular Vesicles* **2017**, *6* (1), 1294368. DOI: 10.1080/20013078.2017.1294368.

83. Aarsund, M.; Nyman, T. A.; Stensland, M. E.; Wu, Y.; Inngjerdingen, M. Isolation of a cytolytic subpopulation of extracellular vesicles derived from NK cells containing NKG7 and cytolytic proteins. *Frontiers in Immunology* **2022**, *13*, 977353. DOI: 10.3389/fimmu.2022.977353.

84. Wu, C.-H.; Li, J.; Li, L.; Sun, J.; Fabbri, M.; Wayne, A. S.; Seeger, R. C.; Jong, A. Y. Extracellular vesicles derived from natural killer cells use multiple cytotoxic proteins and killing mechanisms to target cancer cells. *Journal of Extracellular Vesicles* **2019**, *8* (1), 1588538. DOI: 10.1080/20013078.2019.1588538.

85. Pace, A. L. D.; Tumino, N.; Besi, F.; Alicata, C.; Conti, L. A.; Munari, E.; Maggi, E.; Vacca, P.; Moretta, L. Characterization of Human NK Cell-Derived Exosomes: Role of DNAM1 Receptor in Exosome-Mediated Cytotoxicity against Tumor. *Cancers* **2020**, *12* (3), 661. DOI: 10.3390/cancers12030661.

86. McCune, A.; Kornbluth, J. NK3.3-Derived Extracellular Vesicles Penetrate and Selectively Kill Treatment-Resistant Tumor Cells. *Cancers* **2024**, *16* (1), 90. DOI: 10.3390/cancers16010090.

87. St-Denis-Bissonnette, F.; Qiu, S.; Cummings, S. E.; Kirkby, M.; Haile, Y.; Wassmer, S.; Muradia, G.; Mehic, J.; Stalker, A.; Shrestha, A.; et al. Evaluation of resazurin phenoxazine dye as a highly sensitive cell viability potency assay for natural killer cell-derived extracellular vesicle-based cancer biotherapeutics. *Journal of Extracellular Biology* **2024**, *3* (7), e166. DOI: 10.1002/jex2.166.

88. Khatib, Z. K.; Maleki, A.; Pourfatollah, A. A.; Hamidieh, A. A.; Ferdowsi, S. Antileukemia Activity of Human Natural Killer Cell-Derived Nanomagic Bullets against Acute Myeloid Leukemia (AML). *International Journal of Hematology-Oncology and Stem Cell Research* **2024**, *18* (2), 123-139. DOI: 10.18502/ijhoscr.v18i2.15368.

89. Wang, G.; Hu, W.; Chen, H.; Shou, X.; Ye, T.; Xu, Y. Cocktail Strategy Based on NK Cell-Derived Exosomes and Their Biomimetic Nanoparticles for Dual Tumor Therapy. *Cancers* **2019**, *11* (10), 1560. DOI: 10.3390/cancers11101560.

90. Jiang, Y.; Jiang, H.; Wang, K.; Liu, C.; Man, X.; Fu, Q. Hypoxia enhances the production and antitumor effect of exosomes derived from natural killer cells. *Annals of Translational Medicine* **2021**, *9* (6), 473. DOI: 10.21037/atm-21-347.

91. Lee, J.; Lee, S.-A.; Gu, N.-Y.; Jeong, S. Y.; Byeon, J. S.; Jeong, D.-U.; Ouh, I.-O.; Lee, Y.-H.; Hyun, B.-H. Canine Natural Killer Cell-Derived Exosomes Exhibit Antitumor Activity in a Mouse Model of Canine Mammary Tumor. *BioMed Research International* **2021**, *2021* (1), 6690704. DOI: 10.1155/2021/6690704.

92. Tao, B.; Du, R.; Zhang, X.; Jia, B.; Gao, Y.; Zhao, Y.; Liu, Y. Engineering CAR-NK cell derived exosome disguised nano-bombs for enhanced HER2 positive breast cancer brain metastasis therapy. *Journal of Controlled Release* **2023**, *363*, 692-706. DOI: 10.1016/j.jconrel.2023.10.007.

93. Sulaiman, A.; Wang, L. Bridging the divide: preclinical research discrepancies between triple-negative breast cancer cell lines and patient tumors. *Oncotarget* **2017**, *8* (68), 113269-113281. DOI: 10.18632/oncotarget.22916.

94. Ledford, H. US cancer institute to overhaul tumour cell lines. *Nature* **2016**, *530*, 391. DOI: 10.1038/nature.2016.19364.

95. Nagle, P. W.; Plukker, J. T. M.; Muijs, C. T.; Luijk, P. v.; Coppes, R. P. Patient-derived tumor organoids for prediction of cancer treatment response. *Seminars in Cancer Biology* **2018**, *53*, 258-264. DOI: 10.1016/j.semcancer.2018.06.005.

96. Owonikoko, T. K.; Zhang, G.; Kim, H. S.; Stinson, R. M.; Bechara, R.; Zhang, C.; Chen, Z.; Saba, N. F.; Pakkala, S.; Pillai, R.; et al. Patient-derived xenografts faithfully replicated clinical outcome in a phase II co-clinical trial of arsenic trioxide in relapsed small cell lung cancer. *Journal of Translational Medicine* **2016**, *14* (1), 111. DOI: 10.1186/s12967-016-0861-5.

97. Julien, S.; Merino-Trigo, A.; Lacroix, L.; Pocard, M.; Goéré, D.; Mariani, P.; Landron, S.; Bigot, L.; Nemati, F.; Dartigues, P.; et al. Characterization of a large panel of patient-derived tumor xenografts representing the clinical heterogeneity of human colorectal cancer. *Clinical Cancer Research* **2012**, *18* (19), 5314-5328. DOI: 10.1158/1078-0432.CCR-12-0372.

98. Liu, Y.; Wu, W.; Cai, C.; Zhang, H.; Shen, H.; Han, Y. Patient-derived xenograft models in cancer therapy: technologies and applications. *Signal Transduction and Targeted Therapy 2023 8:1* **2023**, *8* (1), 160. DOI: 10.1038/s41392-023-01419-2.

99. Sikandar, S. S.; Kuo, A. H.; Kalisky, T.; Cai, S.; Zabala, M.; Hsieh, R. W.; Lobo, N. A.; Scheeren, F. A.; Sim, S.; Qian, D.; et al. Role of epithelial to mesenchymal transition associated genes in mammary gland regeneration and breast tumorigenesis. *Nature communications* **2017**, *8* (1), 1669. DOI: 10.1038/s41467-017-01666-2.

100. Gao, H.; Korn, J. M.; Ferretti, S.; Monahan, J. E.; Wang, Y.; Singh, M.; Zhang, C.; Schnell, C.; Yang, G.; Zhang, Y.; et al. High-throughput screening using patient-derived tumor xenografts to predict clinical trial drug response. *Nature Medicine* **2015**, *21* (11), 1318-1325. DOI: 10.1038/nm.3954.

101. Yin, L.; Wang, X.-J.; Chen, D.-X.; Liu, X.-N.; Wang, X.-J. Humanized mouse model: a review on preclinical applications for cancer immunotherapy. *American Journal of Cancer Research* **2020**, *10* (12), 4568-4584.

102. Chen, A.; Neuwirth, I.; Herndler-Brandstetter, D. Modeling the Tumor Microenvironment and Cancer Immunotherapy in Next-Generation Humanized Mice. *Cancers* **2023**, *15* (11), 2989. DOI: 10.3390/cancers15112989.

103. St-Denis-Bissonnette, F.; Kirkby, M.; Wang, L.; Lavoie, J. R. Scalable Biomanufacturing Workflow to Produce and Isolate Natural Killer Cell-Derived Extracellular Vesicle-Based Cancer Biotherapeutics. *Journal of Visualized Experiments* **2024**, (210). DOI: 10.3791/67227.

104. Mediratta, K.; El-Sahli, S.; Marotel, M.; Awan, M. Z.; Kirkby, M.; Salkini, A.; Kurdieh, R.; Abdisalam, S.; Shrestha, A.; Censo, C. D.; et al. Frontiers | Targeting CD73 with flavonoids inhibits cancer stem cells and increases lymphocyte infiltration in a triple-negative breast cancer mouse model. *Frontiers in Immunology* **2024**, *15*, 1366197. DOI: 10.3389/fimmu.2024.1366197.

105. Guillen, K. P.; Fujita, M.; Butterfield, A. J.; Scherer, S. D.; Bailey, M. H.; Chu, Z.; DeRose, Y. S.; Zhao, L.; Cortes-Sanchez, E.; Yang, C.-H.; et al. A human breast cancer-derived xenograft and organoid platform for drug discovery and precision oncology. *Nature Cancer* **2022**, *3* (2), 232-250. DOI: 10.1038/s43018-022-00337-6.

106. Alagkiozidis, I.; Facciabene, A.; Tsiatas, M.; Carpenito, C.; Benencia, F.; Adams, S.; Jonak, Z.; June, C. H.; Daniel J Powell, J.; Coukos, G. Time-dependent cytotoxic drugs selectively cooperate with IL-18 for cancer chemo-immunotherapy. *Journal of Translational Medicine* **2011**, *9* (77). DOI: 10.1186/1479-5876-9-77.

107. Elfarnawany, A.; Dehghani, F. Time- and Concentration-Dependent Adverse Effects of Paclitaxel on Non-Neuronal Cells in Rat Primary Dorsal Root Ganglia. *Toxics* **2023**, *11* (7), 581. DOI: 10.3390/toxics11070581.

108. Cecchetti, S.; Federici, C.; Canese, R.; Iorio, E.; Huber, V.; Pisanu, M. E.; Chirico, M.; Iessi, E.; Camerini, S.; Casella, M.; et al. NK cells-derived extracellular vesicles potency in the B cell lymphoma biotherapy. *Frontiers in immunology* **2024**, *15*, 1503857. DOI: 10.3389/fimmu.2024.1503857.

109. Matchett, E. C.; Kornbluth, J. Extracellular vesicles derived from immortalized human natural killer cell line NK3.3 as a novel therapeutic for multiple myeloma. *Frontiers in Immunology* **2023**, *14*, 1265101. DOI: 10.3389/fimmu.2023.1265101.

110. Nathani, A.; Sun, L.; Li, Y.; Lazarte, J.; Aare, M.; Singh, M. Targeting EGFR-TKI resistance in lung cancer: Role of miR-5193/miR-149-5p loaded NK-EVs and Carboplatin combination. *International Journal of Pharmaceutics* **2025**, *675*, 125573. DOI: 10.1016/j.ijpharm.2025.125573.

111. Nathani, A.; Sun, L.; Khan, I.; Aare, M.; Bagde, A.; Li, Y.; Singh, M. Combined Role of Interleukin-15 Stimulated Natural Killer Cell-Derived Extracellular Vesicles and Carboplatin in Osimertinib-Resistant H1975 Lung Cancer Cells with EGFR Mutations. *Pharmaceutics* **2024**, *16* (1), 83. DOI: 10.3390/pharmaceutics16010083.

112. Wu, J.; Wu, D.; Wu, G.; Bei, H.-P.; Li, Z.; Xu, H.; Wang, Y.; Wu, D.; Liu, H.; Shi, S.; et al. Scale-out production of extracellular vesicles derived from natural killer cells via mechanical stimulation in a seesaw-motion bioreactor for cancer therapy. *Biofabrication* **2022**, *14* (4). DOI: 10.1088/1758-5090/ac7eeb.

113. Yin, T.; Wang, G.; He, S.; Liu, Q.; Sun, J.; Wang, Y. Human cancer cells with stem cell-like phenotype exhibit enhanced sensitivity to the cytotoxicity of IL-2 and IL-15 activated natural killer cells. *Cellular Immunology* **2016**, *300*, 41-45. DOI: 10.1016/j.cellimm.2015.11.009.

114. Luna, J. I.; Grossenbacher, S. K.; Murphy, W. J.; Canter, R. J. Targeting Cancer Stem Cells with Natural Killer Cell Immunotherapy. *Expert Opinion on Biological Therapy* **2017**, *17* (3), 313-324. DOI: 10.1080/14712598.2017.1271874.

115. Ames, E.; Canter, R. J.; Grossenbacher, S. K.; Mac, S.; Chen, M.; Smith, R. C.; Hagino, T.; Perez-Cunningham, J.; Sckisel, G. D.; Urayama, S.; et al. NK Cells Preferentially Target Tumor Cells with a Cancer Stem Cell Phenotype. *The Journal of Immunology* **2015**, *195* (8), 4010-4019. DOI: 10.4049/jimmunol.1500447.

116. Tallerico, R.; Todaro, M.; Franco, S. D.; Maccalli, C.; Garofalo, C.; Sottile, R.; Palmieri, C.; Tirinato, L.; Pangigadde, P. N.; Rocca, R. L.; et al. Human NK Cells Selective Targeting of Colon Cancer–Initiating Cells: A Role for Natural Cytotoxicity Receptors and MHC Class I Molecules. *The Journal of Immunology* **2013**, *190* (5), 2381-2390. DOI: 10.4049/jimmunol.1201542.

117. Castriconi, R.; Daga, A.; Dondero, A.; Zona, G.; Poliani, P. L.; Melotti, A.; Griffero, F.; Marubbi, D.; Spaziante, R.; Bellora, F.; et al. NK Cells Recognize and Kill Human Glioblastoma Cells with Stem Cell-Like Properties. *The Journal of Immunology* **2009**, *182* (6), 3530-3539. DOI: 10.4049/jimmunol.0802845.

118. Pietra, G.; Manzini, C.; Vitale, M.; Balsamo, M.; Ognio, E.; Boitano, M.; Queirolo, P.; Moretta, L.; Mingari, M. C. Natural killer cells kill human melanoma cells with characteristics of cancer stem cells. *International immunology* **2009**, *21* (7), 793-801. DOI: 10.1093/intimm/dxp047.

119. Smyth, T.; Kullberg, M.; Malik, N.; Smith-Jones, P.; Graner, M. W.; Anchordoquy, T. J. Biodistribution and delivery efficiency of unmodified tumor-derived exosomes. *Journal of controlled release* **2015**, *199* (145-155). DOI: 10.1016/j.jconrel.2014.12.013.

120. Lee, T. S.; Kim, Y.; Zhang, W.; Song, I. H.; Tung, C.-H. Facile metabolic glycan labeling strategy for exosome tracking. *Biochimica et Biophysica Acta (BBA) - General Subjects* **2018**, *1862* (5), 1091-1100. DOI: 10.1016/j.bbagen.2018.02.001.

121. Gerwing, M.; Kocman, V.; Stölting, M.; Helfen, A.; Masthoff, M.; Roth, J.; Barczyk-Kahlert, K.; Greune, L.; Schmidt, M. A.; Heindel, W.; et al. Tracking of Tumor Cell–Derived Extracellular Vesicles In Vivo Reveals a Specific Distribution Pattern with Consecutive Biological Effects on Target Sites of Metastasis. *Molecular Imaging and Biology* **2020**, *22* (6), 1501-1510. DOI: 10.1007/s11307-020-01521-9.

122. Wen, S. W.; Sceneay, J.; Lima, L. G.; Wong, C. S. F.; Becker, M.; Krumeich, S.; Lobb, R. J.; Castillo, V.; Wong, K. N.; Ellis, S.; et al. The Biodistribution and Immune Suppressive Effects of Breast Cancer–Derived Exosomes. *Cancer Research* **2016**, *76* (23), 6816-6827. DOI: 10.1158/0008-5472.CAN-16-0868.

123. Si, Y.; Chen, K.; Ngo, H. G.; Guan, J. S.; Totoro, A.; Zhou, Z.; Kim, S.; Kim, T.; Zhou, L.; Liu, X. Targeted EV to Deliver Chemotherapy to Treat Triple-Negative Breast Cancers. *Pharmaceutics* **2022**, *14* (1), 146. DOI: 10.3390/pharmaceutics14010146.

124. Goh, W. J.; Zou, S.; Ong, W. Y.; Torta, F.; Alexandra, A. F.; Schiffelers, R. M.; Storm, G.; Wang, J.-W.; Czarny, B.; Pastorin, G. Bioinspired Cell-Derived Nanovesicles versus Exosomes as Drug Delivery Systems: a Cost-Effective Alternative. *Scientific Reports* **2017**, *7* (1), 14322. DOI: 10.1038/s41598-017-14725-x.

125. Dosil, S. G.; Lopez-Cobo, S.; Rodriguez-GalanIrene, A.; Fernandez-Delgado; Ramirez-Huesca, M.; Milan-Rois, P.; Castellanos, M.; Somoza, A.; Gómez, M. J.; Reyburn, H. T.; et al. Natural killer (NK) cell-derived extracellular-vesicle shuttled microRNAs control T cell responses. *eLife* **2022**, *11*, e76319. DOI: 10.7554/eLife.76319.

126. Rosato, R. R.; Dávila-González, D.; Choi, D. S.; Qian, W.; Chen, W.; Kozielski, A. J.; Wong, H.; Dave, B.; Chang, J. C. Evaluation of anti-PD-1-based therapy against triple-negative breast cancer patient-derived xenograft tumors engrafted in humanized mouse models. *Breast Cancer Research* **2018**, *20* (1), 108. DOI: 10.1186/s13058-018-1037-4.

127. Scherer, S. D.; Riggio, A. I.; Haroun, F.; DeRose, Y. S.; Ekiz, H. A.; Fujita, M.; Toner, J.; Zhao, L.; Li, Z.; Oesterreich, S.; et al. An immune-humanized patient-derived xenograft model of estrogen-independent, hormone receptor positive metastatic breast cancer. *Breast Cancer Research* **2021**, *23* (1), 100. DOI: 10.1186/s13058-021-01476-x.

128. Wang, M.; Yao, L.-C.; Cheng, M.; Cai, D.; Martinek, J.; Pan, C.-X.; Shi, W.; Ma, A.-H.; White, R. W. d. V.; Airhart, S.; et al. Humanized mice in studying efficacy and mechanisms of PD-1-targeted cancer immunotherapy. *The FASEB Journal* **2018**, *32* (3), 1537-1549. DOI: 10.1096/fj.201700740R.

129. Marín-Jiménez, J. A.; Capasso, A.; Lewis, M. S.; Bagby, S. M.; Hartman, S. J.; Shulman, J.; Navarro, N. M.; Yu, H.; Rivard, C. J.; Wang, X.; et al. Testing Cancer Immunotherapy in a Human Immune System Mouse Model: Correlating Treatment Responses to Human Chimerism, Therapeutic Variables and Immune Cell Phenotypes. *Frontiers in Immunology* **2021**, *12*, 607282. DOI: 10.3389/fimmu.2021.607282.

130. Maser, I.-P.; Hoves, S.; Bayer, C.; Heidkamp, G.; Nimmerjahn, F.; Eckmann, J.; Ries, C. H. The Tumor Milieu Promotes Functional Human Tumor-Resident Plasmacytoid Dendritic Cells in Humanized Mouse Models. *Frontiers in Immunology* **2020**, *11*, 2082. DOI: 10.3389/fimmu.2020.02082.

7. Supplemental Information

Supplemental Table 1. List of primers used for RT-qPCR.

Gene	Forward primer sequence	Reverse primer sequence
Gapdh	AATGGGCAGCCGTTAGGAAA	GCGCCCAATACGACCAAATC
Ctgf	AGGAGTGGGTGTGTGACGA	CCAGGCAGTTGGCTCTAATC
Cyr61	AGCCTCGCATCCTATACAACC	TTCTTTCACAAGGCGGCACTC

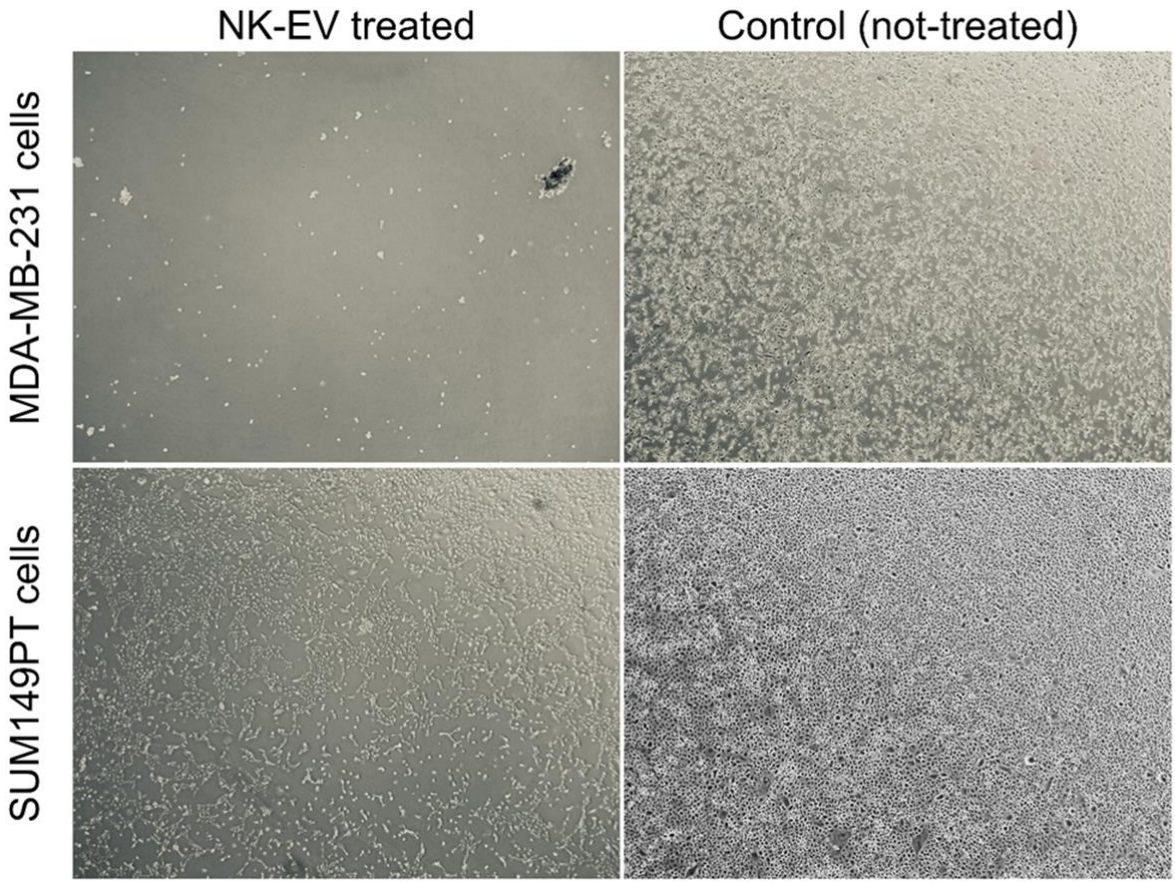

Supplemental Figure 1. NK92-EVs cytotoxic co-culture assay against TNBC cell lines after 24h of treatment.

MDA-MB-231 and SUM149-PT cells were left untreated (right) or co-incubated with a high dose of NK-EVs (1×10^{11} EVs/mL) (left) for 24 hours. Images were acquired on the EVOS FL microscope with a 4X objective.

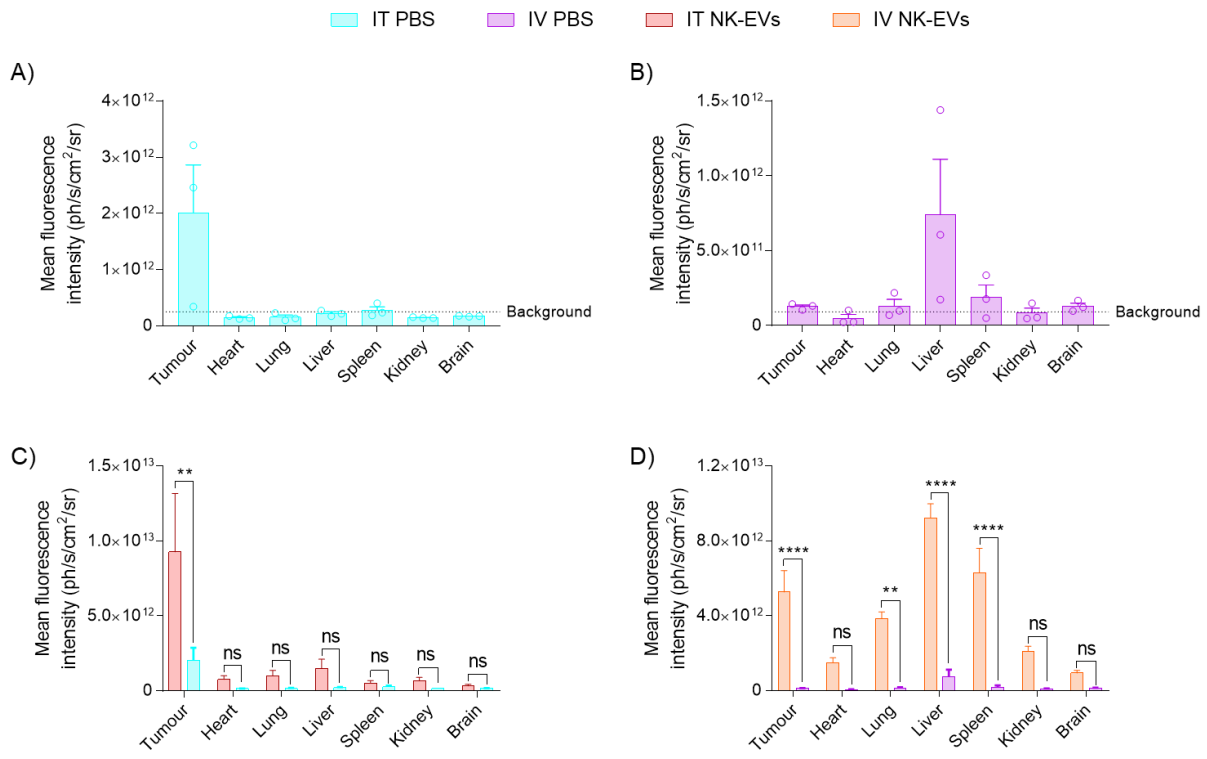

Supplemental Figure 2. Ex vivo biodistribution of IV- or IT-administered DiR-labelled PBS. The Newton 7.0 FT500 was used to collect fluorescent images of the tumours and major organs (heart, lung, liver, spleen, kidney, brain) 24 hours post-treatment. TNBC mice were injected with DiR-labelled PBS A) intratumorally (IT; purple) or B) intravenously (IV; blue), and the data are presented as the mean fluorescence intensity (the black dashed line represents the background signal). A comparison between the average mean fluorescent intensity was performed for DiR-labelled NK-EV and PBS C) IT or D) IV (IT NK-EVs: red, IV NK-EVs: orange). Data are presented as the mean ± SEM, n=3, ns: nonsignificant, **: $p<0.01$, ****: $p<0.0001$.

Appendix A: NK-EV Efficacy in Animal Models

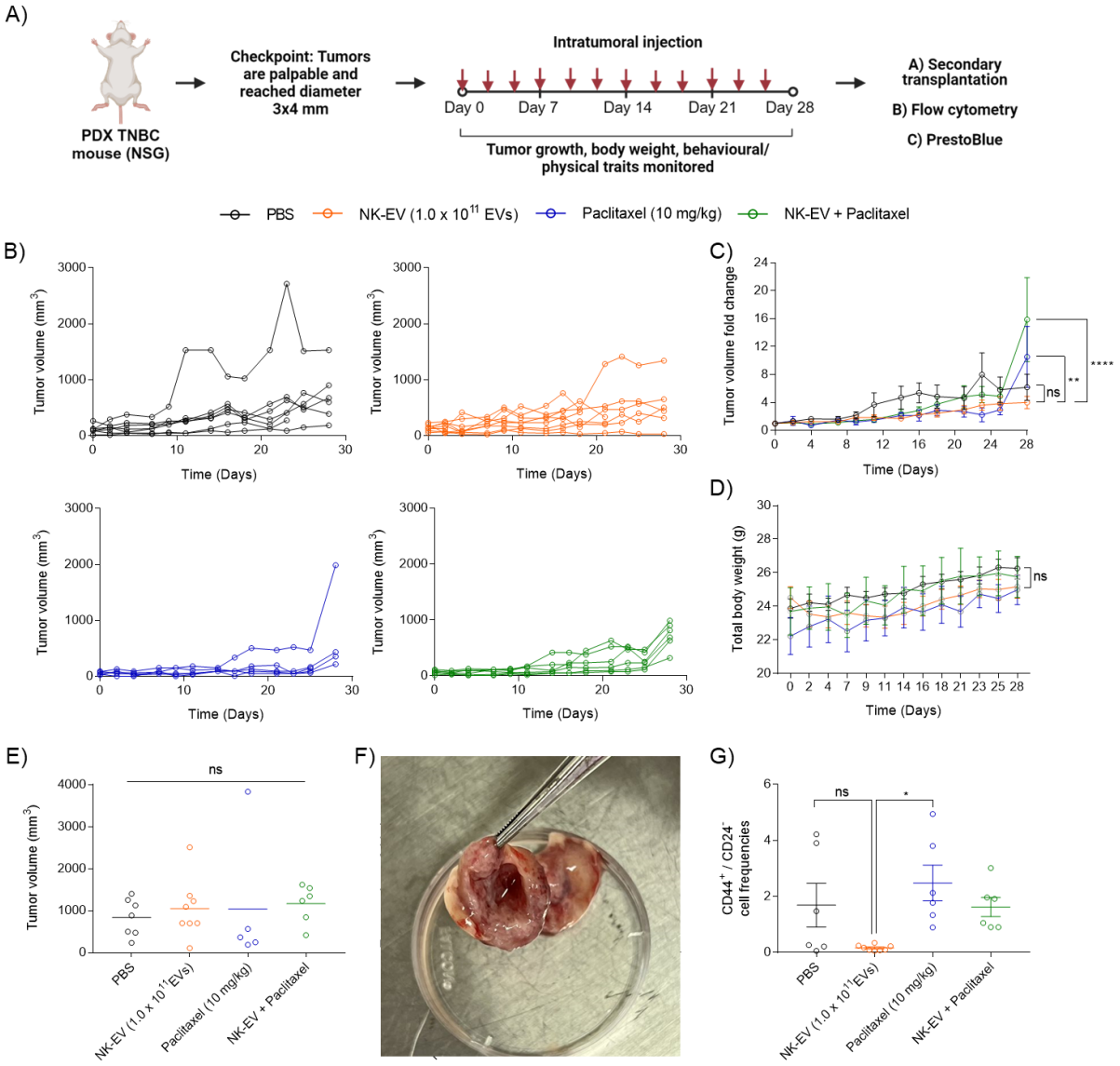

Appendix A: Figure 1. Evaluation of TNBC PDX tumour growth over four weeks of NK-EV treatment. Schematic representation where TNBC PDX HCI-002 mice models are treated with PBS (black), 5.0 × 10^{10} NK-EVs (orange), 10 mg/kg paclitaxel (blue), or a combination of 10 mg/kg paclitaxel and 5.0 × 10^{10} NK-EVs (green). Treatment occurred three times a week for four weeks total, after which tumours were harvested and analyzed using secondary transplantation, flow cytometry, and a resazurin-based cell viability assay. This figure was created using BioRender. B) Individual tumour growth, C) tumour volume fold change, and D) total body weight (g) for each treatment group were evaluated over the entire treatment period. Following tumour harvest, E) tumour volume, F) representative photos of the tumour (pictured above is the NK-EV-treated tumour), and G) tumour weight were recorded. Data are shown as means ± SEM from at least five biological replicates (PBS: n=7; NK-EV: n=8, paclitaxel: n=5, NK-EV + paclitaxel: n=6), ns: non-significant, *: $p<0.05$, **: $p<0.001$, ****: $p<0.0001$.

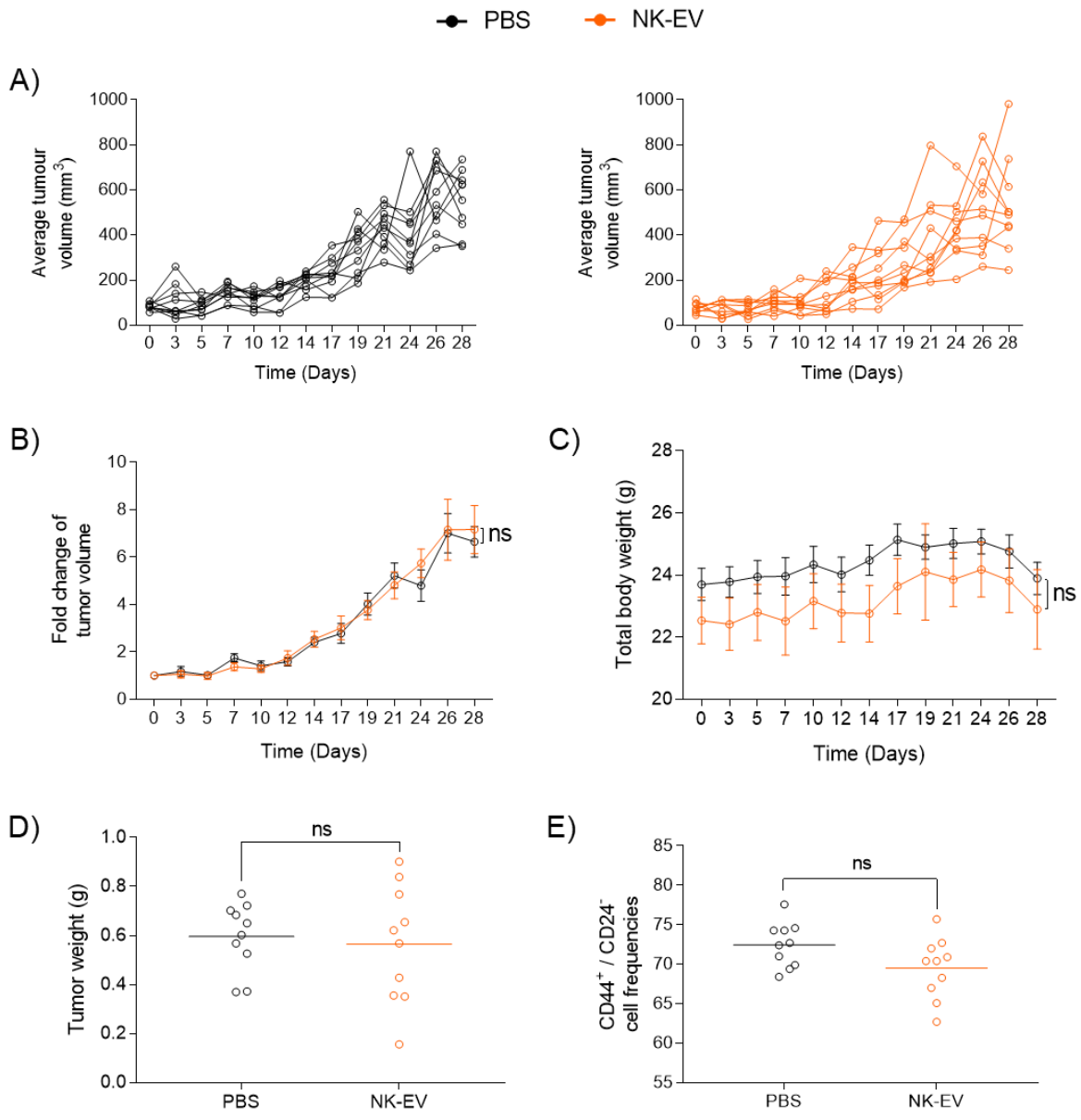

Appendix A: Figure 2. NK-EV treatment did not significantly impact tumour growth in a TNBC cell line-based model. NSG mice were injected orthotopically with RFP-MDA-MB-231 cells onto the mammary fat pad and treated with PBS (black), 5.0 x 10^{10} NK-EVs (orange). Treatment occurred three times a week for four weeks (28 days) total. A) Individual tumour volume, B) tumour volume fold change, and C) total body weight for each treatment group was evaluated over the entire treatment period. Following tumour harvest, D) tumour weight was recorded. E) Flow cytometry was used to assess the frequency of living $CD44^+$ / $CD24^-$ cells. Data are shown as means ± SEM, n=10, ns: non-significant.

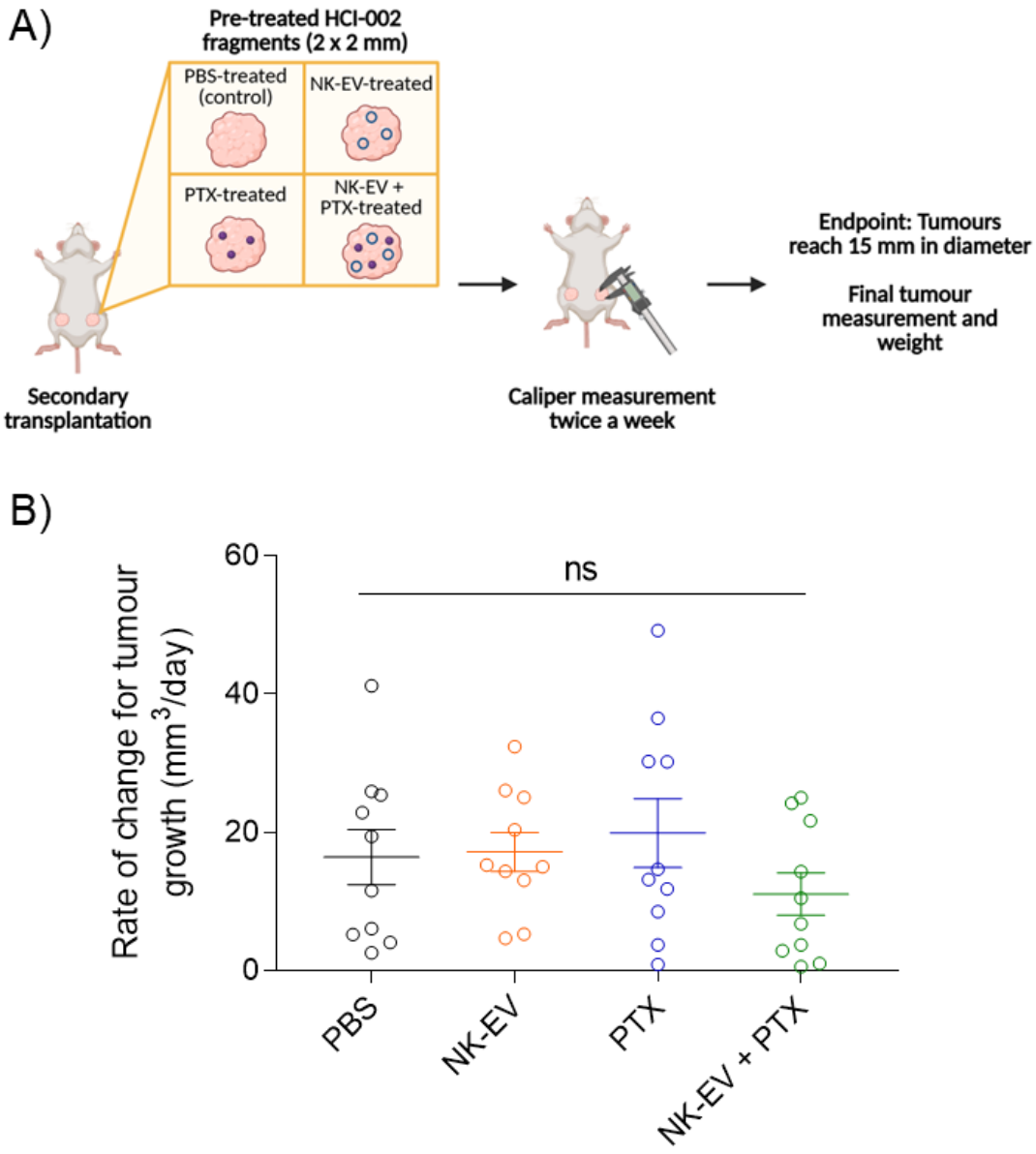

Appendix A: Figure 3. Secondary transplantation of treated PDX tumours following NK-EV treatment. A) Schematic workflow for secondary transplantation of NSG mice. The mice were transplanted with HCI-002 fragments previously treated with PBS (black), 5.0 × 10^{10} NK-EVs (orange), 10 mg/kg paclitaxel (PTX; blue), or a combination of NK-EVs and paclitaxel (green). This figure was created using BioRender. B) The rate of change for tumour growth over the entire time of investigation is presented. Data are shown as mean ± S.E.M., n=10.

Appendix B: Curriculum Vitae

EDUCATION

Master of Science in Microbiology and Immunology 2023 – 2025
University of Ottawa, Ottawa, ON

- **Research project:** Investigating the efficacy of NK cell-derived extracellular vesicles against triple-negative breast cancer
- Supervisors: Dr. Lisheng Wang and Dr. Jessie Lavoie (Health Canada)

Honours Bachelor of Science in Translational and Molecular Medicine 2019 - 2023
University of Ottawa, Ottawa, ON

- **Research project:** Targeting CD73 with flavonoids inhibits triple-negative breast cancer stem cell survival
- Supervisor: Dr. Lisheng Wang

RESEARCH EXPERIENCE

Graduate Researcher September 2023 – Present
University of Ottawa & Stem Cell-based Therapeutics Laboratory, Health Canada, Ottawa, ON

- Supervised by Dr. Lisheng Wang and Dr. Jessie Lavoie.
- Highly familiar with experimentation in a mouse model, including the sterile handling of immunodeficient mice; setting up and maintaining breeding colonies; intravenous, intraperitoneal, subcutaneous, and intratumoral injections; and IVIS fluorescent imaging.
- Conducted and trained students in the transplantation of patient-derived xenografts into an immunodeficient mouse model.
- Trained in cell culturing, patient-derived xenograft, RT-qPCR, cytotoxic co-culture assays, and flow cytometry to assess bulk tumour cell and cancer stem cell viability.
- Experienced in the large-scale biomanufacturing of clinical-grade extracellular vesicles, including hollow-fibre bioreactor production, nanoparticle tracking analysis, and protein/dsDNA quantification.
- Mentored several undergraduate students.

Undergraduate Researcher May 2022 – August 2023
University of Ottawa, ON

- Supervised by Dr. Lisheng Wang.
- Trained in several immunology-related techniques like cell culturing, as well as flow cytometry and RT-qPCR to assess cancer stem cell health.
- Responsible for culturing, expanding, and maintaining an organized collection of the laboratory's patient-derived xenograft lines.

Undergraduate Researcher Jan 2022 – April 2022
University of Ottawa, ON

- Worked under the supervision of Dr. Michael Downey.

- Screened GFP-tagged yeast proteins for histidine polyphosphorylation targets using NCBI Blast and UniProt.
- Experienced in western blotting to test polyphosphorylation of selected proteins.

Summer Student – Co-op May 2021 – August 2021
Brucellosis Reference Laboratory, Canadian Food Inspection Agency, Ottawa, ON

- Worked under the supervision of Dr. Om Surujballi and Niroshan Thanthridge-Don.
- Conducted ELISA and PCR tests to optimize the organization's current detection assay for tuberculosis and brucellosis in livestock.

PROFESSIONAL EXPERIENCE

Teaching Assistant – TMM3104: Cellular Metabolism October 2023 – December 2024
University of Ottawa, Ottawa, ON

- Responsible for the marking and grade distribution of all students enrolled in the course.
- Conducted regular review sessions to reinforce course material.
- Mentored students on relevant course material and proper studying techniques.

Adapted Exams Proctor January 2023 – April 2023
University of Ottawa, Ottawa, ON

- Proctored students taking their exams with the Student Academic Success Services.
- Acted as the direct line of communication between professors and students during examination periods.
- Worked within a team to ensure all exams were accounted for and delivered to the appropriate department.

Tutor-Mentor September 2020 – June 2022
TutorBright, Ottawa, ON

- Tutored students in high school science, math, and English.
- Acted as a mentor, which included developing a study schedule to help organize their time better.
- Developed worksheets meant to test the students' knowledge as extra practice.

EXTRACURRICULAR ACTIVITY

Vice President of Social Media May 2024 – April 2025
Biochemistry, Microbiology, and Immunology Graduate Student Association, Ottawa, ON

- Maintained all social media platforms associated with the student association.
- Aided in the creation of graphics necessary to promote student events and announcements.
- Assisted with the planning and execution of social and academic events for the student body.

Promotions Coordinator May 2022 – May 2023
Translational and Molecular Medicine Student Association, Ottawa, ON

- Created all graphic materials needed to promote TMMSA events using Canva.
- Managed the distribution of TMM's apparel for the 2022-2023 academic year.
- Organized and ran events to promote mental and physical wellbeing as part of the wellness committee.

Student Volunteer January 2020 – May 2021
Let's Talk Science, Ottawa, ON

- Led several classrooms in various science-related activities.
- Acted as a mentor for new volunteers, guiding them through the planning and execution of activities.

PUBLICATIONS

1. El-Sahli, S.; Manturthi, S.; Durocher, E.; Bo, Y.; Akman, A.; Sannan, C.; **Kirkby, M.**; Iroakazi, C. D.; Deyell, H.; Kaczmarek, S.; Lee, S.-H.; Iqbal, U.; Côté, M.; Wang, L.; Gadde, S.; Riley, R.; Kashyap, M.; Billingsley, M.; Mitchell, M. J. Nanoparticle-Mediated mRNA Delivery to Triple-Negative Breast Cancer (TNBC) Patient-Derived Xenograft (PDX) Tumors. ACS Pharmacology & Translational Science. **2025**, 8 (2), 460–469.
2. Manturthi, S.; El-Sahli, S.; Bo, Y.; Durocher, E.; **Kirkby, M.**; Popatia, A.; Mediratta, K.; Daniel, R.; Lee, S.-H.; Iqbal, U.; Côté, M.; Wang, L.; Gadde, S. Nanoparticles Codelivering mRNA and SiRNA for Simultaneous Restoration and Silencing of Gene/Protein Expression In Vitro and In Vivo. ACS Nanoscience Au **2024**, *4* (6), 416–425
3. St-Denis-Bissonnette, F.; **Kirkby, M.**; Wang, L.; Lavoie, J. R. Scalable biomanufacturing workflow to produce and isolate natural killer cell-derived extracellular vesicle-based cancer biotherapeutics. Journal of Visualized Experiments **2024**.
4. St-Denis-Bissonnette, F.; Qiu, S.; Cummings, S. E.; **Kirkby, M.**; Haile, Y.; Wassmer, S.; Muradia, G.; Mehic, J.; Stalker, A.; Shrestha, A.; Ardolino, M.; Lee, S.; Burger, D.; Wang, L.; Lavoie, J. R. Evaluation of resazurin phenoxazine dye as a highly sensitive cell viability potency assay for natural killer cell-derived extracellular vesicle-based cancer biotherapeutics. Journal of Extracellular Biology **2024**, *3*.
5. Mediratta, K.; El-Sahli, S.; Marotel, M.; Awan, M. Z.; **Kirkby, M.**; Salkini, A.; Kurdieh, R.; Abdisalam, S.; Shrestha, A.; Di Censo, C.; Sulaiman, A.; McGarry, S.; Lavoie, J. R.; Liu, Z.; Lee, S.-H.; Li, X.; Sciumè, G.; D'Costa, V. M.; Ardolino, M.; Wang, L. Targeting CD73 with flavonoids inhibits cancer stem cells and increases lymphocyte infiltration in a triple-negative breast cancer mouse model. Frontiers in Immunology **2024**, *15*.
6. **Kirkby, M.**; Popatia, A. M.; Lavoie, J. R.; Wang, L. The potential of hormonal therapies for treatment of triple-negative breast cancer. Cancers **2023**, *15*, 4702.

CONFERENCES AND PRESENTATIONS

Oral Presentation

- M. Kirkby. (February 2025) "Gaining a Deeper Understanding of the Therapeutic Potential of Natural Killer Cell-Derived Extracellular Vesicles in Triple-Negative Breast Cancer and Cancer Stem Cell Populations" *Health Canada Science Forum*, Ottawa, ON.
- M. Kirkby. (February 2024) "Investigating Natural Killer Cell-Derived Extracellular Vesicles in a Clinically Relevant TNBC Model" *BMI Seminar Day*, Ottawa, ON.

Poster Presentation

- M. Kirkby, F. St-Denis-Bissonnette, M. Diab, S. Cummings, G. Maraudia, A. Stalker, M. Ardolino, S. H. Lee, D. Burger, L. Wang, J. R. Lavoie. (April 2025) "Gaining a Deeper Understanding of the Therapeutic Potential of Natural Killer Cell-Derived Extracellular Vesicles in Triple-Negative Breast Cancer and Cancer Stem Cell Populations" *38th Annual Canadian Society for Immunology Meeting*, Gatineau, QC.
- M. Kirkby, F. St-Denis-Bissonnette, M. Diab, S. Cummings, G. Maraudia, A. Stalker, M. Ardolino, S. H. Lee, D. Burger, L. Wang, J. R. Lavoie. (February 2025) "Gaining a Deeper Understanding of the Therapeutic Potential of Natural Killer Cell-Derived Extracellular Vesicles in Triple-Negative Breast Cancer and Cancer Stem Cell Populations" *BMI Poster Day*, Ottawa, ON.
- M. Kirkby, F. St-Denis-Bissonnette, M. Diab, S. Cummings, G. Maraudia, A. Stalker, M. Ardolino, S. H. Lee, D. Burger, L. Wang, J. R. Lavoie. (February 2025) "Gaining a Deeper Understanding of the Therapeutic Potential of Natural Killer Cell-Derived Extracellular Vesicles in Triple-Negative Breast Cancer and Cancer Stem Cell Populations" *Health Canada Science Forum*, Ottawa, ON.

HONOURS AND AWARDS

- Judith E. Raymond Scholarship in Cancer Research, 2025 $5,000
- HCSF Best Student Poster Award – Honourable Mention, 2025
- Ontario Graduate Scholarship – Master's Program, 2024 $15,000
- BMI Seminar Day Top Presenters, 2024 $25
- Canada Graduate Scholarship – Master's Program, 2023 $17,500
- Special Merit Scholarship, 2023 $4,000
- NSERC - Undergraduate Student Research Award, 2023 $7,700
- Merit Scholarship, University of Ottawa, 2020-2023 6 × $1,000
- NSERC - Undergraduate Student Research Award, 2022 $7,600
- University of Ottawa Admission Scholarship, 2019 $3,000

Appendix C: The Potential of Hormonal Therapies for Treatment of Triple-Negative Breast Cancer

Preface: The review article "The Potential of Hormonal Therapies for Treatment of Triple-Negative Breast Cancer" was originally published Open Access in the Cancers journal in 2023 [16].

Citation: Kirkby, M.; Popatia, A. M.; Lavoie, J. R.; Wang, L. The Potential of Hormonal Therapies for Treatment of Triple-Negative Breast Cancer. *Cancers* **2023**, *15* (19), 4702. DOI: 10.3390/cancers15194702.

Author Contributions: Conceptualization: MK and LW; writing—original draft preparation: MK and AMP.; writing—review and editing: MK, AMP, JRL. and LW. All authors have read and agreed to the published version of the manuscript.

Abstract

Triple-negative breast cancer (TNBC) is considered one of the most aggressive forms of breast cancer with poor survival rates compared to other breast cancer subtypes. TNBC is characterized by the absence of the estrogen receptor alpha, progesterone receptor, and the human epidermal growth factor receptor 2, limiting those viable treatment options available to patients with other breast cancer subtypes. Furthermore, due to the particularly high heterogeneity of TNBC, conventional treatments such as chemotherapy are not universally effective, leading to drug resistance and intolerable side effects. Thus, there is a pressing need to discover new therapies beneficial to TNBC patients. This review highlights current findings regarding the roles of three steroid hormone receptors, estrogen receptor beta, the androgen receptor, and the glucocorticoid

receptor, in the progression of TNBC. In addition, we discussed several ongoing and completed clinical trials targeting these hormone receptors in TNBC patients.

1. Introduction

Breast cancer is one of the most lethal and complex diseases that have resulted in the deaths of millions worldwide [1]. Approximately 15% of all breast cancer cases are classified as triple-negative breast cancer (TNBC) which, relative to the other subtypes, has the most aggressive phenotype, the worst overall survival (OS), and a higher occurrence of metastases at the time of diagnosis [2,3]. TNBC is classically defined by a lack of the hormone receptor estrogen receptor alpha (ERα) and the progesterone receptors (PRs) and by an absence of human epidermal growth factor receptor 2 (HER2) [4] (**Figure 1**). As a result, TNBC tumors are not susceptible to the targeted therapies that have been developed for other breast cancer subtypes and TNBC patients most commonly rely on chemotherapy for treatment.

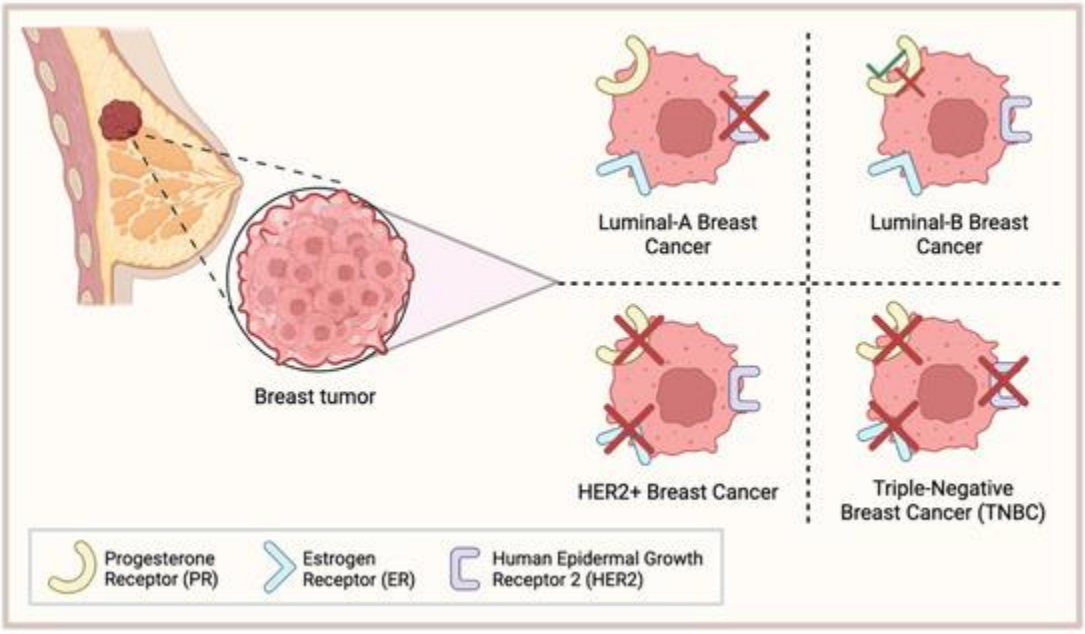

Figure 1. Classification of common breast cancers.
Luminal-A breast cancer lacks expression of HER2; Luminal-B breast cancer is either PR+/−; HER2+ breast cancer lacks PR and ER expression; triple-negative breast cancer (TNBC) lacks expression of PR, ER, and HER2. This figure was made using Biorender.com.

TNBC is considered a fairly heterogenous disease, where four distinct TNBC subtypes have been identified based on their unique gene expression profiles: basal-like 1 (BL1), basal-like 2 (BL2), mesenchymal (M), and luminal androgen receptor (LAR) [5,6]. Each subtype is associated with a unique clinical profile and a differing response to adjuvant and neoadjuvant chemotherapy. Particularly, the BL1 classification was associated with a greater response to chemotherapy and a longer relapse-free survival period [6]. Conversely, the BL2 and LAR phenotypes were more resistant to neoadjuvant chemotherapy and only 18% and 29% of patients achieved a pathological complete response, respectively [6,7]. Thus, in part due to the heterogeneity of this disease, there is a lack of viable treatment options universally available for TNBC patients. This is reflected by TNBC's poor prognosis, where the five-year survival rate for patients with metastatic TNBC is only around 10% [2]. Additionally, approximately 40% of stage I–III TNBC patients will experience relapse following treatment, with the greatest risk present during the first three years post-therapy [3,8]. Thus, there is a critical need to develop novel therapies against this disease.

The aim of this review is to highlight three possible hormone receptors that could be used clinically for TNBC patients. Specifically, we discuss the current research surrounding the role of estrogen receptor beta (ERβ), the androgen receptor (AR), and the glucocorticoid receptor (GR) in the progression of TNBC, as well as their implications on survival and treatment. We also highlight several clinical trials targeting these hormone receptors in TNBC patients and the major outcomes from these studies.

2. Estrogen Receptor Beta

TNBC is commonly characterized by an absence of ERα. Despite this, approximately 5–10% of ERα-negative breast cancer tumors responded positively to treatment with anti-ERα drug tamoxifen [9,10], indicating the possibility of alternative ERα-independent signaling pathways. Growing research has associated the presence of ERβ with the outcome of various TNBC patients. Similar to ERα, ERβ is a steroid hormone receptor that binds various estrogenic compounds, including estradiol-β-17 (E2), to regulate the transcription of its downstream gene targets [11]. Independently of ERα, ERβ is encoded by the gene *ESR2* and can be spliced into five distinct isoforms, ERβ1-5; however, only the full-length variant ERβ1 is functionally capable of binding estrogenic compounds [11,12]. Although ERα and ERβ share a similar genetic identity and are composed of the same five domains, they diverge most significantly in their N-terminal region(18%), which harbor the activation function 1 (AF-1) domain, and C-terminal (18%) region (**Figure 2**), resulting in ER-specific gene regulation [13]. ERβ's classical mechanism of action is functionally similar to that of ERα. In its unbound state, ERβ is bound to the chaperone protein heat shock protein 90 (HSP90) [14]. The binding of its estrogenic compound leads to dimerization of the receptor, dissociation of HSP90, and subsequent translocation to the nucleus. There, ERβ can regulate gene transcription through interactions with the estrogen response elements. ERβ is widely expressed in normal breast epithelial cells and is present in other tissue including the prostate, ovaries, and brain [15,16,17].

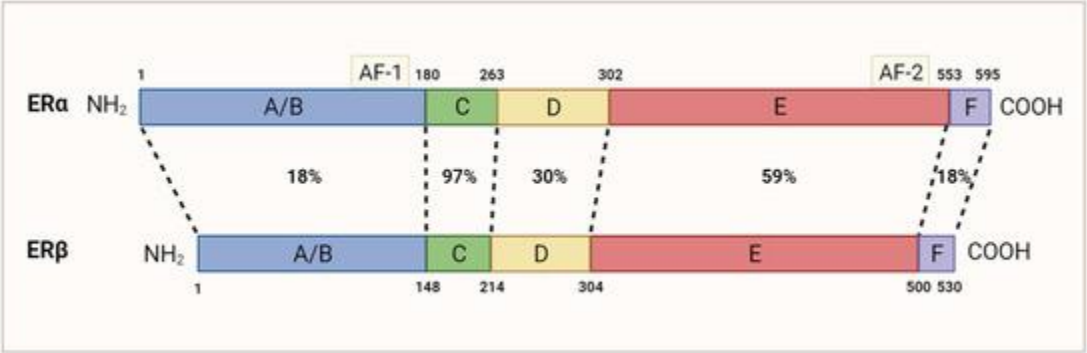

Figure 2. Homology between ERα and ERβ's amino acid sequence. Dotted lines are used to compare domains with the same function.
The N-terminal domain (A/B) containing AF-1 is 18% homologous. The DNA-binding domain (C) is 97% homologous. The hinge domain (D) is 30% homologous. The ligand-binding domain (E), which contains the AF-2 domain, is 59% homologous. The carboxyl-terminal domain (F) is 18% homologous. Adapted from [13]; originally published under Creative Commons Attribution 3.0 Unported (CC BY 3.0) license. Available from: 10.5772/21807. This figure was made using Biorender.com.

3. Estrogen Receptor Beta in the Progression of TNBC

Previously, there has been controversy regarding ERβ's existence within diseased breast tissue. Specifically, previous reports investigating ERβ in breast cancer have used non-specific anti-ERβ antibodies, likely producing a false positive result in regard to ERβ expression [18,19,20]. Since then, several studies using validated anti-ERβ antibodies have generated different results. One study validating the use of antibody PPZ0506 for ERβ detection was unable to detect any transcriptional activity in both normal and diseased breast tissue [20]. In contrast, another study using both antibodies PPZ0506 and PPG5/10 and an optimized immunohistochemistry-based assay demonstrated that approximately 20–30% of all breast carcinomas tested positive for ERβ expression [17]. In TNBC patients specifically, the percentage of ERβ-positive tumors ranged between 25 and 83%; however, the majority of these studies used non-specific antibodies to reach these conclusions [21,22,23,24]. A recent study using the validated CWK-F12 ERβ1 antibody found that 72% of TNBC tumor samples expressed ERβ1,

aligning well with studies using non-specific antibodies; however, its expression was not associated with any TNBC subtype (BL1, BL2, M, or LAR) in particular [25]. Overall, the current findings support the idea that ERβ is expressed in a significant proportion of TNBC tumors; however, further research using validated ERβ antibodies is needed.

The expression of ERβ on TNBC tumors could have several clinical implications. Interestingly, ERβ expression does not depend on the presence or absence of the classical breast cancer markers, indicating that ERβ signaling can function independently of ERα [21,26]. Although several studies have attempted to elucidate Erβ's role in the progression of TNBC, a clear understanding has not been reached. In TNBC cell lines with inducible ERβ1 expression, cellular growth was halted through inhibition of the G1/S cell cycle transition, and this phenomenon was enhanced by the addition of E2 [27]. Furthermore, a knockdown of ERβ at the transcriptional level increased the expression of several pro-tumorigenic genes, including transforming growth factor beta (TGFβ) 1/2 [28].

In direct contrast, a growing number of studies have demonstrated that, under certain conditions, ERβ can instead promote tumor growth in TNBC. As an example, one study demonstrated that ERβ expression in ERα-negative cell lines resulted in increased insulin growth factor (IGF) 2 (IGF2) secretion, upregulation of MAPK/PI3K signaling, and was associated with a decrease in relapse-free survival [29]. The observed discrepancy could be attributed to the differential regulation imposed by ERβ isoforms beyond ERβ1. ERβ2 and ERβ5 were the predominant ERβ isoforms found in human TNBC tumors and cell lines, and an upregulation of either resulted in enhanced cell migration and invasion [30]. Conversely, overexpression of ERβ1 was associated with a suppression of tumor growth and survival. Furthermore, there is a lack of standardization in detection methods, tissue preparation, and antibody selection, as well as minimal

information regarding ERβ's role in each TNBC subtype [29]. Each of these factors could contribute to the conflicting results published so far. Thus, further clarification is needed to fully elucidate the functions of each ERβ isoform in the context of TNBC.

Several researchers have proposed that ERβ's functioning may also depend on other signaling pathways, particularly mutations in tumor suppressor *P53*. Around 80% of all TNBC patients harbor a mutation in the *P53* gene, often resulting in a gain in oncogenic functioning [31]. Mutant p53 can form a complex with p63 and p73, inhibiting their activity and promoting cancer cell metastasis [32,33]. When ERβ is present in vitro, it can interact with mutant p53 to disrupt the complex with either p63 or p73, inhibiting tumor growth [34,35]. ERβ's interaction results in a reconfiguration of mutant p53′s structure, returning its structure to the wildtype form and preventing its oncogenic functioning. In patients with wildtype p53, ERβ alters p53′s transcriptional regulation, resulting in a pro-proliferative phenotype [35]. Similar trends were observed in TNBC patients' OS, where patients expressing mutant p53 and high levels of ERβ had the best outcome. Of note, the sequestration of patient phenotypes may also allow clinicians to predict the benefit of tamoxifen use in TNBC patients. Patients expressing high levels of ERβ and mutant p53 showed an increased responsiveness to tamoxifen treatment while those with wildtype p53 received little to no benefit at all. Thus, ERβ and mutant p53 could serve as useful biomarkers to predict tamoxifen's effectiveness in TNBC patients.

4. Clinical Data regarding Estrogen Receptor Beta in TNBC

Because ERβ is believed to impact the progression of some TNBC tumors, growing research has looked at targeting the receptor in a clinical setting. This section describes the current

clinical data available for targeting ERβ and what results have been obtained thus far. Table 1 summarizes the major findings from clinical trials targeting ERβ.

Table 1. Ongoing or completed clinical trials targeting estrogen receptor beta in TNBC.

Trial (National Clinical Trial Identifier)	Phase		Condition	Interventions	Key Results	References
Tamoxifen			ERβ+/p53-mutant TNBC patient with brain metastases	Tamoxifen	Reduction in tumor volume in the brain metastases; currently, no signs of disease progression.	[36]
Tamoxifen (NCT02062489)	III	(1) (2)	ERα/PR-negative ERβ+ operable breast cancer patients	Adjuvant Tamoxifen	**No preliminary data available.** Study to be completed by May 2026.	[37]
Toremifene (NCT02089854)	IV	(1)	Patients with operable ERβ+ TNBC tumors	Toremifene + Anastrozole	**No preliminary data available.**	[38]
17β-Estradiol (E2)	II	(1)	Metastatic TNBC	E2	**Partial response**: 1/13 patients (Erβ expressing); little effect on **OS** and **PFS;** grade 3–4 **AE** in 4/17 patients; 2 cases of grade 3 dyspnea; 1 case of grade 3 vomiting; 1 case of grade 4 thromboembolism.	[39]
17β-Estradiol (E2) (NCT03941730)	II	(1)	Metastatic TNBC patients overexpressing Erβ	E2	**No preliminary data available.** Study to be completed by April 2024.	[40]

PFS: progression-free survival; OS: median overall survival; AE: adverse events.

4.1. Selective Estrogen Receptor Modulators

Although not traditionally used for ERα-negative tumors, preclinical and clinical research has shown that ERβ can influence the effectiveness of tamoxifen in a small percentage of TNBC patients. In a 2023 case study, the use of tamoxifen in an ERβ-positive / p53-mutant TNBC patient who had experienced brain metastases was evaluated [36]. Treatment with tamoxifen led to a

significant reduction in tumor volume of the brain metastases. This observation was predominantly a result of tamoxifen's ability to increase ERβ's interaction with mutant p53 in the cancerous cells, providing support for the clinical benefit of targeting ERβ in patients. As of today, the patient has shown no signs of disease progression. Although a larger number of patients is needed to validate this finding, this case study was the first to evaluate the status of p53 and ERβ for TNBC treatment. An ongoing phase III clinical trial (NCT02062489) is currently evaluating the effectiveness of adjuvant tamoxifen therapy in ERα/PR-negative, ERβ-positive operable breast cancer patients [37]. The primary objective of this trial is to evaluate tamoxifen's effect on OS and disease-free survival (DFS) in tumors highly expressing ERβ and to determine if Erβ is positivity correlated with a response to estrogen therapy. Results for this study are expected in May 2026.

Toremifene is another FDA-approved nonsteroidal selective estrogen receptor modulator that has demonstrated a similar efficacy and safety profile to tamoxifen [41]. A phase IV clinical trial (NCT02089854) evaluating the use of adjuvant endocrine therapy (toremifene and anastrozole, a nonsteroidal aromatase inhibitor) in patients with operable ERβ-positive TNBC tumors is underway [38]. The effect of this endocrine therapy on DFS and OS will be evaluated to determine its effectiveness relative to the control group (i.e., no adjuvant endocrine therapy). Results for this trial have not been published yet.

4.2. 17β-Estradiol

E2 is the ligand for both ERα and ERβ. As previously mentioned, in TNBC cell lines with inducible expression of ERβ, treatment with E2 promoted G1 cell cycle arrest and tumor regression [27], suggesting that E2 could have clinical potential in treating TNBC. In a phase II clinical trial, the use of high-dose oral E2 was evaluated in 17 patients with metastatic TNBC, regardless of

their ERβ status [39]. Among the 13 patients who expressed high levels of ERβ, only 1 patient demonstrated a partial response to E2 treatment, and treatment was shown to have little effect on OS and progression-free survival (PFS). E2 treatment was generally well tolerated by the patients. Grade 3/4 adverse events (AE) were observed in 4 of the 17 patients evaluated with two cases of grade 3 dyspnea, one case of grade 3 vomiting, and one case of grade 4 thromboembolism reported. Although the trial concluded with minimal effectiveness, the authors do not rule out the use of ERβ entirely. Improved detection of ERβ and the use of alternative ERβ agonists could result in increased clinical benefit for a subset of TNBC patients.

An ongoing phase II clinical trial by Mayo Clinic (NCT03941730) is evaluating the effectiveness of E2 in metastatic TNBC patients overexpressing ERβ [40]. No results have been posted as of this date, and completion of this study is expected in April 2024.

5. Androgen Receptor

One of the most commonly overexpressed steroid nuclear receptors in breast cancer patients is the androgen receptor (AR), with a 70% occurrence leading to increased pathogenesis [42]. This receptor is a single polypeptide that is expressed in 10–43% of TNBC subtypes [43]. The AR has different domains in its structure that allow it to carry out its functions (**Figure 2**). The first domain is the N-terminal region which contains androgen-independent AF-1. The DNA-binding domain (DBD) interacts with incoming androgen signaling components while the hinge domain connects the DBD with the ligand-binding domain (LBD) [44]. Lastly, the C-terminal LBD binds to androgen and anti-androgen ligands contained in the C-terminus with the androgen-dependent activation function 2 domain (**Figure 3**).

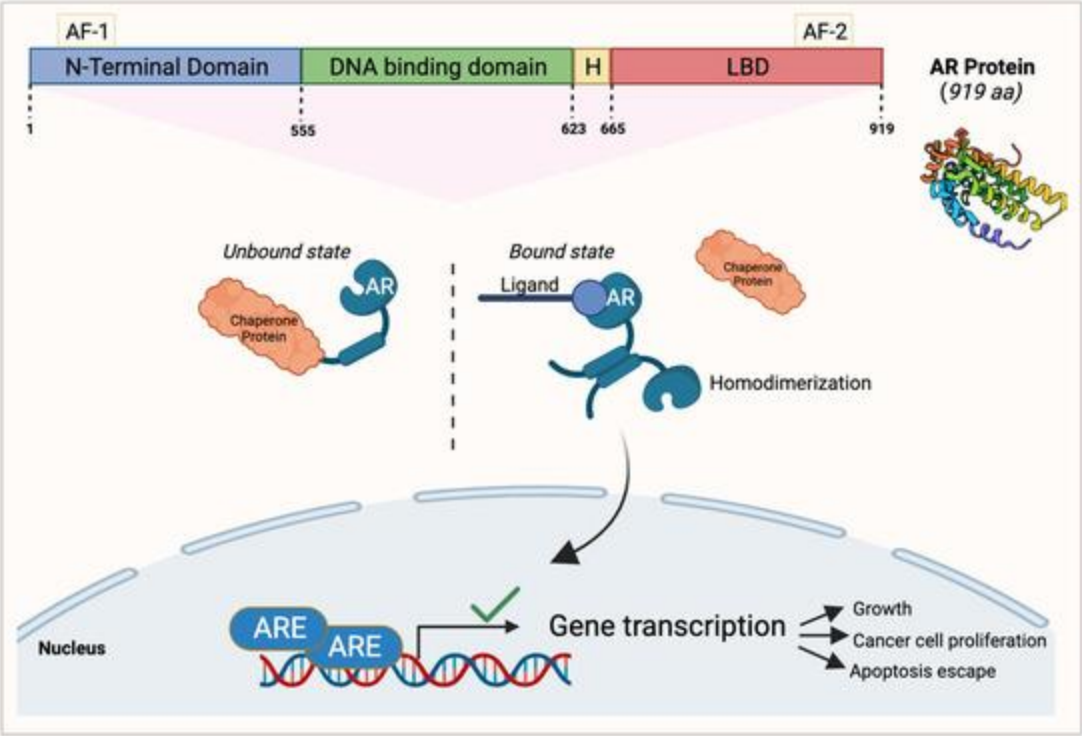

Figure 3. An overview of the androgen receptor (AR) protein structure and its signaling pathway in cancerous cells.
AR's N-terminal region contains androgen-independent activation function 1 (AF-1), followed by the DNA-binding domain, the hinge domain (H), and the ligand-binding domain (LBD) contained in the C-terminus with the AF-2 domain. In AR's unbound state, it interacts with a chaperone protein. When a ligand of interest such as androgen binds to AR, it dissociates from the chaperone protein and homodimerizes. It then translocates to the nucleus to activate gene transcription that enables cell growth, cancer cell proliferation, and apoptosis escape. This figure was made using Biorender.com.

The AR has the capacity to bind to different ligands, such as growth factors including IGF and TGFβ, or endogenous androgens [45,46]; however, when it is unbound, it will interact with chaperone proteins [42]. Once AR binds to a ligand of interest, it will dissociate from the chaperone protein and will reconfigure into a homodimer that induces target gene transcription by translocating into the nucleus and activating a series of signaling events that lead to apoptosis escape and cancer cell proliferation [42,47,48] (Figure 2). AR signaling is important for the

functioning of several organs in the human body including the cardiovascular system, musculoskeletal system, prostate, and the nervous system [49].

6. The Role of the Androgen Receptor in TNBC

The most consistently identified subtype of TNBC that is characterized by AR mRNA and its target genes' expression is the LAR subtype [5,43,50]. LAR TNBCs show increased resistance to both neoadjuvant and adjuvant chemotherapy and demonstrate a poor pathological complete response [7,43,51]. Although AR signaling has been implicated in AR-positive TNBC, its involvement in disease progression is not completely understood. When the LAR subtype was identified, the targeting of AR in LAR cells decreased cell proliferation [5]. TNBC cells expressing high levels of AR increased expression of genes associated with cell cycle progression when compared to AR-negative cell lines [52]. Interestingly, across all the breast cancer subtypes, AR was present on both the primary and metastatic breast carcinomas, with some metastatic tumors showing elevated AR levels [53]. In vitro analysis of TNBC cell lines demonstrated that an upregulation of AR promoted anchorage-independent survival [54], suggesting that AR expression may be essential for successful metastasis to occur. Mechanistically, the presence of androgen can trigger the formation of a complex between AR, Src, FAK, and PI3K to modulate focal adhesion and promote cellular invasion [55]. Additionally, AR was also shown to promote cancer stem cell growth, and treatment with the antiandrogen enzalutamide decreased the formation of mammospheres in vitro and reduced tumor growth in vivo [54]. Because cancer stem cells are capable of initiating tumor growth, the targeting of AR alongside chemotherapy may be a viable method for preventing recurrent disease.

Current studies investigating AR's role as a prognostic marker in breast cancer have yielded controversial results. Several studies analyzing AR-positive and AR-negative TNBC tumors indicate that the expression of AR is associated with an increased OS and DFS [56,57,58]. However, as described above, this is in direct contrast with most experimental results obtained so far. Furthermore, a small number of studies report that AR expression is associated with an increased rate of metastasis [59,60], while others have stated that it has no effect upon OS in TNBC [61,62]. Possible explanations for this discrepancy can include several factors such as the demographic and TNBC subtypes being analyzed, as well as the effect of different AR mutations upon patient outcome [43]. A lack of standardization among the methodologies and AR cut-off percentages used could also contribute to the conflicting results [63]. Despite this, targeting AR is still a viable option as, similar to ERα-positive tumors, AR-positive tumors are dependent on AR function [54]. Therefore, therapies targeting AR are an area of great interest, particularly for the LAR TNBC subtype.

7. Clinical Trials Targeting the Androgen Receptor in TNBC

Because AR has been heavily implicated in the progression of AR-positive LAR and non-LAR TNBC subtypes, several researchers are now looking to target AR as a novel therapeutic avenue for TNBC patients. In this section, the results of several ongoing and recent clinical trials targeting AR are described. The results from these clinical trials are summarized in Table 2.

Table 2. Ongoing or completed clinical trials targeting the androgen receptor in TNBC.

Trial (National Clinical Trial Identifier)	Phase		Condition	Interventions	Key Results	References
Enzalutamide (NCT01889238)	II	(1) (2)	Locally advanced or metastatic AR+ TNBC Intent-to-treat (ITT)—all patients AR expression ≥10%	Enzalutamide	**PFS**: (1) 2.9 months, (2) 3.3 months; **OS:** (1) 12.7 months, (2) 17.6 months; Fatigue (≥2%). Study to be completed by December 2023.	[64]
Enzalutamide (NCT02750358)	II	(1)	Stage I–III AR+ TNBC	Adjuvant Enzalutamide	**DFS:** 1-year: 94%; 2-year: 92%; 3-year: 80%; **Grade 3 or higher AEs related to treatment**: fatigue (6%), hypertension (2%). Study to be completed by May 2024.	[65]
Enobosarm (NCT02971761)	II	(1)	AR+ metastatic TNBC patients	Enobosarm + Pembrolizumab	**Complete response**: 1/16; **Partial response:** 1/16; Stable disease: 2/16; **Response rate** to combination treatment: 13%; **CBR**: 25% after 16 weeks; Grade 3 related AEs—pain (6%), dry skin (6%), diarrhea (6%).	[66]
Bicalutamide (NCT00468715)	II	(1)	ER–/PR– metastatic breast cancer patients highly expressing AR	Bicalutamide	**AR+ expression** (≥10%): 12%; 6-month **CBR**: 19%; **PFS:** 12-week median; Grade 3 AEs related elevated liver enzyme levels in one patient with liver metastases; Grade 3 nausea in 1/28 patients.	[67]
Bicalutamide (NCT02605486)	II	(1)	AR+ metastatic TNBC	Bicalutamide + Palbociclib	At 6-month mark: 35% **progression-free**; 32% **stable disease.** Study to be completed by November 2024.	[68]
Bicalutamide (NCT03090165)	I/II	(1)	Advanced AR+ TNBC patients	Bicalutamide + Ribociclib	**No preliminary data available.** Study to be completed by September 2024.	[69]

Seviteronel	I	(1) (2)	Women with ER+ breast cancer or TNBC 14/19: ER+ 5/19: TNBC	Seviteronel	AEs reported in only 4 patients; 7 women given 450 mg dose of seviteronel, 4/7 patients reached 16-week **CBR**, 2 of these patients diagnosed with TNBC. **Phase II trial** will expand cohort to include men and women with either ER+ or TNBC.	[70]

PFS: progression-free survival; DFS: disease-free survival; OS: median overall survival; CBR: clinical benefit rate; AEs: adverse events.

7.1. Enzalutamide

Enzalutamide is a second-generation antiandrogen that has been FDA-approved for the treatment of metastatic castration-resistant prostate cancer [71]. Enzalutamide works by binding to the ligand-binding domain of AR, inhibiting the binding of androgen ligands to its receptor. As a result, nuclear translocation and chromosomal DNA interactions are prevented, blocking the transcription of target genes and oncogenic processes. A phase II clinical trial (NCT01889238) tested enzalutamide on patients 18 years or older that had locally advanced or metastatic AR-positive TNBC [64]. Patients that had prior treatments for advanced TNBC were eligible for the study; however, patients that had central nervous system metastases, cardiovascular diseases, or a history of seizures were excluded from this study. The patients were divided into two groups: the evaluable subgroup whose AR expression level was ≥10% and the intent-to-treat (ITT) subgroup which included all the patients involved. The results revealed that the PFS was 2.9 months in the ITT subgroup compared to 3.3 months in the evaluable subgroup. Additionally, the median OS was 12.7 months in the ITT subgroup compared to 17.6 months in the evaluable subgroup. Enzalutamide was well tolerated by most participants in this study. Fatigue was the only grade 3

or greater AE related to treatment, occurring in ≥2% of patients, with all other serious AEs being attributed to disease progression. This study is expected to be completed by December 2023.

Another phase II clinical study (NCT02750358) evaluated adjuvant enzalutamide treatment in patients with stage I–III AR-positive TNBC who had completed their standard-of-care treatment [65]. A total of 50 patients were initially enrolled in the study; however, only 35 patients completed at least one year of enzalutamide treatment to meet the trial's endpoint for feasibility. Of the evaluated patients, the 1-year DFS, 2-year DFS, and 3-year DFS were 94%, 92%, and 80%, respectively. Enzalutamide was well tolerated in these patients and demonstrated low toxicity. The only grade 3 or higher AEs reported were fatigue (6%) and hypertension (2%). This study's expected completion date is May 2024.

7.2. Enobosarm

Enobosarm is a non-steroidal selective androgen receptor modulator that, in AR-positive TNBC tumors, showed an ability to inhibit tumor growth [72]. In a phase II clinical trial (NCT02971761), a combination of enobosarm and pembrolizumab, an anti-PD-1 immunotherapy, was tested on AR-positive metastatic TNBC patients [66]. A total of 18 patients were initially enrolled in the trial and only 16 patients were evaluated for efficacy. This combinational therapy returned some clinical benefit, with 1 of 16 patients achieving a complete response, 1 of 16 patients receiving a partial response, and 2 of 16 patients with stable disease. Additionally, the response rate for this combination treatment was 13% and the clinical benefit rate (CBR) was 25% after 16 weeks. Enobosarm and pembrolizumab treatment was generally well tolerated, with the only grade 3 AEs reported being pain (6%), dry skin (6%), and diarrhea (6%).

7.3. Bicalutamide

Bicalutamide is a first-generation non-steroidal AR antagonist that is currently FDA-approved for the treatment of prostate cancer [73]. Bicalutamide binds AR through competitive inhibition, preventing its translocation to the nucleus and any further signaling. A phase II trial (NCT00468715) investigated bicalutamide's efficacy and safety in ER-/PR-negative metastatic breast cancer patients that were highly expressing AR [67]. A total of 51 of the 424 (12%) screened patients tested positive for AR expression (≥10%), and 26 patients were evaluable for the study's primary endpoint. In the evaluated patients, a 6-month CBR of 19% and a 12-week median PFS were achieved. Bicalutamide showed low levels of toxicity and no grade 4/5 AEs were reported. Grade 3 AEs related to elevated liver enzyme levels (aspartate aminotransferase, bilirubin, and alkaline phosphatase) were reported in one patient who had liver metastases, so it is unclear whether the events could be attributed to disease progression or to treatment. Otherwise, 1 of the 28 patients evaluated for safety reported grade 3 nausea.

Some researchers have begun exploring bicalutamide's effectiveness in combination with other therapeutics for treating AR-positive TNBC patients. Particularly, the cyclin-dependent kinase (CDK)4/6-retinoblastoma pathway has been implicated in the progression of breast cancer, and some TNBC cell lines have demonstrated sensitivity to the use of CDK4/6 inhibitors [74]. An ongoing phase II clinical trial (NCT02605486) investigating bicalutamide in combination with CDK4/6 inhibitor palbociclib in AR-positive metastatic TNBC has demonstrated potential clinical benefit [68]. A total of 31 of the 33 enrolled patients were evaluated for the study's endpoints. At the six-month mark, 11 of 31 patients were progression-free, and 10 of 31 patients had stable disease. The bicalutamide and palbociclib combination was fairly well tolerated by patients. The expected study completion date for this trial is November 2024. Another phase I/II clinical trial

(NCT03090165) is investigating the use of bicalutamide in combination with the CDK4/6 inhibitor ribociclib in advanced AR-positive TNBC patients [69]. From the phase I clinical data, this combinational therapy has been well tolerated by patients and no unexpected toxicities have been reported. The study's expected completion date is September 2024.

7.4. Seviteronel

Seviteronel possesses the ability to inhibit both AR and cytochrome P450 17α-hydroxylase/17,20-lyase (CYP17 lyase), the enzyme required for androgen production [75]. Additionally, seviteronel promoted the radiosensensitization of TNBC cell lines and decreased tumor volume when used in conjunction with radiation. An open-label phase I clinical study aimed to determine the appropriate dosage of seviteronel in women with ERα-positive breast cancer or TNBC, as well as its safety [70]. A total of 19 women were evaluated in this study, where 14 of the patients were classified as ER-positive while the other 5 were classified as TNBC. AR status was not considered at this time. Seviteronel was generally well tolerated by patients, with grade 3 or higher AEs being reported in only four subjects. Additionally, in the seven women given a 450 mg dose of seviteronel, the recommended phase 2 dose, four of the patients reached the 16-week CBR, with two of these patients being diagnosed with TNBC. Phase II of this clinical trial will expand the cohort to include men and women with either ER-positive breast cancer or TNBC.

8. Glucocorticoid Receptor

GR is a nuclear hormone receptor that is ubiquitously expressed and activated upon the binding of its respective ligand, glucocorticoid. Glucocorticoids are steroid hormones that are released by the adrenal glands and play significant and broad roles in metabolism, anti-

inflammation, immune responses, and fetal development [76]. The GR structure is composed of a disordered amino-terminal domain (NTD), a DBD, and an LBD [77]. In its unbound state, GR resides in the cytoplasm, protected in a chaperone complex during its folding stages. However, once the glucocorticoid ligand binds to GR's LBD, GR becomes activated and translocates to the nucleus where its DBD domain participates in specific DNA binding. Consequently, GR will then recruit various transcription factors that will further activate or repress target gene expression (Figure 4).

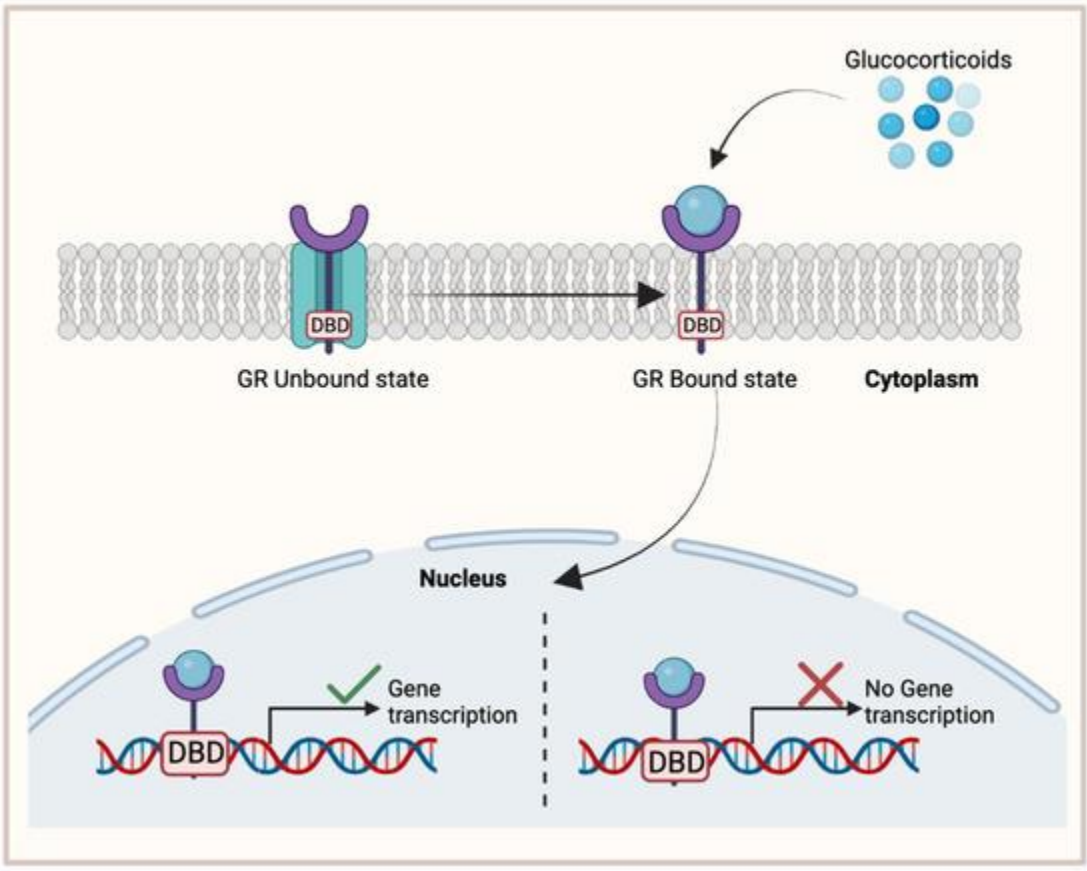

Figure 4. Glucocorticoid receptor (GR) binding mechanism, activating target gene expression.
In its unbound state, GR is located in the cytoplasm with a chaperone complex. Once bound to its ligand, glucocorticoid, GR translocates to the nucleus where its DNA-binding domain (DBD) will activate or inhibit target gene expression. This figure was made using Biorender.com.

9. Glucocorticoid Receptor in TNBC

The expression levels of GR on TNBC cells vary considerably in different studies, ranging from 0% to 84% [78,79,80,81,82]. This discrepancy can be largely attributed to the lack of standardization among antibodies and methods used to detect GR on cells. Generally, the presence of GR on TNBC cells is associated with a poor patient prognosis and a worse OS [78,79]. This is in direct contrast with ERα-positive patients where the presence of GR corresponds to a better prognosis [83], suggesting that regulation of GR through ERα can heavily impact whether GR imparts a proliferative or antiproliferative functioning. TNBC patients with high GR expression are typically more resistant to chemotherapy-induced apoptosis, a phenomenon that is likely mediated through the GR-mediated upregulation of several pro-survival genes, including *MPK-1* and *SGK-1* [83,84]. In basal-like TNBC, GR and STAT3 bind the same regulatory region, cooperatively promoting the expression of hundreds of basal-like genes that are associated with cell proliferation, stemness, and the epithelial–mesenchymal transition (EMT) [85].

GR signaling in TNBC cells depends heavily upon its external environment. An abundance of TGFβ1 or cellular stress in the tumor microenvironment activates p39 MAPK signaling, resulting in ligand-independent but p38-dependent GR phosphorylation at Ser134 (pS134-GR), ultimately promoting TNBC invasion and anchorage-independent growth [86]. Additionally, pS134-GR promotes the expression of MAP_3K_5, an activator of p38 MAPK signaling, suggesting that GR participates in a feedforward loop in response to stressors present in the environment. Additionally, pS134-GR regulates several genes involved in metabolic reprogramming to favor cell migration [78], demonstrating GR's essential role in metastasis.

Interestingly, GR signaling could possibly have a bi-faceted role in chemotherapy response. High GR expression in TNBC patients was associated with an increased responsiveness to

anthracycline-based chemotherapy; however, it demonstrated a poor response to taxane-based therapy [87]. In ERα-negative patients who were given glucocorticoid alongside their anthracycline treatment, OS was improved, while ERα-negative patients treated with glucocorticoid alone showed a worse OS [88]. The mechanism of action behind GR's interactions with anthracycline and taxane is not well understood; however, this observation allows for the potential use of GR as a biomarker for the outcome of different chemotherapies in TNBC.

10. The Clinical Use of RU486 (Mifepristone) in GR-Positive TNBC

RU486, otherwise known as mifepristone, is an antiprogesterone and anti-glucocorticosteroid agent that has a high affinity for PR and GR [89]. RU486 is capable of binding either receptor, maintaining them in an unfavorable conformation to inhibit any downstream signaling. RU486 is predominantly used to terminate pregnancy during the early developmental stages; however, preclinical data obtained in breast cancer cell lines and TNBC mice models suggest that it could function as a hormonal therapy as well [90,91,92,93]. Table 3 summarizes the results of clinical trials testing mifepristone in TNBC.

Table 3. Ongoing or completed clinical trials targeting the glucocorticoid receptor in TNBC.

Trial (National Clinical Trial Identifier)	Phase	Condition	Interventions	Key Results	References
Mifepristone RU486 + Nab-paclitaxel (NCT01493310)	I (1)	Advanced GR+ breast cancer patients TNBC + patients	RU486 + nab-paclitaxel	**Complete response:** 2/6; **Partial response:** 2/6; **Stable disease:** 1/6; **Progressive disease:** 1/6; Some patients experienced neutropenia.	[94]
Mifepristone RU486 + Nab-paclitaxel vs.	II (1)	Advanced GR+ TNBC	Nab-paclitaxel + Placebo	**OS (2):** 9 months; **OS (1):** 6 months; **PFS:** not significantly improved by	[95]

Placebo (NCT02788981)		(2)	13/29: Nab-paclitaxel + placebo 16/29: Nab-paclitaxel + RU486	Nab-paclitaxel + RU486	addition of RU486; **Grade 3 AE:** Neutropenia. Study to be completed by August 2024.	
Mifepristone RU486 + Eribulin (NCT02014337)	I/II	(1)	Patients with operable GR+ TNBC	RU486 + Eribulin	**Phase I:** 16 patients with meta-static breast cancer; **Phase II:** 21 patients with TNBC; **Phase II dose combinational treatment partial response:** 3/23; **Stable disease:** 8/23; **Progressive disease:** 11/23; **Inconclusive:** 1/23; **Median PFS:** 9 weeks; **Grade 3/4 AEs:** neutropenia, neuropathy, fatigue, hypokalemia, nausea.	[96]

PFS: progression-free survival; OS: median overall survival; AEs: adverse events.

A randomized phase I clinical trial (NCT01493310) completed in 2018 was designed to determine the pharmacokinetics and toxicity of chemotherapy agent nab-paclitaxel (Abraxane, an albumin-bound nanoparticle formulation of paclitaxel) when used in combination with mifepristone in advanced GR-positive breast cancer patients [94]. A total of nine patients were enrolled in the trial, where six were diagnosed with TNBC. Of the six TNBC patients, two of them had a complete response, two had a partial response, one had stable disease, and one had progressive disease. Pharmacokinetic studies revealed that administration of mifepristone successfully delayed nab-paclitaxel clearance in a number of patients. Combinational treatment had manageable levels of toxicity, with some patients experiencing neutropenia as a result of this therapy.

A phase II, randomized, placebo-controlled clinical trial (NCT02788981) is investigating the use of nab-paclitaxel with or without mifepristone in patients with advanced GR-positive TNBC [95]. Of the 29 patients enrolled in the trial, 13 received nab-paclitaxel and a placebo, while the other 16 patients received the nab-paclitaxel and mifepristone combination. OS in the combination group was 9 months, while nab-paclitaxel alone was 6 months, though PFS was not significantly improved by the addition of mifepristone. The combinational treatment was generally well tolerated by patients, with the most reported grade 3 AE being neutropenia. This study is expected to be completed by August 2024.

A phase I/II clinical trial (NCT02014337) investigated the safety and efficacy of mifepristone in combination with eribulin, another FDA-approved chemotherapy agent for breast cancer, in patients with GR-positive TNBC [96]. Phase I included 16 patients with metastatic breast cancer while phase II had 21 patients with TNBC specifically. Across phase I and II, there were 23 evaluable patients at the recommended phase II dose (mifepristone 300 mg/day and eribulin 1.1 mg/m^2). Following combinational treatment, three patients had a partial response, eight had stable disease, eleven patients had progressive disease, and one was still inconclusive. The median PFS was 9 weeks, which was generally better than the use of eribulin alone. In terms of safety, this combinational treatment was well tolerated, and the most commonly reported AE was neutropenia. Grade 3/4 AEs were limited to neutropenia, neuropathy, fatigue, hypokalemia, and nausea.

11. Conclusions

The inherent lack of distinct cellular targets and the pronounced heterogeneity of TNBC tumors has led to a significant deficiency in treatment options, resulting in a more challenging

prognosis for TNBC patients. As a result, researchers have been exploring alternative therapeutic avenues for TNBC. Targeting steroid hormonal receptors, such as ERβ, GR, and AR, has shown some potential in inhibiting cancer cell proliferation and curbing tumor growth in biological models. These receptors could also be considered as biomarkers for determining patient prognosis and sensitivity to related treatments. Specifically, the presence of AR is associated with improved OS while GR is associated with a worsened outcome in TNBC, and patients expressing ERβ and mutant p53 had an increased responsiveness to tamoxifen treatment.

Clinical trials targeting these receptors in TNBC patients expressing high levels of ERβ, AR, or GR demonstrated moderate improvement of survival and patient outcome, particularly in patients with metastatic disease. The majority of therapies were well tolerated by patients, with a limited number of grade 3 or higher AEs. Thus, it appears that the use of these hormonal therapies could provide some benefit to a substantial proportion of TNBC patients.

12. Future Directions

While the current findings are promising, further research is needed to resolve gaps in the literature. Primarily, the majority of studies do not account for the heterogeneity of TNBC tumors. Subtype-dependent regulation of receptor signaling could partially explain the range of patient responses reported in clinical trials. Additionally, insight into the interactions between these hormone receptors is needed. While a small number of studies have reported on the crosstalk between the various hormone receptors [97,98,99,100], their mechanism of action is still largely unknown. Thus, further research regarding these hormonal receptors in TNBC could lead to a new effective treatment for some patients.

References

1. Sung, H.; Ferlay, J.; Siegel, R.L.; Laversanne, M.; Soerjomataram, I.; Jemal, A.; Bray, F. Global Cancer Statistics 2020: GLOBOCAN Estimates of Incidence and Mortality Worldwide for 36 Cancers in 185 Countries. *CA Cancer J. Clin.* **2021**, *71*, 209–249. [Google Scholar] [CrossRef]
2. Hsu, J.-Y.; Chang, C.-J.; Cheng, J.-S. Survival, Treatment Regimens and Medical Costs of Women Newly Diagnosed with Metastatic Triple-Negative Breast Cancer. *Sci. Rep.* **2022**, *12*, 729. [Google Scholar] [CrossRef]
3. Dent, R.; Trudeau, M.; Pritchard, K.I.; Hanna, W.M.; Kahn, H.K.; Sawka, C.A.; Lickley, L.A.; Rawlinson, E.; Sun, P.; Narod, S.A. Triple-Negative Breast Cancer: Clinical Features and Patterns of Recurrence. *Clin. Cancer Res.* **2007**, *13*, 4429–4434. [Google Scholar] [CrossRef]
4. Orrantia-Borunda, E.; Anchondo-Nuñez, P.; Acuña-Aguilar, L.E.; Gómez-Valles, F.O.; Ramírez-Valdespino, C.A. Subtypes of Breast Cancer. In *Breast Cancer*; Mayrovitz, H.N., Ed.; Exon Publications: Brisbane, Australia, 2022; ISBN 978-0-645-33203-2. [Google Scholar]
5. Lehmann, B.D.; Bauer, J.A.; Chen, X.; Sanders, M.E.; Chakravarthy, A.B.; Shyr, Y.; Pietenpol, J.A. Identification of Human Triple-Negative Breast Cancer Subtypes and Preclinical Models for Selection of Targeted Therapies. *J. Clin. Investig.* **2011**, *121*, 2750–2767. [Google Scholar] [CrossRef]
6. Lehmann, B.D.; Jovanović, B.; Chen, X.; Estrada, M.V.; Johnson, K.N.; Shyr, Y.; Moses, H.L.; Sanders, M.E.; Pietenpol, J.A. Refinement of Triple-Negative Breast Cancer Molecular Subtypes: Implications for Neoadjuvant Chemotherapy Selection. *PLoS ONE* **2016**, *11*, e0157368. [Google Scholar] [CrossRef]
7. Santonja, A.; Sánchez-Muñoz, A.; Lluch, A.; Chica-Parrado, M.R.; Albanell, J.; Chacón, J.I.; Antolín, S.; Jerez, J.M.; de la Haba, J.; de Luque, V.; et al. Triple Negative Breast Cancer Subtypes and Pathologic Complete Response Rate to Neoadjuvant Chemotherapy. *Oncotarget* **2018**, *9*, 26406–26416. [Google Scholar] [CrossRef]
8. Stewart, R.L.; Updike, K.L.; Factor, R.E.; Henry, N.L.; Boucher, K.M.; Bernard, P.S.; Varley, K.E. A Multigene Assay Determines Risk of Recurrence in Patients with Triple-Negative Breast Cancer. *Cancer Res.* **2019**, *79*, 3466–3478. [Google Scholar] [CrossRef]
9. Manna, S.; Holz, M.K. Tamoxifen Action in ER-Negative Breast Cancer. *Sign Transduct. Insights* **2016**, *5*, 1–7. [Google Scholar] [CrossRef]
10. Early Breast Cancer Trialists' Collaborative Group. Tamoxifen for Early Breast Cancer: An Overview of the Randomised Trials. *Lancet* **1998**, *351*, 1451–1467. [Google Scholar] [CrossRef]
11. Zhao, C.; Dahlman-Wright, K.; Gustafsson, J.-Å. Estrogen Receptor β: An Overview and Update. *Nucl. Recept. Signal* **2008**, *6*, e003. [Google Scholar] [CrossRef]
12. Božović, A.; Mandušić, V.; Todorović, L.; Krajnović, M. Estrogen Receptor Beta: The Promising Biomarker and Potential Target in Metastases. *Int. J. Mol. Sci.* **2021**, *22*, 1656. [Google Scholar] [CrossRef] [PubMed]
13. Roca, P.; Oliver, J.; Sastre-Serra, J.; Nadal-Serrano, M.; Roca, P.; Oliver, J.; Sastre-Serra, J.; Nadal-Serrano, M. The Importance of ERα/ERβ Ratio in Breast Cancer: Mitochondrial Function and Oxidative Stress. In *Breast Cancer—Carcinogenesis, Cell Growth and Signalling Pathways*; IntechOpen: London, UK, 2011; ISBN 978-953-307-714-7. [Google Scholar]
14. Mal, R.; Magner, A.; David, J.; Datta, J.; Vallabhaneni, M.; Kassem, M.; Manouchehri, J.; Willingham, N.; Stover, D.; Vandeusen, J.; et al. Estrogen Receptor Beta (ERβ): A Ligand Activated Tumor Suppressor. *Front. Oncol.* **2020**, *10*, 587386. [Google Scholar] [CrossRef] [PubMed]
15. Kuiper, G.G.; Shughrue, P.J.; Merchenthaler, I.; Gustafsson, J.A. The Estrogen Receptor Beta Subtype: A Novel Mediator of Estrogen Action in Neuroendocrine Systems. *Front. Neuroendocrinol.* **1998**, *19*, 253–286. [Google Scholar] [CrossRef] [PubMed]
16. Crandall, D.L.; Busler, D.E.; Novak, T.J.; Weber, R.V.; Kral, J.G. Identification of Estrogen Receptor Beta RNA in Human Breast and Abdominal Subcutaneous Adipose Tissue. *Biochem. Biophys. Res. Commun.* **1998**, *248*, 523–526. [Google Scholar] [CrossRef]
17. Hawse, J.R.; Carter, J.M.; Aspros, K.G.M.; Bruinsma, E.S.; Koepplin, J.W.; Negron, V.; Subramaniam, M.; Ingle, J.N.; Rech, K.L.; Goetz, M.P. Optimized Immunohistochemical Detection of Estrogen Receptor Beta Using Two

Validated Monoclonal Antibodies Confirms Its Expression in Normal and Malignant Breast Tissues. *Breast Cancer Res. Treat.* **2020**, *179*, 241–249. [Google Scholar] [CrossRef]
18. Wu, X.; Subramaniam, M.; Negron, V.; Cicek, M.; Reynolds, C.; Lingle, W.L.; Goetz, M.P.; Ingle, J.N.; Spelsberg, T.C.; Hawse, J.R. Development, Characterization, and Applications of a Novel Estrogen Receptor Beta Monoclonal Antibody. *J. Cell Biochem.* **2012**, *113*, 711–723. [Google Scholar] [CrossRef]
19. Nelson, A.W.; Groen, A.J.; Miller, J.L.; Warren, A.Y.; Holmes, K.A.; Tarulli, G.A.; Tilley, W.D.; Katzenellenbogen, B.S.; Hawse, J.R.; Gnanapragasam, V.J.; et al. Comprehensive Assessment of Estrogen Receptor Beta Antibodies in Cancer Cell Line Models and Tissue Reveals Critical Limitations in Reagent Specificity. *Mol. Cell Endocrinol.* **2017**, *440*, 138–150. [Google Scholar] [CrossRef]
20. Andersson, S.; Sundberg, M.; Pristovsek, N.; Ibrahim, A.; Jonsson, P.; Katona, B.; Clausson, C.-M.; Zieba, A.; Ramström, M.; Söderberg, O.; et al. Insufficient Antibody Validation Challenges Oestrogen Receptor Beta Research. *Nat. Commun.* **2017**, *8*, 15840. [Google Scholar] [CrossRef]
21. Gruvberger-Saal, S.K.; Bendahl, P.-O.; Saal, L.H.; Laakso, M.; Hegardt, C.; Edén, P.; Peterson, C.; Malmström, P.; Isola, J.; Borg, Å.; et al. Estrogen Receptor β Expression Is Associated with Tamoxifen Response in ERα-Negative Breast Carcinoma. *Clin. Cancer Res.* **2007**, *13*, 1987–1994. [Google Scholar] [CrossRef]
22. Honma, N.; Horii, R.; Iwase, T.; Saji, S.; Younes, M.; Takubo, K.; Matsuura, M.; Ito, Y.; Akiyama, F.; Sakamoto, G. Clinical Importance of Estrogen Receptor-β Evaluation in Breast Cancer Patients Treated with Adjuvant Tamoxifen Therapy. *JCO* **2008**, *26*, 3727–3734. [Google Scholar] [CrossRef]
23. Reese, J.M.; Suman, V.J.; Subramaniam, M.; Wu, X.; Negron, V.; Gingery, A.; Pitel, K.S.; Shah, S.S.; Cunliffe, H.E.; McCullough, A.E.; et al. ERβ1: Characterization, Prognosis, and Evaluation of Treatment Strategies in ERα-Positive and -Negative Breast Cancer. *BMC Cancer* **2014**, *14*, 749. [Google Scholar] [CrossRef] [PubMed]
24. Guo, L.; Zhu, Q.; Aisimutuola, M.; Yilamu, D.; Liu, S.; Jakulin, A. Expression and Prognostic Value of Estrogen Receptor β in Patients with Triple-Negative and Triple-Positive Breast Cancer. *Exp. Ther. Med.* **2015**, *9*, 2147–2150. [Google Scholar] [CrossRef] [PubMed]
25. Takano, E.A.; Younes, M.M.; Meehan, K.; Spalding, L.; Yan, M.; Allan, P.; Fox, S.B.; Redfern, A.; Clouston, D.; Giles, G.G.; et al. Estrogen Receptor Beta Expression in Triple Negative Breast Cancers Is Not Associated with Recurrence or Survival. *BMC Cancer* **2023**, *23*, 459. [Google Scholar] [CrossRef] [PubMed]
26. Novelli, F.; Milella, M.; Melucci, E.; Di Benedetto, A.; Sperduti, I.; Perrone-Donnorso, R.; Perracchio, L.; Venturo, I.; Nisticò, C.; Fabi, A.; et al. A Divergent Role for Estrogen Receptor-Beta in Node-Positive and Node-Negative Breast Cancer Classified According to Molecular Subtypes: An Observational Prospective Study. *Breast Cancer Res.* **2008**, *10*, R74. [Google Scholar] [CrossRef]
27. Shanle, E.K.; Zhao, Z.; Hawse, J.; Wisinski, K.; Keles, S.; Yuan, M.; Xu, W. Research Resource: Global Identification of Estrogen Receptor β Target Genes in Triple Negative Breast Cancer Cells. *Mol. Endocrinol.* **2013**, *27*, 1762–1775. [Google Scholar] [CrossRef]
28. Schüler-Toprak, S.; Häring, J.; Inwald, E.C.; Moehle, C.; Ortmann, O.; Treeck, O. Agonists and Knockdown of Estrogen Receptor β Differentially Affect Invasion of Triple-Negative Breast Cancer Cells in Vitro. *BMC Cancer* **2016**, *16*, 951. [Google Scholar] [CrossRef]
29. Austin, D.; Hamilton, N.; Elshimali, Y.; Pietras, R.; Wu, Y.; Vadgama, J. Estrogen Receptor-Beta Is a Potential Target for Triple Negative Breast Cancer Treatment. *Oncotarget* **2018**, *9*, 33912–33930. [Google Scholar] [CrossRef]
30. Yan, S.; Dey, P.; Ziegler, Y.; Jiao, X.; Kim, S.H.; Katzenellenbogen, J.A.; Katzenellenbogen, B.S. Contrasting Activities of Estrogen Receptor Beta Isoforms in Triple Negative Breast Cancer. *Breast Cancer Res. Treat.* **2021**, *185*, 281–292. [Google Scholar] [CrossRef]
31. Koboldt, D.C.; Fulton, R.S.; McLellan, M.D.; Schmidt, H.; Kalicki-Veizer, J.; McMichael, J.F.; Fulton, L.L.; Dooling, D.J.; Ding, L.; Mardis, E.R.; et al. Comprehensive Molecular Portraits of Human Breast Tumours. *Nature* **2012**, *490*, 61–70. [Google Scholar] [CrossRef]

32. Noll, J.E.; Jeffery, J.; Al-Ejeh, F.; Kumar, R.; Khanna, K.K.; Callen, D.F.; Neilsen, P.M. Mutant P53 Drives Multinucleation and Invasion through a Process That Is Suppressed by ANKRD11. *Oncogene* **2012**, *31*, 2836–2848. [Google Scholar] [CrossRef]
33. Adorno, M.; Cordenonsi, M.; Montagner, M.; Dupont, S.; Wong, C.; Hann, B.; Solari, A.; Bobisse, S.; Rondina, M.B.; Guzzardo, V.; et al. A Mutant-P53/Smad Complex Opposes P63 to Empower TGFbeta-Induced Metastasis. *Cell* **2009**, *137*, 87–98. [Google Scholar] [CrossRef] [PubMed]
34. Bado, I.; Nikolos, F.; Rajapaksa, G.; Gustafsson, J.-Å.; Thomas, C. ERβ Decreases the Invasiveness of Triple-Negative Breast Cancer Cells by Regulating Mutant P53 Oncogenic Function. *Oncotarget* **2016**, *7*, 13599–13611. [Google Scholar] [CrossRef] [PubMed]
35. Mukhopadhyay, U.K.; Oturkar, C.C.; Adams, C.; Wickramasekera, N.; Bansal, S.; Medisetty, R.; Miller, A.; Swetzig, W.M.; Silwal-Pandit, L.; Børresen-Dale, A.-L.; et al. TP53 Status as a Determinant of Pro- vs Anti-Tumorigenic Effects of Estrogen Receptor-Beta in Breast Cancer. *J. Natl. Cancer Inst.* **2019**, *111*, 1202–1215. [Google Scholar] [CrossRef]
36. Scarpetti, L.; Oturkar, C.C.; Juric, D.; Shellock, M.; Malvarosa, G.; Post, K.; Isakoff, S.; Wang, N.; Nahed, B.; Oh, K.; et al. Therapeutic Role of Tamoxifen for Triple-Negative Breast Cancer: Leveraging the Interaction Between ERβ and Mutant P53. *Oncologist* **2023**, *28*, 358–363. [Google Scholar] [CrossRef] [PubMed]
37. Evaluation of Tamoxifen's Efficacy for ER/PR Negative, ER-Beta Positive Operable Breast Cancer Patients. Available online: https://www.smartpatients.com/trials/NCT02062489 (accessed on 10 September 2023).
38. Peking Union Medical College Hospital. Evaluation of Adjuvant Endocrine Therapy for Operable ER-Beta Positive, ER-Alpha/PR Negative, Her-2 Negative Breast Cancer Patients; 2016. Available online: clinicaltrials.gov (accessed on 17 September 2023).
39. Wisinski, K.B.; Xu, W.; Tevaarwerk, A.J.; Saha, S.; Kim, K.; Traynor, A.; Dietrich, L.; Hegeman, R.; Patel, D.; Blank, J.; et al. Targeting Estrogen Receptor Beta in a Phase 2 Study of High-Dose Estradiol in Metastatic Triple-Negative Breast Cancer: A Wisconsin Oncology Network Study. *Clin. Breast Cancer* **2016**, *16*, 256–261. [Google Scholar] [CrossRef]
40. Mayo Clinic. Therapeutic Targeting of ER Beta in Triple Negative Breast Cancer; 2023. Available online: clinicaltrials.gov (accessed on 7 September 2023).
41. Hong, J.; Huang, J.; Shen, L.; Zhu, S.; Gao, W.; Wu, J.; Huang, O.; He, J.; Zhu, L.; Chen, W.; et al. A Prospective, Randomized Study of Toremifene vs. Tamoxifen for the Treatment of Premenopausal Breast Cancer: Safety and Genital Symptom Analysis. *BMC Cancer* **2020**, *20*, 663. [Google Scholar] [CrossRef]
42. Gucalp, A.; Traina, T.A. Triple-Negative Breast Cancer: Role of the Androgen Receptor. *Cancer J.* **2010**, *16*, 62–65. [Google Scholar] [CrossRef]
43. Bhattarai, S.; Klimov, S.; Mittal, K.; Krishnamurti, U.; Li, X.B.; Oprea-Ilies, G.; Wetherilt, C.S.; Riaz, A.; Aleskandarany, M.A.; Green, A.R.; et al. Prognostic Role of Androgen Receptor in Triple Negative Breast Cancer: A Multi-Institutional Study. *Cancers* **2019**, *11*, 995. [Google Scholar] [CrossRef]
44. Tan, M.H.E.; Li, J.; Xu, H.E.; Melcher, K.; Yong, E. Androgen Receptor: Structure, Role in Prostate Cancer and Drug Discovery. *Acta Pharmacol. Sin.* **2015**, *36*, 3–23. [Google Scholar] [CrossRef]
45. Elgehama, A.; Sun, L.; Yu, B.; Guo, W.; Xu, Q. Selective Targeting of the Androgen Receptor-DNA Binding Domain by the Novel Antiandrogen SBF-1 and Inhibition of the Growth of Prostate Cancer Cells. *Invest. New Drugs* **2021**, *39*, 442–457. [Google Scholar] [CrossRef]
46. Zhu, M.-L.; Kyprianou, N. Androgen Receptor and Growth Factor Signaling Cross-Talk in Prostate Cancer Cells. *Endocr. Relat. Cancer* **2008**, *15*, 841–849. [Google Scholar] [CrossRef] [PubMed]
47. Bryan, R.M.; Mercer, R.J.; Bennett, R.C.; Rennie, G.C.; Lie, T.H.; Morgan, F.J. Androgen Receptors in Breast Cancer. *Cancer* **1984**, *54*, 2436–2440. [Google Scholar] [CrossRef] [PubMed]
48. Persijn, J.P.; Korsten, C.B.; Engelsman, E. Oestrogen and Androgen Receptors in Breast Cancer and Response to Endocrine Therapy. *Br. Med. J.* **1975**, *4*, 503. [Google Scholar] [CrossRef]
49. Rana, K.; Davey, R.A.; Zajac, J.D. Human Androgen Deficiency: Insights Gained from Androgen Receptor Knockout Mouse Models. *Asian J. Androl.* **2014**, *16*, 169–177. [Google Scholar] [CrossRef] [PubMed]

50. Burstein, M.D.; Tsimelzon, A.; Poage, G.M.; Covington, K.R.; Contreras, A.; Fuqua, S.A.W.; Savage, M.I.; Osborne, C.K.; Hilsenbeck, S.G.; Chang, J.C.; et al. Comprehensive Genomic Analysis Identifies Novel Subtypes and Targets of Triple-Negative Breast Cancer. *Clin. Cancer Res.* **2015**, *21*, 1688–1698. [Google Scholar] [CrossRef] [PubMed]
51. Masuda, H.; Baggerly, K.A.; Wang, Y.; Zhang, Y.; Gonzalez-Angulo, A.M.; Meric-Bernstam, F.; Valero, V.; Lehmann, B.D.; Pietenpol, J.A.; Hortobagyi, G.N.; et al. Differential Response to Neoadjuvant Chemotherapy among 7 Triple-Negative Breast Cancer Molecular Subtypes. *Clin. Cancer Res.* **2013**, *19*, 5533–5540. [Google Scholar] [CrossRef] [PubMed]
52. Christenson, J.L.; O'Neill, K.I.; Williams, M.M.; Spoelstra, N.S.; Jones, K.L.; Trahan, G.D.; Reese, J.; Van Patten, E.T.; Elias, A.; Eisner, J.R.; et al. Activity of Combined Androgen Receptor Antagonism and Cell Cycle Inhibition in Androgen Receptor Positive Triple Negative Breast Cancer. *Mol. Cancer Ther.* **2021**, *20*, 1062–1071. [Google Scholar] [CrossRef]
53. Cimino-Mathews, A.; Hicks, J.L.; Illei, P.B.; Halushka, M.K.; Fetting, J.H.; De Marzo, A.M.; Park, B.H.; Argani, P. Androgen Receptor Expression Is Usually Maintained in Initial Surgically-Resected Breast Cancer Metastases, But Often Lost in End-Stage Metastases Found at Autopsy. *Hum. Pathol.* **2012**, *43*, 1003–1011. [Google Scholar] [CrossRef]
54. Barton, V.N.; Christenson, J.L.; Gordon, M.A.; Greene, L.I.; Rogers, T.J.; Butterfield, K.; Babbs, B.; Spoelstra, N.S.; D'Amato, N.C.; Elias, A.; et al. Androgen Receptor Supports an Anchorage-Independent, Cancer Stem Cell-like Population in Triple-Negative Breast Cancer. *Cancer Res.* **2017**, *77*, 3455–3466. [Google Scholar] [CrossRef]
55. Giovannelli, P.; Di Donato, M.; Auricchio, F.; Castoria, G.; Migliaccio, A. Androgens Induce Invasiveness of Triple Negative Breast Cancer Cells Through AR/Src/PI3-K Complex Assembly. *Sci. Rep.* **2019**, *9*, 4490. [Google Scholar] [CrossRef]
56. Asano, Y.; Kashiwagi, S.; Goto, W.; Tanaka, S.; Morisaki, T.; Takashima, T.; Noda, S.; Onoda, N.; Ohsawa, M.; Hirakawa, K.; et al. Expression and Clinical Significance of Androgen Receptor in Triple-Negative Breast Cancer. *Cancers* **2017**, *9*, 4. [Google Scholar] [CrossRef] [PubMed]
57. Lyalkin, S.A.; Verevkina, N.O.; Alekseyenko, O.O.; Syvak, L.A. Prognostic Role of Androgen Receptor Expression in Patients with Metastatic Triple Negative Breast Cancer. *Exp. Oncol.* **2020**, *42*, 140–143. [Google Scholar] [CrossRef] [PubMed]
58. Wang, C.; Pan, B.; Zhu, H.; Zhou, Y.; Mao, F.; Lin, Y.; Xu, Q.; Sun, Q. Prognostic Value of Androgen Receptor in Triple Negative Breast Cancer: A Meta-Analysis. *Oncotarget* **2016**, *7*, 46482–46491. [Google Scholar] [CrossRef]
59. Hu, R.; Dawood, S.; Holmes, M.D.; Collins, L.C.; Schnitt, S.J.; Cole, K.; Marotti, J.D.; Hankinson, S.E.; Colditz, G.A.; Tamimi, R.M. Androgen Receptor Expression and Breast Cancer Survival in Postmenopausal Women. *Clin. Cancer Res.* **2011**, *17*, 1867–1874. [Google Scholar] [CrossRef]
60. McGhan, L.J.; McCullough, A.E.; Protheroe, C.A.; Dueck, A.C.; Lee, J.J.; Nunez-Nateras, R.; Castle, E.P.; Gray, R.J.; Wasif, N.; Goetz, M.P.; et al. Androgen Receptor-Positive Triple Negative Breast Cancer: A Unique Breast Cancer Subtype. *Ann. Surg. Oncol.* **2014**, *21*, 361–367. [Google Scholar] [CrossRef] [PubMed]
61. Sridhar, N.; Glisch, C.; Jawa, Z.; Chaudhary, L.N.; Kamaraju, S.; Burfeind, J.; Charlson, J.; Chitambar, C.R.; Jorns, J.M.; Cheng, Y.C. Androgen Receptor Expression in Patients with Triple Negative Breast Cancer Treated with Neoadjuvant Chemotherapy: A Single Institution Study. *J. Cancer* **2022**, *13*, 2472–2476. [Google Scholar] [CrossRef] [PubMed]
62. Mrklić, I.; Pogorelić, Z.; Capkun, V.; Tomić, S. Expression of Androgen Receptors in Triple Negative Breast Carcinomas. *Acta Histochem.* **2013**, *115*, 344–348. [Google Scholar] [CrossRef] [PubMed]
63. Dubrava, A.L.; Kyaw, P.S.P.; Newman, J.; Pringle, J.; Westhuyzen, J.; La Hera Fuentes, G.; Shakespeare, T.P.; Sakalkale, R.; Aherne, N.J. Androgen Receptor Status in Triple Negative Breast Cancer: Does It Correlate with Clinicopathological Characteristics? *Breast Cancer Targets Ther.* **2023**, *15*, 359–371. [Google Scholar] [CrossRef]

64. Traina, T.A.; Miller, K.; Yardley, D.A.; Eakle, J.; Schwartzberg, L.S.; O'Shaughnessy, J.; Gradishar, W.; Schmid, P.; Winer, E.; Kelly, C.; et al. Enzalutamide for the Treatment of Androgen Receptor-Expressing Triple-Negative Breast Cancer. *J. Clin. Oncol.* **2018**, *36*, 884–890. [Google Scholar] [CrossRef]
65. Walsh, E.M.; Gucalp, A.; Patil, S.; Edelweiss, M.; Ross, D.S.; Razavi, P.; Modi, S.; Iyengar, N.M.; Sanford, R.; Troso-Sandoval, T.; et al. Adjuvant Enzalutamide for the Treatment of Early-Stage Androgen-Receptor Positive, Triple-Negative Breast Cancer: A Feasibility Study. *Breast Cancer Res. Treat.* **2022**, *195*, 341–351. [Google Scholar] [CrossRef]
66. Yuan, Y.; Lee, J.S.; Yost, S.E.; Frankel, P.H.; Ruel, C.; Egelston, C.A.; Guo, W.; Gillece, J.D.; Folkerts, M.; Reining, L.; et al. A Phase II Clinical Trial of Pembrolizumab and Enobosarm in Patients with Androgen Receptor-Positive Metastatic Triple-Negative Breast Cancer. *Oncologist* **2021**, *26*, 99-e217. [Google Scholar] [CrossRef] [PubMed]
67. Gucalp, A.; Tolaney, S.; Isakoff, S.J.; Ingle, J.N.; Liu, M.C.; Carey, L.A.; Blackwell, K.; Rugo, H.; Nabell, L.; Forero, A.; et al. Phase II Trial of Bicalutamide in Patients with Androgen Receptor–Positive, Estrogen Receptor–Negative Metastatic Breast Cancer. *Clin. Cancer Res.* **2013**, *19*, 5505–5512. [Google Scholar] [CrossRef] [PubMed]
68. Gucalp, A.; Boyle, L.A.; Alano, T.; Arumov, A.; Gounder, M.M.; Patil, S.; Feigin, K.; Edelweiss, M.; D'Andrea, G.; Bromberg, J.; et al. Phase II Trial of Bicalutamide in Combination with Palbociclib for the Treatment of Androgen Receptor (+) Metastatic Breast Cancer. *JCO* **2020**, *38*, 1017. [Google Scholar] [CrossRef]
69. Sharifi, M.; Wisinski, K.; Burkard, M.; Tevaarwerk, A.; Tamkus, D.; Chan, N.; Truica, C.; Danciu, O.; Hoskins, K.; O'Regan, R. Abstract OT1-02-01: Phase I Trial of Bicalutamide and Ribociclib in Androgen Receptor-Positive Triple Negative Breast Cancer. *Cancer Res.* **2019**, *79*, OT1-02–01. [Google Scholar] [CrossRef]
70. Bardia, A.; Gucalp, A.; DaCosta, N.; Gabrail, N.; Danso, M.; Ali, H.; Blackwell, K.L.; Carey, L.A.; Eisner, J.R.; Baskin-Bey, E.S.; et al. Phase 1 Study of Seviteronel, a Selective CYP17 Lyase and Androgen Receptor Inhibitor, in Women with Estrogen Receptor-Positive or Triple-Negative Breast Cancer. *Breast Cancer Res. Treat.* **2018**, *171*, 111–120. [Google Scholar] [CrossRef]
71. Menon, M.P.; Higano, C.S. Enzalutamide, a Second Generation Androgen Receptor Antagonist: Development and Clinical Applications in Prostate Cancer. *Curr. Oncol. Rep.* **2013**, *15*, 69–75. [Google Scholar] [CrossRef] [PubMed]
72. Narayanan, R.; Ahn, S.; Cheney, M.D.; Yepuru, M.; Miller, D.D.; Steiner, M.S.; Dalton, J.T. Selective Androgen Receptor Modulators (SARMs) Negatively Regulate Triple-Negative Breast Cancer Growth and Epithelial:Mesenchymal Stem Cell Signaling. *PLoS ONE* **2014**, *9*, e103202. [Google Scholar] [CrossRef]
73. Rice, M.A.; Malhotra, S.V.; Stoyanova, T. Second-Generation Antiandrogens: From Discovery to Standard of Care in Castration Resistant Prostate Cancer. *Front. Oncol.* **2019**, *9*, 801. [Google Scholar] [CrossRef]
74. Hu, Y.; Gao, J.; Wang, M.; Li, M. Potential Prospect of CDK4/6 Inhibitors in Triple-Negative Breast Cancer. *Cancer Manag. Res.* **2021**, *13*, 5223–5237. [Google Scholar] [CrossRef]
75. Michmerhuizen, A.R.; Chandler, B.; Olsen, E.; Wilder-Romans, K.; Moubadder, L.; Liu, M.; Pesch, A.M.; Zhang, A.; Ritter, C.; Ward, S.T.; et al. Seviteronel, a Novel CYP17 Lyase Inhibitor and Androgen Receptor Antagonist, Radiosensitizes AR-Positive Triple Negative Breast Cancer Cells. *Front. Endocrinol.* **2020**, *11*, 35. [Google Scholar] [CrossRef]
76. Marchi, D.; van Eeden, F.J.M. Homeostatic Regulation of Glucocorticoid Receptor Activity by Hypoxia-Inducible Factor 1: From Physiology to Clinic. *Cells* **2021**, *10*, 3441. [Google Scholar] [CrossRef] [PubMed]
77. Postel, S.; Wissler, L.; Johansson, C.A.; Gunnarsson, A.; Gordon, E.; Collins, B.; Castaldo, M.; Köhler, C.; Öling, D.; Johansson, P.; et al. Quaternary Glucocorticoid Receptor Structure Highlights Allosteric Interdomain Communication. *Nat. Struct. Mol. Biol.* **2023**, *30*, 286–295. [Google Scholar] [CrossRef] [PubMed]
78. Dwyer, A.R.; Perez Kerkvliet, C.; Truong, T.H.; Hagen, K.M.; Krutilina, R.I.; Parke, D.N.; Oakley, R.H.; Liddle, C.; Cidlowski, J.A.; Seagroves, T.N.; et al. Glucocorticoid Receptors Drive Breast Cancer Cell Migration and Metabolic Reprogramming via PDK4. *Endocrinology* **2023**, *164*, bqad083. [Google Scholar] [CrossRef] [PubMed]

79. Noureddine, L.M.; Trédan, O.; Hussein, N.; Badran, B.; Le Romancer, M.; Poulard, C. Glucocorticoid Receptor: A Multifaceted Actor in Breast Cancer. *Int. J. Mol. Sci.* **2021**, *22*, 4446. [Google Scholar] [CrossRef]
80. Abduljabbar, R.; Negm, O.H.; Lai, C.-F.; Jerjees, D.A.; Al-Kaabi, M.; Hamed, M.R.; Tighe, P.J.; Buluwela, L.; Mukherjee, A.; Green, A.R.; et al. Clinical and Biological Significance of Glucocorticoid Receptor (GR) Expression in Breast Cancer. *Breast Cancer Res. Treat.* **2015**, *150*, 335–346. [Google Scholar] [CrossRef]
81. Baker, G.M.; Murphy, T.; Block, T.; Nguyen, D.; Lynch, F.J. Development and Validation of an Immunohistochemistry Assay to Assess Glucocorticoid Receptor Expression for Clinical Trials of Mifepristone in Breast Cancer. *CMAR* **2015**, *7*, 361–368. [Google Scholar] [CrossRef]
82. Buxant, F.; Engohan-Aloghe, C.; Noël, J.-C. Estrogen Receptor, Progesterone Receptor, and Glucocorticoid Receptor Expression in Normal Breast Tissue, Breast In Situ Carcinoma, and Invasive Breast Cancer. *Appl. Immunohistochem. Mol. Morphol.* **2010**, *18*, 254. [Google Scholar] [CrossRef]
83. Pan, D.; Kocherginsky, M.; Conzen, S.D. Activation of the Glucocorticoid Receptor Is Associated with Poor Prognosis in Estrogen Receptor-Negative Breast Cancer. *Cancer Res.* **2011**, *71*, 6360–6370. [Google Scholar] [CrossRef]
84. Wu, W.; Chaudhuri, S.; Brickley, D.R.; Pang, D.; Karrison, T.; Conzen, S.D. Microarray Analysis Reveals Glucocorticoid-Regulated Survival Genes That Are Associated with Inhibition of Apoptosis in Breast Epithelial Cells. *Cancer Res.* **2004**, *64*, 1757–1764. [Google Scholar] [CrossRef]
85. Conway, M.E.; McDaniel, J.M.; Graham, J.M.; Guillen, K.P.; Oliver, P.G.; Parker, S.L.; Yue, P.; Turkson, J.; Buchsbaum, D.J.; Welm, B.E.; et al. STAT3 and GR Cooperate to Drive Gene Expression and Growth of Basal-Like Triple-Negative Breast Cancer. *Cancer Res.* **2020**, *80*, 4355–4370. [Google Scholar] [CrossRef]
86. Perez Kerkvliet, C.; Dwyer, A.R.; Diep, C.H.; Oakley, R.H.; Liddle, C.; Cidlowski, J.A.; Lange, C.A. Glucocorticoid Receptors Are Required Effectors of TGFβ1-Induced P38 MAPK Signaling to Advanced Cancer Phenotypes in Triple-Negative Breast Cancer. *Breast Cancer Res.* **2020**, *22*, 39. [Google Scholar] [CrossRef] [PubMed]
87. Elkashif, A.; Bingham, V.; Haddock, P.; Humphries, M.P.; McQuaid, S.; Mullan, P.B.; McCarthy, H.O.; Buckley, N.E. Glucocorticoid Receptor Expression Predicts Good Outcome in Response to Taxane-Free, Anthracycline-Based Therapy in Triple Negative Breast Cancer. *J. Oncol.* **2020**, *2020*, e3712825. [Google Scholar] [CrossRef] [PubMed]
88. Lin, C.-H.; Chuang, P.-Y.; You, S.-L.; Chiang, C.-J.; Huang, C.-S.; Wang, M.-Y.; Chao, M.; Lu, Y.-S.; Cheng, A.-L.; Tang, C.-H. Effect of Glucocorticoid Use on Survival in Patients with Stage I–III Breast Cancer. *Breast Cancer Res. Treat.* **2018**, *171*, 225–234. [Google Scholar] [CrossRef] [PubMed]
89. Cadepond, F.; Ulmann, A.; Baulieu, E.-E. RU486 (MIFEPRISTONE): Mechanisms of Action and Clinical Uses. *Annu. Rev. Med.* **1997**, *48*, 129–156. [Google Scholar] [CrossRef] [PubMed]
90. Musgrove, E.A.; Sutherland, R.L. Effects of the Progestin Antagonist RU 486 on T-47D Breast Cancer Cell Cycle Kinetics and Cell Cycle Regulatory Genes. *Biochem. Biophys. Res. Commun.* **1993**, *195*, 1184–1190. [Google Scholar] [CrossRef]
91. Bardon, S.; Vignon, F.; Chalbos, D.; Rochefort, H. RU486, a Progestin and Glucocorticoid Antagonist, Inhibits the Growth of Breast Cancer Cells via the Progesterone Receptor. *J. Clin. Endocrinol. Metab.* **1985**, *60*, 692–697. [Google Scholar] [CrossRef]
92. Yu, S.; Yan, C.; Wu, W.; He, S.; Liu, M.; Liu, J.; Yang, X.; Ma, J.; Lu, Y.; Jia, L. RU486 Metabolite Inhibits CCN1/Cyr61 Secretion by MDA-MB-231-Endothelial Adhesion. *Front. Pharmacol.* **2019**, *10*, 1296. [Google Scholar] [CrossRef]
93. Jang, J.H.; Woo, S.M.; Um, H.J.; Park, E.J.; Min, K.-J.; Lee, T.-J.; Kim, S.H.; Choi, Y.H.; Kwon, T.K. RU486, a Glucocorticoid Receptor Antagonist, Induces Apoptosis in U937 Human Lymphoma Cells through Reduction in Mitochondrial Membrane Potential and Activation of P38 MAPK. *Oncol. Rep.* **2013**, *30*, 506–512. [Google Scholar] [CrossRef]
94. Nanda, R.; Stringer-Reasor, E.M.; Saha, P.; Kocherginsky, M.; Gibson, J.; Libao, B.; Hoffman, P.C.; Obeid, E.; Merkel, D.E.; Khramtsova, G.; et al. A Randomized Phase I Trial of Nanoparticle Albumin-Bound Paclitaxel

with or without Mifepristone for Advanced Breast Cancer. *SpringerPlus* **2016**, *5*, 947. [Google Scholar] [CrossRef]
95. Chen, N.; Saha, P.; Rampurwala, M.M.; Kamaraju, S.; Hahn, O.M.; Howard, F.M.; Fleming, G.F.; Matossian, M.; Freeman, J.Q.; Karrison, T.; et al. A Randomized Phase II Trial of Nab-Paclitaxel with or without Mifepristone for Advanced Triple-Negative Breast Cancer. *JCO* **2023**, *41*, e13103. [Google Scholar] [CrossRef]
96. Han, H.; Wilks, S.; Paplomata, E.; Modiano, M.; Becerra, C.; Braiteh, F.; Spira, A.; Pluard, T.; Richards, D.; Conzen, S.; et al. Abstract P6-12-15: Efficacy Results of a Phase 1/2 Study of Glucocorticoid Receptor (GR) Antagonist Mifepristone (MIFE) in Combination with Eribulin in GR-Positive Triple-Negative Breast Cancer (TNBC). *Cancer Res.* **2017**, *77*, P6-12–15. [Google Scholar] [CrossRef]
97. Rosette, C.; Agan, F.J.; Rosette, N.; Mazzetti, A.; Moro, L.; Gerloni, M. The Dual Androgen Receptor and Glucocorticoid Receptor Antagonist CB-03-10 as Potential Treatment for Tumors That Have Acquired GR-Mediated Resistance to AR Blockade. *Mol. Cancer Ther.* **2020**, *19*, 2256–2266. [Google Scholar] [CrossRef] [PubMed]
98. Kanai, A.; McNamara, K.M.; Iwabuchi, E.; Miki, Y.; Onodera, Y.; Guestini, F.; Khalid, F.; Sagara, Y.; Ohi, Y.; Rai, Y.; et al. Significance of Glucocorticoid Signaling in Triple-Negative Breast Cancer Patients: A Newly Revealed Interaction with Androgen Signaling. *Breast Cancer Res. Treat.* **2020**, *180*, 97–110. [Google Scholar] [CrossRef] [PubMed]
99. Anestis, A.; Sarantis, P.; Theocharis, S.; Zoi, I.; Tryfonopoulos, D.; Korogiannos, A.; Koumarianou, A.; Xingi, E.; Thomaidou, D.; Kontos, M.; et al. Estrogen Receptor Beta Increases Sensitivity to Enzalutamide in Androgen Receptor-Positive Triple-Negative Breast Cancer. *J. Cancer Res. Clin. Oncol.* **2019**, *145*, 1221–1233. [Google Scholar] [CrossRef]
100. Song, W.; Tang, L.; Xu, Y.; Sun, Q.; Yang, F.; Guan, X. ERβ1 Inhibits Metastasis of Androgen Receptor-Positive Triple-Negative Breast Cancer by Suppressing ZEB1. *J. Exp. Clin. Cancer Res.* **2017**, *36*, 75. [Google Scholar] [CrossRef]

Appendix D. Scalable Biomanufacturing Workflow to Produce and Isolate Natural Killer Cell-Derived Extracellular Vesicle-Based Cancer Biotherapeutics

Preface: This work was adapted from the method paper "Scalable Biomanufacturing Workflow to Produce and Isolate Natural Killer Cell-Derived Extracellular Vesicle-Based Cancer Biotherapeutics" originally published in the Journal of Visualized Experiments in 2024. This work was published as a co-first author with Frederic St-Denis-Bissonnette.

Citation: St-Denis-Bissonnette, F.; Kirkby, M.; Wang, L.; Lavoie, J. R. Scalable Biomanufacturing Workflow to Produce and Isolate Natural Killer Cell-Derived Extracellular Vesicle-Based Cancer Biotherapeutics. *Journal of Visualized Experiments* **2024**, (210). DOI: 10.3791/67227.

Author Contributions: Conceptualization, FSTDB, MK, LW, JRL; NTA experimentation and analysis: FSTDB, MK; EV cytotoxicity assay: FSTDB; EV cytotoxicity analyses: FSTDB, MK, LW, JRL; Statistical analysis: FSTDB; writing—original draft preparation, FSTDB and MK; writing—review and editing, FSTDB, MK, LW, JRL. All authors have read and agreed to the published version of the manuscript.

Abstract

Natural killer cell-derived extracellular vesicles (NK-EVs) are being investigated as cancer biotherapeutics. They possess unique properties as cytotoxic nanovesicles targeting cancer cells and as immunomodulatory communicators. A scalable biomanufacturing workflow enables the production of large quantities of high-purity NK-EVs to meet the pre-clinical and clinical demands. The workflow employs a closed-loop hollow-fiber bioreactor, enabling continuous

production of NK-EVs from the NK92-MI cell line under serum-free, xeno-free, feeder-free, and antibiotic-free conditions in compliance with Good Manufacturing Practices standards. This protocol-driven study outlines the biomanufacturing workflow for isolating NK-EVs using size-exclusion chromatography, ultrafiltration, and filter-based sterilization. Essential NK-EV product characterization is performed via nanoparticle tracking analysis, and their functionality is assessed through a validated cell viability-based potency assay against cancer cells. This scalable biomanufacturing process holds significant potential to advance the clinical translation of NK-EV-based cancer biotherapeutics by adhering to best practices and ensuring reproducibility.

Introduction

In the 21st century, remarkable advancements have been achieved in the battle against cancer. This is mainly due to the rise of cancer immunotherapeutics, a class of drugs that harnesses the immune system to fight cancer. Natural killer cell-derived extracellular vesicles (NK-EVs) represent promising contenders in the expanding realm of immunotherapy. Integrative to innate and adaptive immunity, NK cells play a crucial role in the body's defense against virus-infected, stressed, and malignant cells. They employ a comprehensive arsenal of anti-cancer machinery to eliminate abnormal cells through cytotoxic means[1,2,3]. Among these mechanisms is the production and secretion of EVs, nanoscale bilayer structures containing various biomolecules, such as proteins, RNAs, and DNAs, crucial for facilitating intercellular communication[4,5,6]. NK-EVs emerge as promising cell-free therapeutics due to their unique carrier properties. These include their small size, allowing filter-based sterilization, high biocompatibility, preferential accumulation within tumors, broad cargo delivery spectrum, capacity to overcome biological barriers such as the blood-brain barrier, and minimal toxicity profile. For several reasons, NK-EVs

obviate the need for patient lymphodepletion via chemotherapy before administration: 1) conventionally, lymphodepletion is employed to create a more hospitable environment for cell-based therapy, enabling infused cells to proliferate and exert their therapeutic effects; 2) unlike cells, EVs lack the replication capacity and are substantially smaller in scale; 3) EVs operate through distinct mechanisms and exhibit diminished immunogenicity compared to cells[5,6,7]. Furthermore, NK-EVs consistently exhibited *in vitro* efficacy against various cancer models and have also shown immunomodulatory effects on immune cells that foster anti-cancer responses[8,9]. *In vivo* results corroborate these findings, showcasing cancer regression following NK-EV treatment and negligible toxicities[10,11,12]. Therefore, NK-EV-based therapeutics hold great promise to address the challenges of treating cold, immunologically inert solid tumors[13,14,15,16,17].

Our recent study addresses a significant bottleneck to the clinical translation of NK-EVs through biomanufacturing[7]. The article presents a proof-of-concept for a cost-effective and scalable biomanufacturing workflow of NK-EVs meticulously designed to ensure in-process quality control testing. This approach continuously produced large quantities of high-purity NK-EV-based cancer biotherapeutics, with thorough product characterization conducted according to the MISEV2018 guidelines[18]. The scalability of the biomanufacturing workflow can be achieved by increasing cartridge size or having multiple bioreactors running in parallel. Similarly, the scalability of the EV isolation workflow can be easily attainable using techniques like Fast Protein Liquid Chromatography (FPLC) based size-exclusion chromatography (SEC), ultrafiltration (UF), and filter-based sterilization. The closed-loop hollow-fiber bioreactor (HFB) system grew the IL-2-self-sufficient NK cell line (NK92-MI cells) without requiring serum supplementation, a feeder system, and antibiotics. This was accomplished using a commercially available chemically defined and xeno-free medium (a GMP version is now commercially available). As a result, large

quantities of NK cells (10^9 viable cells) and NK-EVs (10^{12} EVs) were successfully produced within 5 - 7 days using a single medium-size bioreactor cartridge, with both products extensively characterized. Throughout the biomanufacturing process, cell health was monitored daily using quantifiable metrics such as pH, glucose, and lactate levels, along with visual indicators such as media color and any sign of contamination, which are essential predictors of cell and EV quality. Post-harvest evaluation of NK cell viability and functionality generated in the HFB system, particularly cytotoxicity, revealed a significant enhancement compared to flask-based cultures[7]. Likewise, purified NK-EVs exhibited a high purity profile, devoid of bacteria, mycoplasma, common viral entities, and cellular components, and with negligible endotoxin levels. Importantly, purified NK-EVs constituted over 99.9% of all nanoparticles found in the final product[7]. Lastly, these purified NK-EVs retained key NK characteristics, including surface markers (CD2, CD45, CD56), cytokine payload (GzmB, PFN, IFN-g), and demonstrated potent cytotoxicity against leukemic K562 cells, the gold-standard line for assessing NK cell cytotoxicity[7].

The present protocol details the scalable biomanufacturing workflow discussed above. It elucidates the methodology for isolating NK-EVs produced using FPLC-SEC coupled with UF and filter-based sterilization. Additionally, the protocol describes pivotal steps, including product characterization using nanoparticle tracking analysis (NTA), quality assessment using various tools (protein/dsDNA quantification and microbial testing), and functional validation of the purified NK-EV product against cancer cells by cell viability assay. Typically, this workflow yields 1.0 - 1.5 mL of NK-EV product with an average concentration of 1.18 x 10^{12} EVs/mL[7], totaling a minimum of 1 x 10^{12} EVs based on approximately 40 mL of EV-rich CM. This process allows product release for various downstream applications, such as investigatory, preclinical, and multi-omics (proteomics, transcriptomics, genomics, metabolomics, lipidomics, and epigenomics)

studies demanding high quantities of high-quality EVs while holding potential for clinical translation, with demonstrated reproducibility.

Protocol

1. NK-EV biomanufacturing from NK92-MI cells using a closed-loop bioreactor

NOTE: NK-EVs are manufactured using a scalable biomanufacturing workflow that adheres to Good Manufacturing Practices (GMP) and utilizes the NK92-MI cells (see **Figure 1**). Our recent publication has detailed insights into the biomanufacturing procedure and NK-EV products' identity and safety profiles[7].

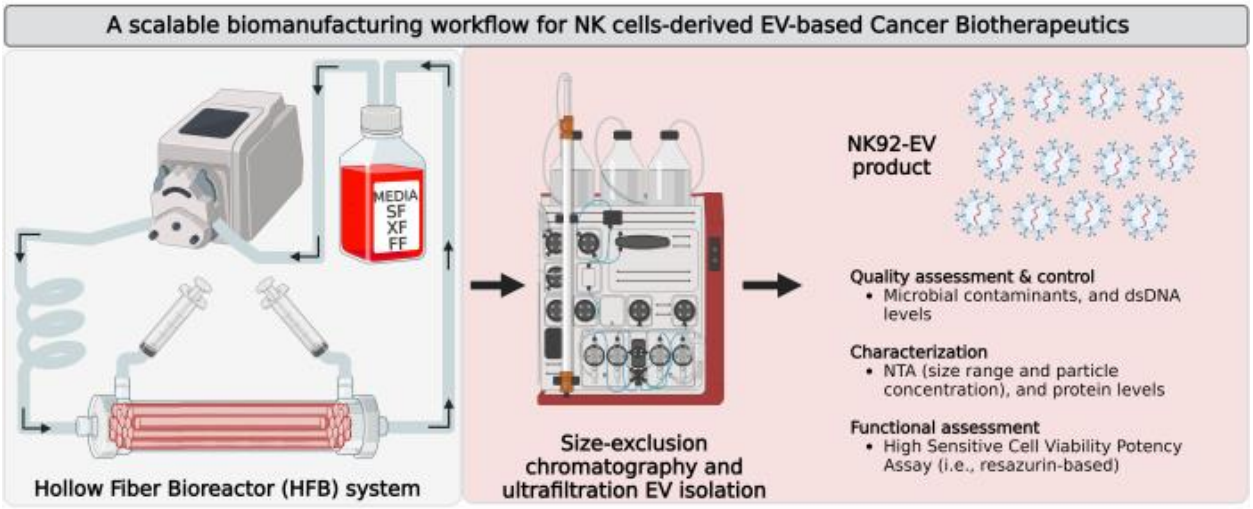

Figure 1: Biomanufacturing of natural killer cell-derived extracellular vesicles (NK-EVs) in a closed-loop hollow-fiber bioreactor (HFB) with scalable isolation workflow.
Schematic representation of the biomanufacturing workflow to generate large quantities of high-purity NK-EV products. IL-2 self-sufficient NK92-MI cells are seeded into a closed-loop HFB cartridge and cultured under serum-free (SF), xeno-free (XF), feeder-free, and antibiotic-free conditions, where they are grown for continual EV-rich conditioned medium collection. NK-EV isolation from EV-rich CM is performed by Fast Protein Liquid Chromatography-based size exclusion chromatography (FPLC-SEC) coupled with ultrafiltration (UF). NK-EVs are characterized and assessed through multiple assays, and their functionality against K562 leukemia

cells is evaluated using a viability potency assay. This figure has been modified from[7](created with Biorender.com).

1. Starting from 1 - 5 x 10^6 NK92-MI cells and maintaining a cell density between 3 - 8 x 10^5 cells/mL, culture the cells in T25 - T175 flasks using a pre-warmed culture medium. Incubate at 37 °C with 5% CO_2 (see **Table of Materials**). Replace the medium every 2 - 3 days until 1 x 10^8 NK92-MI cells are produced of at least 70% viability. NOTE: Keep 1/5th-1/3rd of the conditioned medium (CM) when reseeding the cells, as it contains favorable growth factors.
2. Perform medium HFB cartridge preparation and NK cell inoculation as described below. NOTE: All manipulations should be performed inside a class II biosafety cabinet to ensure and maintain sterility. Before moving the cartridge system into the biosafety cabinet, generously spray with 70% ethanol, paying special attention to the reservoir bottleneck and the syringe connections.
    1. Prepare the HFB cartridge according to the manufacturer's instructions[19] (see **Table of Materials**; see **Figure 2**) as described below.
        1. Wrap Luer Lock connections with wax film and adjust the pump flow rate according to the manufacturer's instructions[19]. Condition the HFB cartridge by allowing 150 mL of sterile phosphate-buffered saline (PBS; see **Table of Materials**) to circulate for at least five days.
        2. To remove the air from the extracellular capillary space (ECS; volume is approximately 29 mL), inject approximately 40 mL of PBS through the left ECS port and allow the air to escape through the right ECS port. While doing that, close the left and right end port clamps. Ensure the syringe is always connected to the left and right ECS ports.

3. Once completed, put the cartridge on the flow pump (see **Table of Materials**) inside the incubator set to 37 °C and 5% CO_2. Ensure there are no leaks after a few days of circulation.

2. Replace the PBS with 150 mL of culture medium in the reservoir bottle and the ECS 2 days before seeding cells into the cartridge. Repeat the previous conditioning steps (step 1.2.1.) using the culture medium but for 2 days of circulation.
3. Before seeding cells, replace the contents in the reservoir bottle and the ECS with 250 mL of fresh culture medium.
4. Acquire the culture flask from the incubator and transfer the cells to a 50 mL tube. Spin at 300 x *g* for 5 min. Resuspend the cell pellet using 21 mL of culture medium.
5. Prepare two aliquots of 20.5 µL each from the cell suspension for cell counting on an automated cell counter (see **Table of Materials**). To each 20.5 µL cell suspension aliquot, add an equal amount of AO/PI dye (see **Table of Materials**) and mix up and down at least 10x.
   NOTE: We do not recommend Trypan Blue for accurate NK cell counting. Alternatively, use a hemocytometer for manual counting.
6. Load 20 µL into each counting chamber of the counting slide and perform automated cell counting using the appropriate program. Calculate the average live cell concentration and note viability.
7. Mix the NK cell solution a few times before aspirating it using a 20 mL syringe and an 18 G needle to maintain sterility. This solution should contain approximately 1 x 10^8 live NK cells in approximately 20 mL or about 5 x 10^6 cells/mL.

8. After removing the needle from the syringe, gently inject the NK cells into the cartridge through the left ECS port. To ensure uniform cell dispersion throughout the cartridge, gently reciprocate the cell solution at least 10x using the syringes connected to the left and right ECS ports.
   NOTE: the solution should have equal turbidity across both syringes, with the left and right end ports closed.
9. Open the left and right end port and inject what remains within the syringes. Close the left and right ECS ports using the clamps.
10. Transfer the cartridge to the incubator and let it sit for 30 min before properly installing it on the flow pump. Leave the cartridge in for biomanufacturing. Adjust the flow rate according to the manufacturer.
11. To monitor cell health metrics, acquire a 0.5 mL aliquot of medium daily from the thoroughly mixed medium in the reservoir bottle and store it at -20 °C after verifying glucose and pH levels. L-lactate levels can be verified later (see **Table of Materials**).
12. Replace the medium in the reservoir (250 - 500 mL) every 1 - 2 days to maintain the glucose content above 50% of the initial levels found in the medium and pH above 7.0 (range from 7.0 - 8.0).

3. Perform NK-EV-rich CM collection daily after 1 day of rest when first seeding the cartridge as described below.
   1. Move the cartridge system into the biosafety cabinet. Gently inject approximately 21 mL of culture medium through the left ECS port to push an equivalent volume

of EV-rich CM through the right ECS - do not mix (see **Figure 3**). NOTE: Always use new plasticware to prevent contamination.

2. Transfer EV-rich CM solution into a 50 mL tube and centrifuge at 300 x *g* for 5 min. Meanwhile, move the cartridge system back into the incubator on the flow pump.
3. Transfer the supernatant to a new tube and centrifuge at 2000 x *g* for 10 min. Again, transfer the supernatant into a new tube. Then, aliquot the EV-rich CM equally across 3, 50 mL tubes (~7 mL/tube) and store at −80 °C until further processing. NOTE: Sequentially harvested EV-rich CM is pooled across these three tubes, generating three technical replicate sample tubes.

4. Perform HFB-NK cell harvest to continue producing EV-rich CM using the same HFB cartridge as described below.
NOTE: NK cells can be harvested from the HFB's ECS by performing the HFB-NK cell harvest protocol" once the cartridge reaches confluence (maximum of 1 x 10^9 cells). This happens after 5 - 7 days for each lot or when the glucose content is found to be below the limit of detection of the glucose meter (e.g., no reading or readings of ~ 0) for 2 consecutive days. If this is the final cell harvest, the medium can be substituted for PBS to flush the cartridge and retrieve the cells.
    1. Harvest EV-rich CM exactly as detailed above in step 1.3.
    2. Inject approximately 50 mL of the medium through the left ECS port. To ensure homogenous cell dispersion throughout the cartridge, gently push back and forth the cell solution using the syringes connected to the left and right ECS ports at least 10x to loosen up cells before ultimately pushing and collecting them with a syringe

through the right ECS port. Transfer the harvested EV-rich CM into a 50 mL tube. Set aside at 37 °C (water bath or incubator) for now.
NOTE: The push-back action helps to dislodge the cells before they are fully expelled and collected by a syringe through the right ECS port. The solution should have equal turbidity across both syringes, with the left and right end ports closed. Tapping on the bioreactor cartridge (physical disturbance) can help preemptively dislodge the cell cluster at the bottom of the cartridge. Aggressive back-forth mixing of the cell suspension can negatively affect the viability of the recovered cells. Care and patience should be applied to maximize viability.

3. Repeat the last step 2x. In total, 150 mL of cell suspension should be recovered. Centrifuge at 300 x *g* for 5 min. Discard supernatant.
4. Resuspend both cell pellets in 20 mL of fresh medium each and combine them. Collect two aliquots of 20.5 µL each of the cell suspension for cell counting on an automated cell counter (see **Table of Materials**).
NOTE: Typically, numerous cell dilutions using PBS as diluent are required to fall within the cell counter's dynamic range.
5. To the 20.5 µL cell suspension aliquot, add an equal amount of AO/PI dye (see **Table of Materials**) and mix up and down at least 10x. Load 20 µL into each counting chamber of the counting slide and perform automated cell counting using the appropriate program.
6. Average the live cell concentration of all dilution-corrected counts, determine the total amount of live cells, and record the viability. As detailed above, to continuously produce EV-rich CM using the same bioreactor cartridge, reseed 1 x

10^8 HFB-produced NK cells.

NOTE: If desired, HFB-produced NK cells can be stored using a cryopreservation freezing medium and a freezing container to control the freezing rate (see **Table of Materials**).

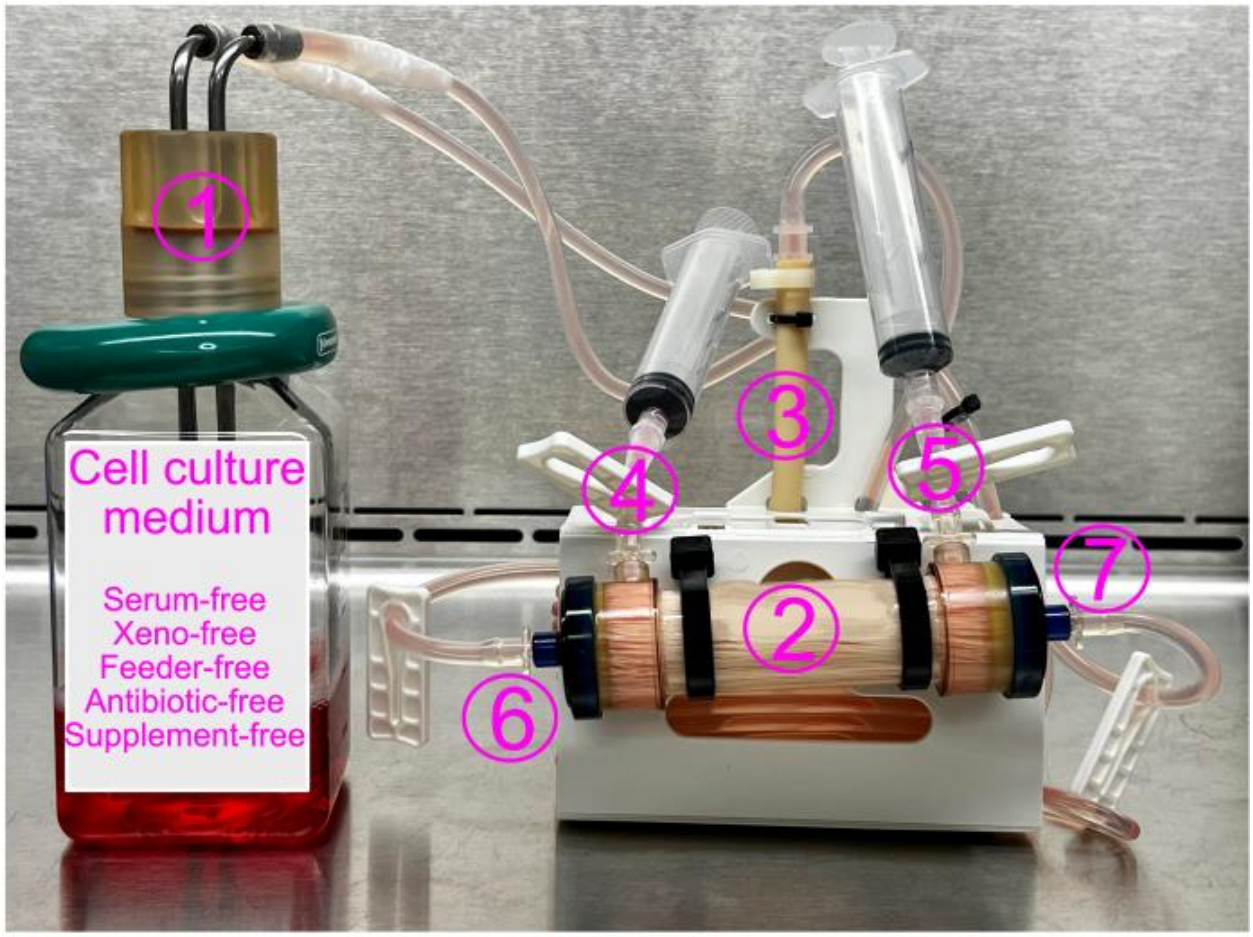

Figure 2: Hollow-Fiber Bioreactor (HFB) system component and set-up.
The reservoir bottle (1) contains the complete medium that circulates through the bioreactor cartridge (2) by the action of a peristaltic pump (not shown) acting on the pump tubing (3). Cells are introduced into the extracellular capillary space (ECS) through the left (4) and right (5) ECS side ports. Once the ECS slide clamps are closed, the left (6) and right (7) end side ports are open to allow the medium to circulate throughout the system. Notice the addition of wax film on the

Luer Lock connection near the reservoir cap of the medium bottle to prevent potential contamination.

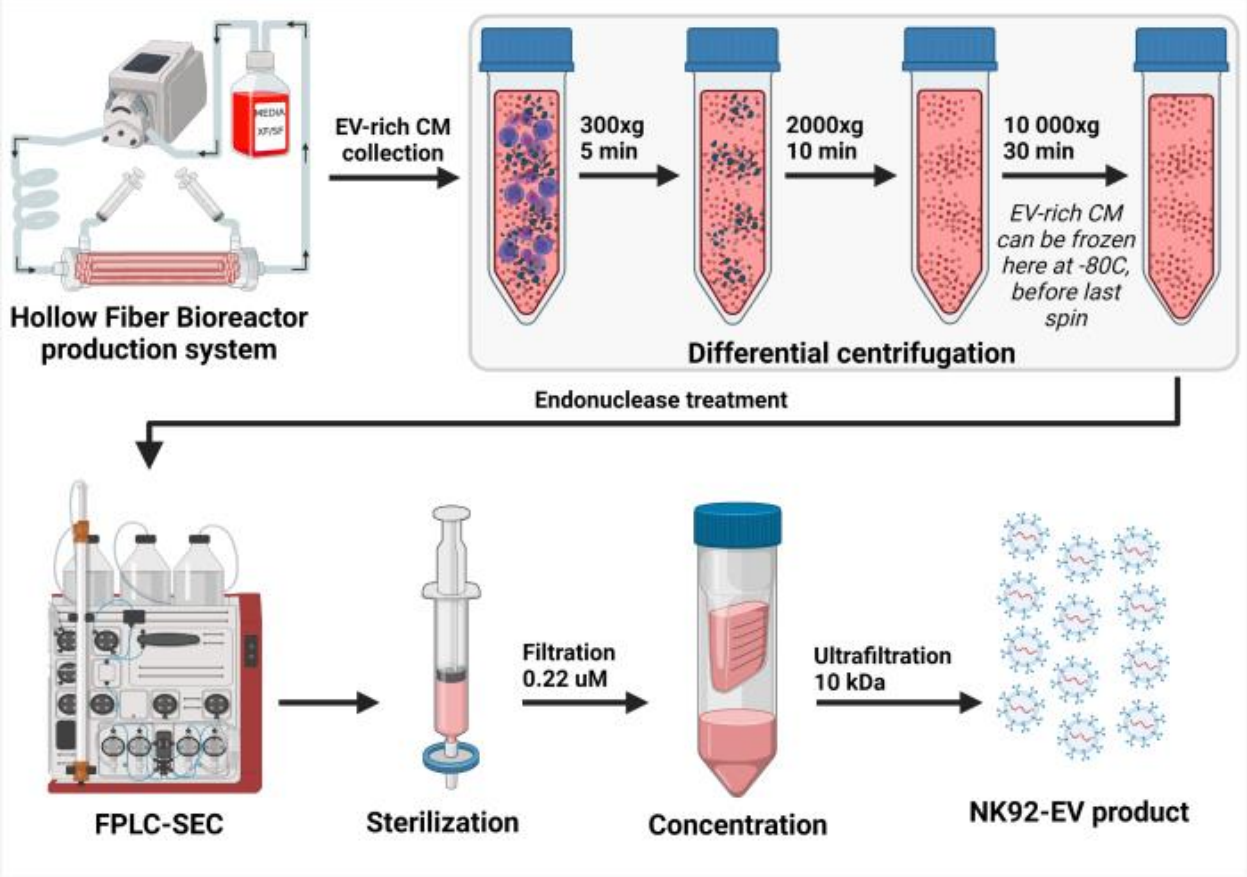

Figure 3: Schematic representation of the NK-EV isolation process.
After daily collection of EV-rich conditioned medium (CM), the solution was differentially centrifugated to remove cells (first spin at 300 x *g* for 5 min) and cellular debris (second spin at 2000 x *g* for 10 min). Cleared EV-rich CM was stored at -80 °C until further processing. Once ready for NK-EV isolation, frozen EV-rich CM is thawed and centrifuged one more time to ensure the removal of cellular debris (third spin at 10,000 x *g* for 30 min). Then, the EV-rich CM is treated for 2 - 4 h at 37 °C with endonuclease to digest nucleic acids considered host cell contaminants. Next, the EV-rich CM is processed by Fast Protein Liquid Chromatography-based size-exclusion chromatography (FPLC-SEC) for EV purification using a bimodal resin. Eluted fractions of approximately 10 - 15 mL are combined and filtered with 0.22 µM filters to ensure the sterility of the final NK-EV product. Ultrafiltration allows the product to be concentrated by a factor of about 35 - 50X, yielding a guaranteed concentration of over 1 x 10^{12} EVs/mL, totaling 1.0 - 1.5 mL. This figure has been modified from[7](created with Biorender.com).

2. NK-EV purification by FPLC-SEC coupled with UF and filter-based sterilization

1. Prepare the following solutions and filter them twice using a 0.1 µm filter (see **Table of Materials**): water (conductivity of 0 mS/cm), PBS: 50 mL of 10x PBS + 450 mL of water (conductivity around 14.7 mS/cm), 20% ethanol, cleaning solution (0.5 M NaOH and 30% isopropyl alcohol in water).
2. Perform FPLC system initiation according to manufacturer's instructions (see **Table of Materials**). Perform pre- and post-run clean-in-place (CIP) steps according to manufacturer's instructions. Wash all lines and the column resin and rinse using double-filtered (DF) water, cleaning solution, DF-water, and DF-PBS.
   NOTE: It is worth noting that CIP can be done on another day if needed.
3. Use a chromatography column packed with a bimodal resin (see **Table of Materials**) with a bed height of 20 cm. Make connections using the drip-to-drip method to ensure no air is introduced inside the column.
4. Set up the fraction collector with appropriate collection tubes and change the fractionation settings to the desired collection volume (e.g., 15 mL). Place enough tubes and two additional tubes to collect the entire sample volume.
5. Carry out sample preparation as described below.
    1. Take 40 - 80 mL of EV-rich CM from the -80 °C freezer and thaw quickly at 37 °C. Load the sample into the ultracentrifuge and spin at 10,000 x *g* for 30 min at 4 °C.

       NOTE: Tubes must be balanced accurately by weight, not by volume.
    2. After spinning, collect the supernatant and transfer it to a new tube. To reduce dsDNA levels, treat the EV-rich CM with 50 U/mL of endonuclease and 1.5 mM

of $MgCl_2$ (see **Table of Materials**). Incubate for 2 - 4 h in an incubator (37 °C), allowing moderate mixing.

6. Once the system (lines and column) is ready for EV isolation, load the EV-rich CM into a 60 mL syringe and connect it to the sample line. Start the system by clicking **Manual Run** and set the flow rate to 0. Follow the software prompts to save the run pre-emptively, then click **Start**.
7. Select **Line B (DF-PBS)** and run at a flow velocity of 150 cm/h (flow rate of 2.0 mL/min). Make sure the solution runs through the column.
8. Once the conductivity stabilizes, press Auto Zero UV. Change the flow path to direct the sample to the waste bottle before the column. Make sure no bubbles are introduced into the system.
9. After a maximum of 5 - 20 s, direct the sample to the column. Click **Fractionation** once the UV readings reach approximately 230 mAU.
10. Once the sample is completely injected through the system, switch the buffer system over to DF-PBS (at the sample valve) to continue purification. Click **Fractionation** again when the UV value reaches approximately 1600 mAU.
    NOTE: This corresponds to the intersection between UV readings and conductivity readings. Longer fractionation only dilutes the retentate without increasing EV yield.
11. Combine all the fractions (diluted NK-EVs) and store them at 4 °C until ready for filter-based sterilization and ultrafiltration (UF).
12. Continue running DF-PBS until the UV value reaches approximately 1000 mAU. After this, stop running and save the chromatogram as a PDF document.

3. NK-EV product filter-based sterilization and concentration by UF

1. Cool down the centrifuge to 10 °C. Sanitize every component of the UF apparatus (see **Table of Materials**) by rinsing with 20 - 30 mL of 90% ethanol. Spin at 4000 x *g* for 5 - 10 min.

   NOTE: The filter is made of 10 kDa MWCO regenerated cellulose.
2. Discard the flow through and then repeat the rinse using sterile PBS to equilibrate the device. Repeat 2x in total.
3. To maximize sterility, filter the diluted NK-EV solution using a 0.22 μm syringe filter pre-wet with DF-PBS (see **Table of Materials**). Collect the filtrate directly into the sterilized concentration apparatus.
4. Spin at 4000 x *g* for 15 - 40 min (spin time is sample dependent). Mix the solution within the top filter compartment using a serological pipette after spinning. Spin at 4000 x *g* for an additional 10 min.

   NOTE: The mixing step is optional as it simply eases the concentration step by preventing the membrane from being clogged by EVs.
5. Temporarily set aside the flow-through and collect the NK-EV sample by inverting the filtration device and attaching it to the collecting device.
6. Spin at 2000 x *g* for 2 min. Transfer the purified NK-EV product into a 2 mL tube. Store the purified NK-EV product at 4 °C for short-term use (≤ 7 days) or frozen at -20 °C for long-term use.

4. NK-EV characterization by Nanoparticle Tracking Analysis (NTA)

1. Prepare the solution and filter it twice at 0.1 µm (see **Table of Materials**): water, PBS, cleaning solution (10% bleach (CAUTION) in water).
2. Initiate the NTA system according to the manufacturer's instructions. Similarly, perform the pre- and post-run clean-in-place (CIP) steps. Wash all lines and rinse using double-filtered (DF) water, cleaning solution, and DF water. Equilibrate the lines using DF-PBS.
3. Verify the flow cell and check for air bubbles. Remove bubbles if present. Once clear, carefully re-insert the flow cell into the NTA instrument. NOTE: Although not recommended by the manufacturer, very difficult-to-remove air bubbles can easily be removed by rinsing with 20% ethanol and then DF-water.
4. Once the flow cell is in place and the door is closed, click **Start Camera**. With the lines filled with DF-PBS, the screen should show an absolute minimum number of particles.
5. Change capture settings to a screen gain of 2 and a camera level of 14. Also, turn on the heater to temperature-stabilize the flow cell.
6. Click **Standard measurement** to create a script under the SOP tab for collecting one capture over 1 min at a flow rate of 30 particles/frame and 23 °C.
7. Just below, add the folder and file name to the pathway name to save the data.
8. Prepare dilutions of the purified NK-EV product using DF-PBS in advance. When running NTA, accurate quantification requires 30 - 80 particles/frame.
9. Vortex the sample before loading it into the syringe (see **Table of Materials**).
10. Carefully connect the 1 mL acquisition syringe to the instrument loading line. No air should be present as it will negatively affect the acquisition and analysis. Slowly push half of the sample through, leaving around 0.5 mL in the syringe.

11. Once particles are visible on the screen, focus the camera to have a maximum of one halo around each particle. Click **Infuse** under the Hardware tab at a rate of 1000 for 5 s. Then, bring it down to a rate of 30.
12. Press **Run Script** and follow the prompts. The software will ensure the temperature is set and ask if the settings are correct. Click **Yes** and follow the software prompts.
13. After completing the capture, click **Cancel** when the software asks to process or export files. Click **Infuse** under the Hardware tab at a rate of 1000 for 10 - 15 s. In the meantime, turn back on the heater and the camera. Then, bring the rate down to 30 until the particles move.
14. Gather four more captures by repeating the previous steps. Once a total of five captures have been recorded per dilutions, perform analysis after importing all five captures.
15. Select the files to be processed by highlighting them. Click **Process Selected Files**. Under the Process tab, adjust the analysis settings to a screen gain of 2 and a detection threshold of 15. Settings are sample-dependent; ensure that 30 - 80 particles per frame are visible.
16. Check and click **OK** for analysis.
17. Once the files are processed, the software will ask to export them. Click **Yes** without clicking additional boxes or click **Export**.
18. Repeat for all EV dilutions or samples. Shut down the NTA instrument after all samples are completed and CIP is done.

5. Quality assurance testing

1. Perform microbial testing using two tests: 1) a small aliquot of purified NK-EVs is spiked into autoclaved LB broth medium, and 2) a small aliquot of purified NK-EVs is used for mycoplasma PCR detection (see **Table of Materials**).
    1. Test 1: culture LB medium at 37 °C for up to 5 days of with positive and negative controls included. Record the OD_{600}, if needed.
    2. Test 2: perform mycoplasma PCR detection according to the manufacturer's protocol.
2. Quantify protein and dsDNA on purified NK-EV dilutions using fluorometer-based assays as per manufacturer's instructions (see **Table of Materials**).

6. Potency evaluation of NK-EV treated cancer cells using a validated highly sensitive resazurin-based cell viability assay [20]

1. Culture human K562 leukemia cells using RPMI-1640 with 10% heat-inactivated FBS for a few days before performing the potency assay (see **Table of Materials**). Maintain density between 2 - 8 x 10^5 cells/mL and replace media every 2 - 3 days.
2. Acquire a 96-well flat-bottom plate (see **Table of Materials**) and pre-emptively add the volume of assay medium (supplemented with 5% EV-depleted FBS) required for normalization purposes (see **Table of Materials**). The final volume is 150 µL/well. NOTE: Use a repeater pipettor to reduce well-to-well variation.
3. Acquire the cell culture and transfer the cells to a tube. Spin at 300 x *g* for 5 min. Resuspend the cell pellet into a single-cell solution using 2 - 5 mL of assay medium.

4. Collect an aliquot of 20.5 µL of the cell suspension for cell counting on an automated cell counter (see **Table of Materials**).
5. To the 20.5 µL cell suspension aliquot, add an equal amount of AO/PI dye (see **Table of Materials**) and mix up and down at least 10x.

   NOTE: We recommend AO/PI for accurate cell counting. Alternatively, use a hemocytometer for manual counting.
6. Load 20 µL into each counting chamber of the counting slide and perform automated cell counting using the appropriate program. Average the live cell concentration and record the viability.
7. Transfer approximately 1 x 10^6 cells into a secondary tube. Dilute the cells to precisely 7 mL of assay medium and repeat cell counting. The concentration should be approximately 1.2 - 1.5 x 10^5live cells/mL.
8. As detailed above, adjust the single-cell suspension concentration to 1 x 10^5 live cells/mL and repeat cell counting if needed.

   NOTE: The coefficient of variation between technical duplicate counts should be less than 25%; typically, it is less than 5% with AO/PI counting.
9. Once the desired concentration is achieved, transfer 50 µL (± 1 µL) of this solution into each well to get as close as possible to 5000 cells/well (4900 - 5100 cells/well). Prepare technical triplicates for each assay condition and use a repeater pipettor to reduce well-to-well variation.
10. Transfer the plate to an orbital shaker (350 - 500 RPM) for 2 min. Transfer cells back to the incubator until ready to proceed with NK-EV treatment.
11. Prepare the required NK-EV dilutions (1:5, 1:10, and 1:100) using an assay medium.

12. From these dilutions, test the following EV concentrations: 1 x 10^8, 5 x 10^8, 1 x 10^9, 5 x 10^9, 1 x 10^{10}, 5 x 10^{10} and 1 x 10^{11} particles/mL. The dosing volume is limited to 20% of the total assay volume.
13. Once ready, transfer the required volume of a given dilution to the wells requiring a desired EV concentration for treatment. Add 15 µL of 10x Triton-X to the positive control well (see **Table of Materials**). The final well volume should be normalized to 150 µL.
14. Add the plate to an orbital shaker (350 - 500 RPM) for 2 min. Incubate the cells at 37 °C in the 5% CO_2 incubator for 3 h.
15. Pre-warm the plate reader (see **Table of Materials**) at 37 °C and load the following script: 37 °C (reduces temperature-related variation), 450 RPM mixing for 1 min (ensures sample homogeneity), and read.
16. Add 15 µL of the resazurin-based reagent to each well (see **Table of Materials**). Protect the reagent from light and use a repeater pipettor to reduce well-to-well variation.
17. Add the plate to an orbital shaker (350 - 500 RPM) for 2 min. Transfer the plate to the incubator and incubate for 60 min. Remove air bubbles using an ethanol-dipped pipette tip. Read plate using an excitation of 560 nm and an emission of 590 nm.
18. Data analysis: Average technical replicates were averaged and correct for background before performing a dose-response analysis using a non-linear regression for the inhibition effect showing the log(inhibitor) vs. normalized response-variable slope without constraint. Record the Hillslope and EC_{50} values.

Results

NK-EVs possess inherent cytotoxic functions and have demonstrated high efficacy against various cancer models. However, there needs to be more standardization among current studies regarding a biomanufacturing workflow suitable for the large-scale production of NK-EVs[6,21]. Our previous study described the feasibility of a closed-looped hollow-fiber bioreactor (HFB) system to produce large quantities of high-purity NK-EV products[7]. As a follow-up, this protocol-based study details the biomanufacturing workflow and demonstrates its reproducibility by producing and isolating the NK-EV product (**Figure 1**). Furthermore, essential product characterization and validation are required before product release is performed, whereby new and original data are presented in this study.

The HFB system was selected for NK-EV production due to its ease of use, reliability, scalability, and GMP compliance[7]. In reference to the HFB system set-up, the NK cells are injected through the left ECS port and seeded into the bioreactor cartridge (**Figure 2**). At the same time, the media bottle is connected to the HFB through the side ports, and the media is allowed to flow throughout the system. The NK cells are cultured in serum-free, xeno-free, feeder-free, and antibiotic-free medium, where the media is replaced when the glucose content falls below 50% to maintain and maximize cell health over time. CM is collected daily, processed through differential centrifugations, and kept frozen (-80 °C) until ready for further processing. Afterward, EV isolation is conducted through a combination of differential centrifugations and FPLC-SEC coupled with UF and filtration (**Figure 3**). This results in a concentrated and sterile NK-EV product with a final volume of approximately 1.0 - 1.5 mL. A representative chromatogram of the FPLC-SEC isolation of NK-EVs is provided (**Figure 4**). Before FPLC-SEC processing, the NK-EV-rich CM is treated with endonuclease, significantly reducing dsDNA levels, a potential host (NK) cell

contaminant[7]. Thus, the described EV isolation workflow removes cellular debris and RNA/DNA contaminants from the NK-EV product, which is essential for ensuring a low and unwanted immunogenic potential and that the final product is suitable for downstream studies.

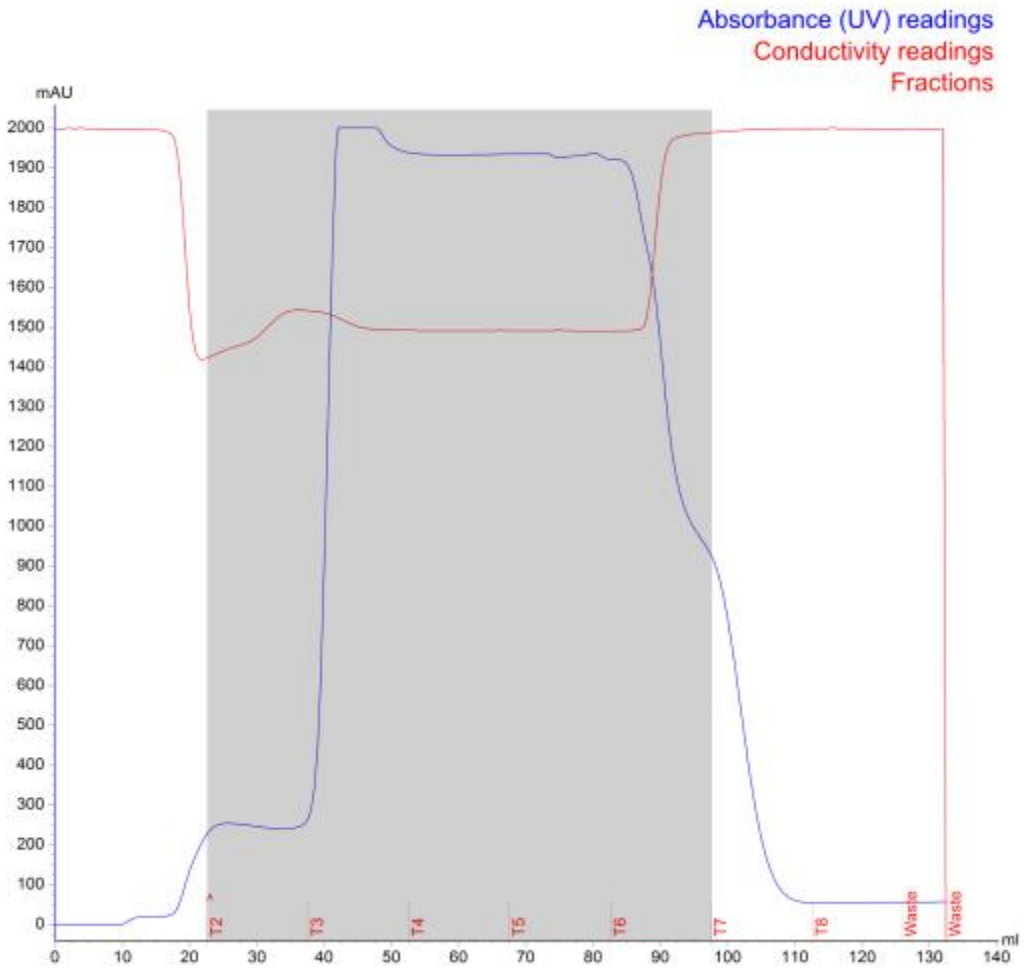

Figure 4: NK-EV isolation chromatogram generated during Fast Protein Liquid Chromatography size Exclusion.
The blue line represents the absorbance (mAU; maximum reading of 2000 mAU), the red line represents the conductivity, the red text represents the run log, and the gray shaded area represents the fractionated NK-EVs (denoted by fractions T2 - T7).

Following isolation, basic NK-EV characterization and quality assurance testing are used to evaluate if the NK-EV product can be released for further downstream experimentation. NK-EV

product particle size range and concentration are measured using nanoparticle tracking analysis (NTA), with sizes ranging from 76.30 - 174.30 nm in diameter (D_{10} of 78.38 ± 2.07 nm, D_{50} of 106.72 ± 2.43 nm, and D_{90} of 169.80 ± 4.17 nm) and an average concentration of 1.39 x 10^{12} EVs/mL (**Figure 5A-B**). Additionally, fluorometer quantification showed a protein and dsDNA concentration of 298.90 ± 66.62 mg/mL and 225.60 ± 37.7 ng/mL for the final product, respectively (**Figure 5C-D**). This corresponds to an average ratio of 5.06 x 10^6 EV/µg of protein and 6.16 x 10^{12} EV/µg of DNA. Microbial and mycoplasma testing both returned negative results (data not shown). These results are consistent with the characterization of NK-EVs from previous work[7]. The earlier publication[7] also provides a further in-depth characterization of the NK-EV products following the MISEV guidelines (i.e., TEM, western blot, endotoxin level, viral entities, and flow cytometry for surface antigens and cytokines).

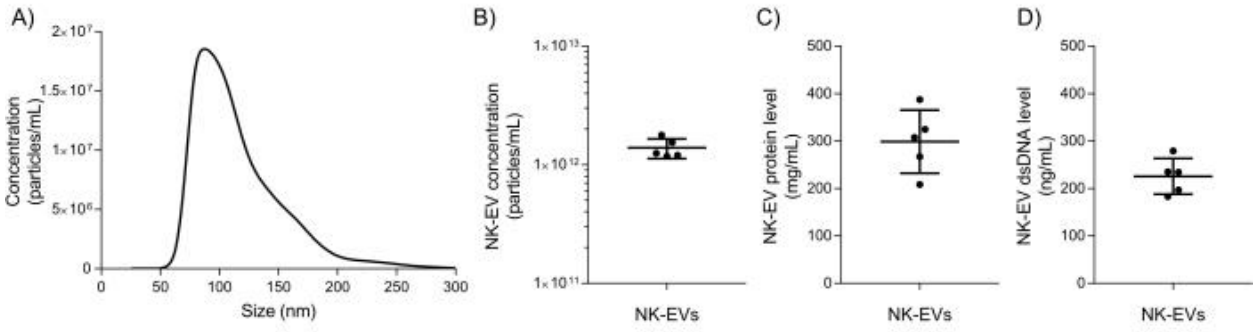

Figure 5: Purified NK-EV product characterization.
(**A**) NK-EV product size distribution measured by NTA, shown as mean from 5 independent experiments, each with 10 technical replicates (5 video captures x 2 dilutions). (**B**) NK-EV particle product concentration (particles/mL) measured by NTA, presented as mean ± SD from 5 independent experiments, each with technical duplicates. (**C**) NK-EV product protein concentration (mg/mL) was measured by using a fluorometer, presented as mean ± SD from 5 independent experiments, each with technical triplicates. (**D**) NK-EV product dsDNA concentration (ng/mL) measured by using a fluorometer, presented as mean ± SD from 5 independent experiments, each with technical triplicates.

Lastly, the NK-EV product's functionality (i.e., cytotoxicity against cancer cells) was assessed using a validated highly sensitive resazurin-based cell viability assay following NK-EV treatment against leukemic cell line K562[7,20]. K562 cell treatment with NK-EVs for 3 h produced a dose-dependent effect on cell viability, corresponding to an EC_{50} of 9.33 x 10^9 EVs/mL (i.e., the dosage that corresponds to the killing of 50% of the cell population; **Figure 6A-B**). Thus, following the outlined product release criteria, the NK-EV product is deemed suitable for further experimentation.

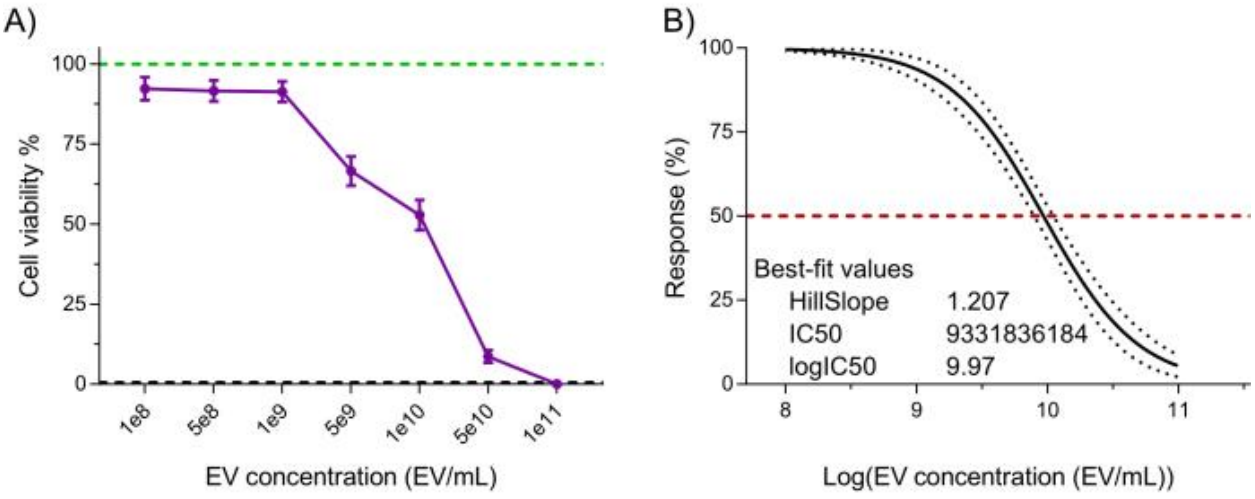

Figure 6: Purified NK-EV product functional validation.
NK-EVs demonstrate a dose-dependent cytotoxicity against human K562 leukemia cells treated at various NK-EV concentrations for 3 hours using a highly sensitivity resazurin-based cell viability assay. (**A**) Normalized assay readouts (green line represents the untreated K562 leukemia cell control, and the black dashed line represents lysed K562 leukemia dead cell control; detergent-treated). Data are shown as mean ± SEM from 11 independent experiments with technical triplicates. (**B**) EC_{50} curve analysis with a variable slope for NK-EV treatment with 95% confidence interval/prediction bands (red dashed line represents 50% response).

Discussion

Several studies suggest that NK-EVs possess vast potential as an anti-cancer therapeutic[4,5,7,9,16,22,23,24,25,26,27,28,29,30]. However, a scalable GMP-compliant biomanufacturing

system capable of yielding large quantities of high-purity NK-EVs is required for further pre-clinical testing and future clinical applications. To address this issue, a previous study used a closed-looped HFB system to continuously produce NK cells and NK-EV-rich CM suitable for downstream experimentation. Due to their 3D design, HFB systems closely reflect the conditions of the vascular system and possess an incredibly high surface-area-to-volume ratio, permitting upwards of a billion cells to remain in culture, ultimately leading to improved EV production[7,31,32]. Importantly, this work was the first to ever report using an HFB system for culturing NK cells, likely due to the cell line IL-2 self-sufficiency[7].

Additional steps must be taken to ensure the sterility of the HFB system and the production of high-purity NK-EVs. These precautions are especially crucial in the absence of a sterile, clean room, which may be the case for several research facilities. Before entering the biosafety cabinet, the HFB system is meticulously sprayed with 70% ethanol to disinfect all external surfaces. Additionally, wax film is wrapped around all Luer Lock connections to minimize the risk of contamination. This is particularly important as this biomanufacturing workflow does not use antibiotics, which are known to affect the biochemical profile of cell and cell-derived products[33]. Various metrics were used to assess cell health during cell product biomanufacturing. For example, daily assessments of the reservoir media's pH, glucose, and lactate levels were conducted as these are vital cell health surrogates for monitoring. In addition to quantitative assessments, qualitative observations of the HFB system (e.g., media color and visual signs of contamination such as turbidity) are also helpful for monitoring cell health. Cell counts on daily retrieved CM have not been found to be a representative metric of viability for the health of the culture (data not shown). This is likely a result of dead cells retrieved during CM sampling that were found within the tubing where media was not allowed to circulate (the small section between the ECS and the ECS syringe

port), thereby undervaluing the viability of the overall cell culture. Only harvested NK cells produced by the HFB at the end of a production lot can provide a reliable metric of the culture's health. These cells consistently showed viability values above 70% across production lots[7]. Together, these quality assessment methods ensure the continuous production of high-purity NK-EVs.

Several isolation techniques have been developed to purify and isolate EVs[34]. One method, SEC, utilizes a column packed with a porous material - resin - allowing for molecule separation based on size discrimination. Here, the larger EVs are eluted through the column faster; this method is known as flow-through purification based on size exclusion. At the same time, smaller contaminants (dsDNA, free-floating proteins like endonuclease, salts, phenol red, etc.) are left behind and further retained within the resin by electrostatic forces (i.e., a bimodal resin was used). SEC-based processing removes non-EV-bound proteins while maintaining the original EV structure and functionality[35,36]. Furthermore, SEC-based purification is easily scalable without compromising the high yield and purity, making it a suitable choice for isolating NK-EVs for biotherapeutic uses. Despite these advantages, SEC has some drawbacks, such as the relatively diluted flow-through (eluent); hence, UF is required for product concentration, but it also permits buffer exchange. The non-sterile UF apparatus is rinsed with 70% ethanol and PBS and kept in the biosafety cabinet prior to use to ensure sterility. Typically, the flow-through can be concentrated to 35x-50x of the initial volume while removing small molecules that could have made their way into the eluent. Differential centrifugation and endonuclease treatment are performed before FPLC-SEC coupled with UF to remove residual cells, cellular debris, and long strands of antigenic dsDNA[7].

Following NK-EV product isolation, characterization, and functional validation are performed per the guidelines in MISEV2018 and MISEV2023 to determine the product's suitability for further use[6,18]. Each isolation yields 1.0 - 1.5 mL of high-purity NK-EV product at a minimum concentration of 1 x 10^{12} EVs/mL, with an average concentration of 1.39 x 10^{12} particles/mL. Previously, Gupta et al. determined that the median EV dosage *in vivo* is 3.37 x 10^{8} EVs/kg of body weight of mice[37]. Treating with the median dosage would require 8.43 x 10^{6} EVs/mouse with a body weight of 25 g, a value far below the guaranteed minimum (1 x 10^{12} particles/mL) obtained through this workflow. Thus, the described biomanufacturing workflow can produce more than enough NK-EVs for pre-clinical experimentation or to meet dosing targets. Each isolation is tested for mycoplasma and microbial presence as part of the product's quality control assessment. In addition, a previous study demonstrated the absence of common viral entities and endotoxin in the final product and the absence of cellular components considered host cell contaminants (by western blot analysis)[7,34]. Lastly, functional assessment was performed using a validated highly sensitive resazurin-based cell viability assay to assess the NK-EVs' functionality[20]. The described viability assay functions by reducing resazurin (weakly fluorescent) to resorufin (highly fluorescent) by metabolically active cells, allowing for the assessment of cell viability following NK-EV treatment. Compared to other alternative cell viability assays, the resazurin-based assay used in the study is highly sensitive to changes in cell viability (very low background noise) and allows for shortened incubation time to observe results (less than 30 min to obtain statistically significant results)[20]. Generally, the NK-EVs exhibit a dose-dependent effect upon K562 viability. Together, the results presented represent an NK-EV product that has met the product release criteria for pre-clinical evaluation and is suitable for downstream applications.

In conclusion, this protocol-based study describes the biomanufacturing of NK-EVs with clinical-grade potential. As discussed, the NK-EVs are produced using a closed-loop HFB system under serum-free, xeno-free, feeder-free, and antibiotic-free conditions[7]. A combination of FPLC-SEC/UF isolates and purifies the NK-EV product. Before releasing the products for downstream application, the NK-EVs must be characterized and functionally validated to ensure they are suitable for use. As demonstrated, following this biomanufacturing protocol can successfully generate a large quantity of high-purity NK-EVs that exhibit on-target cytotoxicity against cancer cells. Therefore, the described biomanufacturing protocol may be an asset for future studies that require the production of clinical-grade NK-EVs.

References

1. Cheng, M., Chen, Y., Xiao, W., Sun, R., Tian, Z. **NK cell-based immunotherapy for malignant diseases.** *Cell Mol Immunol*. **10** (3), 230-252 (2013).
2. Sheridan, C. **Industry appetite for natural killer cells intensifies.** *Nat Biotechnol*. **41** (2), 159-161 (2023).
3. Shimasaki, N., Coustan-Smith, E., Kamiya, T., Campana, D. **Expanded and armed natural killer cells for cancer treatment.** *Cytotherapy*. **18** (11), 1422-1434 (2016).
4. Elsharkasy, O. M., et al. **Extracellular vesicles as drug delivery systems: Why and how.** *Adv Drug Deliv Rev*. **159**, 332-343 (2020).
5. St-Denis-Bissonnette, F., et al. **Applications of extracellular vesicles in triple-negative breast cancer.** *Cancers*. **14** (2), 451 (2022).
6. Welsh, J. A., et al. **Minimal information for studies of extracellular vesicles (MISEV2023): From basic to advanced approaches.** *J Extracell Vesicles*. **13** (2), e12404 (2024).
7. St-Denis-Bissonnette, F., et al. **A clinically relevant large-scale biomanufacturing workflow to produce natural killer cells and natural killer cell-derived extracellular vesicles for cancer immunotherapy.** *J Extracell Vesicles*. **12** (12), e12387 (2023).
8. Federici, C., et al. **Natural-killer-derived extracellular vesicles: Immune sensors and interactors.** *Front Immunol*. **11**, 262 (2020).
9. Lugini, L., et al. **Immune surveillance properties of human NK cell-derived exosomes.** *J Immunol*. **189** (6), 2833-2842 (2012).
10. Zhu, L., et al. **Novel alternatives to extracellular vesicle-based immunotherapy - exosome mimetics derived from natural killer cells.** *Artif Cells Nanomed Biotechnol*. **46** (sup3), S166-S179 (2018).
11. Cochran, A. M., Kornbluth, J. **Extracellular vesicles from the human natural killer cell line NK3.3 have broad and potent anti-tumor activity.** *Front Cell Dev Biol*. **9**, 698639 (2021).
12. Kim, H. Y., et al. **Delivery of human natural killer cell-derived exosomes for liver cancer therapy: an in vivo study in subcutaneous and orthotopic animal models.** *Drug Deliv*. **29** (1), 2897-2911 (2022).
13. Alvarez-Erviti, L., et al. **Delivery of siRNA to the mouse brain by systemic injection of targeted exosomes.** *Nat Biotechnol*. **29** (4), 341-345 (2011).

14. El-Sahli, S., et al. **A triple-drug nanotherapy to target breast cancer cells, cancer stem cells, and tumor vasculature.** *Cell Death Dis*. **12** (1), 8 (2021).
15. Sulaiman, A., et al. **Co-targeting bulk tumor and CSCs in clinically translatable TNBC patient-derived xenografts via combination nanotherapy.** *Mol Cancer Ther*. **18** (10), 1755-1764 (2019).
16. Farcas, M., Inngjerdingen, M. **Natural killer cell-derived extracellular vesicles in cancer therapy.** *Scand J Immunol*. **92** (4), e12938 (2020).
17. Murphy, D. E., et al. **Extracellular vesicle-based therapeutics: natural versus engineered targeting and trafficking.** *Exp Mol Med*. **51**, 1-12 (2019).
18. Thery, C., et al. **Minimal information for studies of extracellular vesicles 2018 (MISEV2018): a position statement of the International Society for Extracellular Vesicles and update of the MISEV2014 guidelines.** *J Extracell Vesicles*. **7** (1), 1535750 (2018).
19. FiberCell-Systems. **.** *FiberCell systems user manual & quick start guide*. , (2024).
20. St-Denis-Bissonnette, F., et al. **Evaluation of resazurin phenoxazine dye as a highly sensitive cell viability potency assay for natural killer cell-derived extracellular vesicle-based cancer biotherapeutics.** *J Extracell Biology*. **3** (7), e166 (2024).
21. Herrmann, I. K., Wood, M. J. A., Fuhrmann, G. **Extracellular vesicles as a next-generation drug delivery platform.** *Nat Nanotechnol*. **16** (7), 748-759 (2021).
22. Andaloussi, E. L. A., Mager, I., Breakefield, X. O., Wood, M. J. **Extracellular vesicles: biology and emerging therapeutic opportunities.** *Nat Rev Drug Discov*. **12** (5), 347-357 (2013).
23. Federici, C., et al. **Exosome release and low pH belong to a framework of resistance of human melanoma cells to cisplatin.** *PLoS One*. **9** (2), e88193 (2014).
24. Yanez-Mo, M., et al. **Biological properties of extracellular vesicles and their physiological functions.** *J Extracell Vesicles*. **4**, 27066 (2015).
25. Neviani, P., et al. **Natural killer-derived exosomal miR-186 inhibits neuroblastoma growth and immune escape mechanisms.** *Cancer Res*. **79** (6), 1151-1164 (2019).
26. Sun, H., et al. **Natural killer cell-derived exosomal miR-3607-3p inhibits pancreatic cancer progression by targeting IL-26.** *Front Immunol*. **10**, 2819 (2019).
27. Jiang, Y., et al. **Engineered exosomes: a promising drug delivery strategy for brain disease.** *Curr Med Chem*. **29** (17), 3111-3124 (2022).
28. Dosil, S. G., et al. **Natural killer (NK) cell-derived extracellular-vesicle shuttled microRNAs control T cell responses.** *Elife*. **11**, e76319 (2022).
29. Geeurickx, E., et al. **The generation and use of recombinant extracellular vesicles as biological reference material.** *Nat Commun*. **10** (1), 3288 (2019).
30. Nathani, A., et al. **Combined role of interleukin-15 stimulated natural killer cell-derived extracellular vesicles and carboplatin in osimertinib-resistant H1975 lung cancer cells with EGFR mutations.** *Pharmaceutics*. **16** (1), 83 (2024).
31. Gobin, J., et al. **Hollow-fiber bioreactor production of extracellular vesicles from human bone marrow mesenchymal stromal cells yields nanovesicles that mirrors the immuno-modulatory antigenic signature of the producer cell.** *Stem Cell Res Ther*. **12** (1), 127 (2021).
32. Sun, L., et al. **A 3D culture system improves the yield of MSCs-derived extracellular vesicles and enhances their therapeutic efficacy for heart repair.** *Biomed Pharmacother*. **161**, 114557 (2023).
33. Ryu, A. H., Eckalbar, W. L., Kreimer, A., Yosef, N., Ahituv, N. **Use antibiotics in cell culture with caution: genome-wide identification of antibiotic-induced changes in gene expression and regulation.** *Sci Rep*. **7** (1), 7533 (2017).
34. Meng, W., et al. **Prospects and challenges of extracellular vesicle-based drug delivery system: considering cell source.** *Drug Deliv*. **27** (1), 585-598 (2020).
35. Yang, Y., et al. **Extracellular vesicles isolated by size-exclusion chromatography present suitability for RNomics analysis in plasma.** *J Transl Med*. **19** (1), 104 (2021).

36. Gamez-Valero, A., et al. **Size-exclusion chromatography-based isolation minimally alters extracellular vesicles' characteristics compared to precipitating agents.** *Sci Rep*. **6**, 33641 (2016).
37. Gupta, D., Zickler, A. M., El Andaloussi, S. **Dosing extracellular vesicles.** *Adv Drug Deliv Rev*. **178**, 178 (2021).

Appendix E. Rights and Permissions

49 Spadina Ave. Suite 200
Toronto ON M5V 2J1 Canada
www.biorender.com

Confirmation of Publication and Licensing Rights - Open Access

July 8th, 2025

Subscription Type:	*Lab - Academic*
Agreement number:	*RT28HHQ2B1*
Publisher Name:	*University of Ottawa*
Figure Title:	*The YAP/TAZ signaling pathway in mammalian cells.*
Citation to Use:	*Created in BioRender. Kirkby, M. (2025) https://BioRender.com/zghqgne*

To whom this may concern,

This document ("Confirmation") hereby confirms that Science Suite Inc. dba BioRender ("BioRender") has granted the following BioRender user: Melanie Kirkby ("User") a BioRender Academic Publication License in accordance with BioRender's Terms of Service and Academic License Terms ("License Terms") to permit such User to do the following on the condition that all requirements in this Confirmation are met:

1) publish their Completed Graphics created in the BioRender Services containing both User Content and BioRender Content (as both are defined in the License Terms) in publications (journals, textbooks, websites, etc.); and
2) sublicense such Completed Graphics under "open access" publication sublicensing models such as CC-BY 4.0 and more restrictive models, so long as the conditions set forth herein are fully met.

Requirements of User:

1) All Completed Graphics to be published in any publication (journals, textbooks, websites, etc.) must be accompanied by the following citation either as a caption, footnote or reference for each figure that includes a Completed Graphic:
"Created in BioRender. Kirkby, M. (2025) https://BioRender.com/zghqgne ".
2) All terms of the License Terms including all Prohibited Uses are fully complied with. E.g. For Academic License Users, no commercial uses (beyond publication in journals, textbooks or websites) are permitted without obtaining or switching to a BioRender Industry Plan.
3) A Reader (defined below) may request that the User allow their figure to be a public template for Readers to view, copy, and modify the figure. It is up to the User to determine what level of access to grant.

Open-Access Journal Readers:

Open-Access journal readers ("Reader") who wish to view and/or re-use a particular Completed Graphic in an Open-Access journal subject to CC-BY sublicensing may do so by clicking on the URL link in the

applicable citation for the subject Completed Graphic.

The re-use/modification options below are available after the Reader requests the User to adapt their

figure as a BioRender template and the User has granted such access.

1) View-Only/Free Plan Use: A Reader who wishes to only view the Completed Graphic may do so in the BioRender Services as either a BioRender Free Plan user or simply as a viewer. By becoming a BioRender Free Plan user, the Reader may view, modify and re-use the Completed Graphic as permitted under BioRender's Basic License Terms (e.g. personal use only, no publishing or commercial use permitted).
2) Re-Use/Publish with No Modifications: For any re-use and re-publication of a Completed Graphic with no modification(s) to the Completed Graphic made by the Reader, a Reader may do so by citing the original author using the citation noted above with the Completed Graphic. The Reader must also comply with the underlying License Terms which apply to the Completed Graphic as noted above (e.g. no commercial use for Academic License).
3) Re-Use/Publish with Modifications: For any re-use and re-publication of a Completed Graphic with a modification(s) made by the Reader, the Reader may do so by becoming a BioRender user themselves under either an Academic or Industry Plan, citing the original author using the citation noted above with the Completed Graphic and complying with the applicable License Terms.

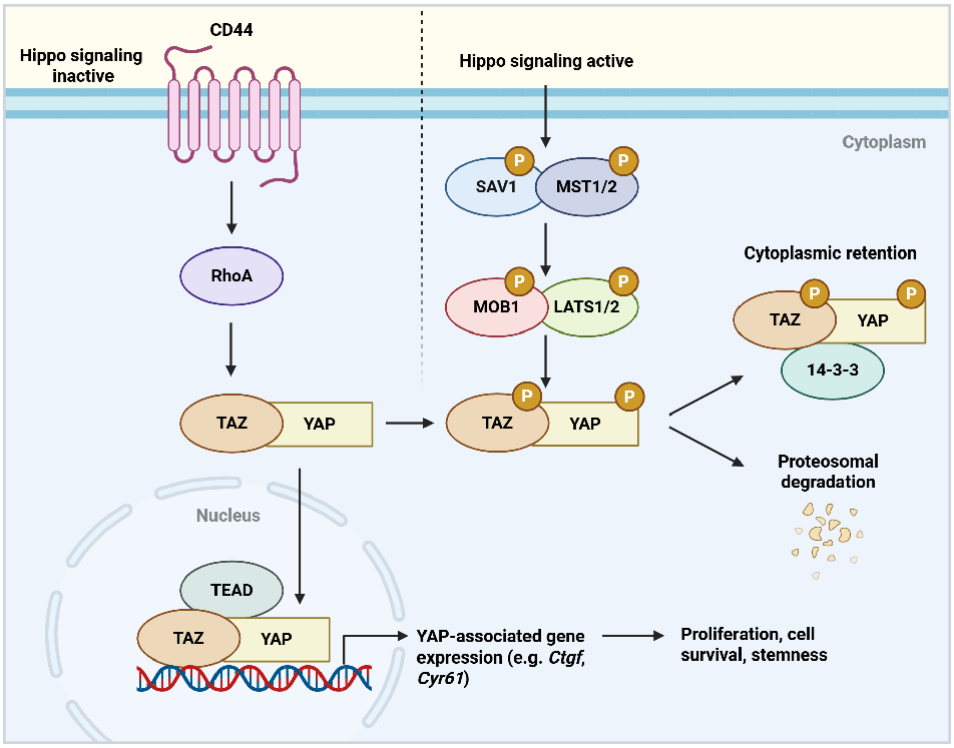

For any questions regarding this document, or other questions about publishing with BioRender, please refer to our BioRender Publication Guide, or contact BioRender Support at support@biorender.com.

49 Spadina Ave. Suite 200
Toronto ON M5V 2J1 Canada
www.biorender.com

Confirmation of Publication and Licensing Rights - Open Access

July 8th, 2025

Subscription Type:	*Lab - Academic*
Agreement number:	*RZ28HHQ9VQ*
Publisher Name:	*University of Ottawa*
Figure Title:	*Representative schematic of the NK-EV's composition.*
Citation to Use:	*Created in BioRender. Kirkby, M. (2025) https://BioRender.com/t546o0i*

To whom this may concern,

This document ("Confirmation") hereby confirms that Science Suite Inc. dba BioRender ("BioRender") has granted the following BioRender user: Melanie Kirkby ("User") a BioRender Academic Publication License in accordance with BioRender's Terms of Service and Academic License Terms ("License Terms") to permit such User to do the following on the condition that all requirements in this Confirmation are met:

1) publish their Completed Graphics created in the BioRender Services containing both User Content and BioRender Content (as both are defined in the License Terms) in publications (journals, textbooks, websites, etc.); and
2) sublicense such Completed Graphics under "open access" publication sublicensing models such as CC-BY 4.0 and more restrictive models, so long as the conditions set forth herein are fully met.

Requirements of User:

1) All Completed Graphics to be published in any publication (journals, textbooks, websites, etc.) must be accompanied by the following citation either as a caption, footnote or reference for each figure that includes a Completed Graphic:
"Created in BioRender. Kirkby, M. (2025) https://BioRender.com/t546o0i ".
2) All terms of the License Terms including all Prohibited Uses are fully complied with. E.g. For Academic License Users, no commercial uses (beyond publication in journals, textbooks or websites) are permitted without obtaining or switching to a BioRender Industry Plan.
3) A Reader (defined below) may request that the User allow their figure to be a public template for Readers to view, copy, and modify the figure. It is up to the User to determine what level of access to grant.

Open-Access Journal Readers:

Open-Access journal readers ("Reader") who wish to view and/or re-use a particular Completed Graphic in an Open-Access journal subject to CC-BY sublicensing may do so by clicking on the URL link in the

applicable citation for the subject Completed Graphic.

The re-use/modification options below are available after the Reader requests the User to adapt their

figure as a BioRender template and the User has granted such access.

1) View-Only/Free Plan Use: A Reader who wishes to only view the Completed Graphic may do so in the BioRender Services as either a BioRender Free Plan user or simply as a viewer. By becoming a BioRender Free Plan user, the Reader may view, modify and re-use the Completed Graphic as permitted under BioRender's Basic License Terms (e.g. personal use only, no publishing or commercial use permitted).
2) Re-Use/Publish with No Modifications: For any re-use and re-publication of a Completed Graphic with no modification(s) to the Completed Graphic made by the Reader, a Reader may do so by citing the original author using the citation noted above with the Completed Graphic. The Reader must also comply with the underlying License Terms which apply to the Completed Graphic as noted above (e.g. no commercial use for Academic License).
3) Re-Use/Publish with Modifications: For any re-use and re-publication of a Completed Graphic with a modification(s) made by the Reader, the Reader may do so by becoming a BioRender user themselves under either an Academic or Industry Plan, citing the original author using the citation noted above with the Completed Graphic and complying with the applicable License Terms.

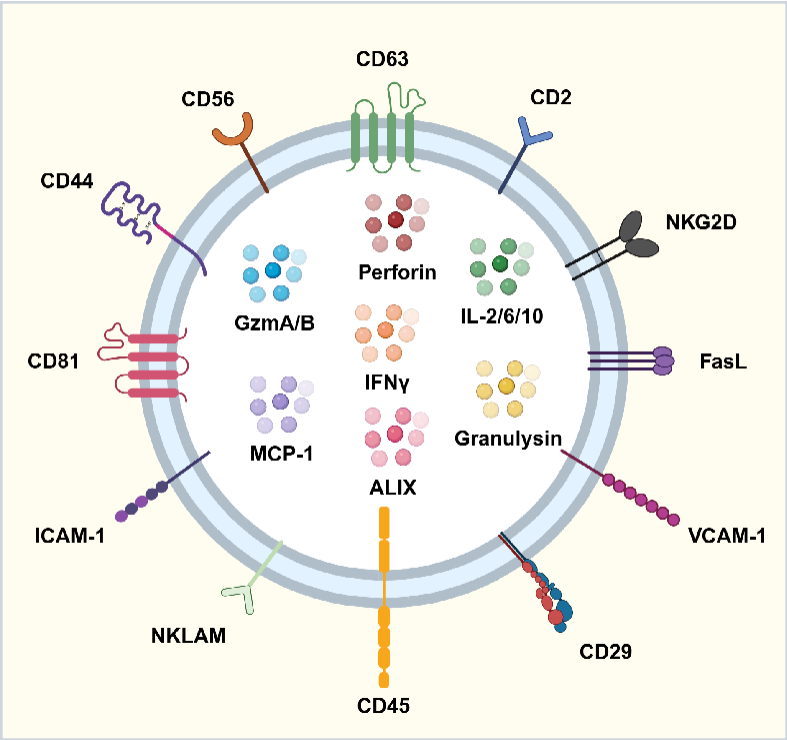

For any questions regarding this document, or other questions about publishing with BioRender, please refer to our BioRender Publication Guide, or contact BioRender Support at support@biorender.com.

49 Spadina Ave. Suite 200
Toronto ON M5V 2J1 Canada
www.biorender.com

Confirmation of Publication and Licensing Rights - Open Access

July 29th, 2025

Subscription Type:	*Lab - Academic*
Agreement number:	*FD28KGEBFH*
Publisher Name:	*University of Ottawa*
Figure Title:	*Cell viability of various TNBC cell lines following NK-EV treatment.*
Citation to Use:	*Created in BioRender. St-denis-bissonnette, F. (2025) https://BioRender.com/1pz6h3l*

To whom this may concern,

This document ("Confirmation") hereby confirms that Science Suite Inc. dba BioRender ("BioRender") has granted the following BioRender user: Melanie Kirkby ("User") a BioRender Academic Publication License in accordance with BioRender's Terms of Service and Academic License Terms ("License Terms") to permit such User to do the following on the condition that all requirements in this Confirmation are met:

1) publish their Completed Graphics created in the BioRender Services containing both User Content and BioRender Content (as both are defined in the License Terms) in publications (journals, textbooks, websites, etc.); and
2) sublicense such Completed Graphics under "open access" publication sublicensing models such as CC-BY 4.0 and more restrictive models, so long as the conditions set forth herein are fully met.

Requirements of User:

1) All Completed Graphics to be published in any publication (journals, textbooks, websites, etc.) must be accompanied by the following citation either as a caption, footnote or reference for each figure that includes a Completed Graphic:
"Created in BioRender. St-denis-bissonnette, F. (2025) https://BioRender.com/1pz6h3l ".
2) All terms of the License Terms including all Prohibited Uses are fully complied with. E.g. For Academic License Users, no commercial uses (beyond publication in journals, textbooks or websites) are permitted without obtaining or switching to a BioRender Industry Plan.
3) A Reader (defined below) may request that the User allow their figure to be a public template for Readers to view, copy, and modify the figure. It is up to the User to determine what level of access to grant.

Open-Access Journal Readers:

Open-Access journal readers (“Reader”) who wish to view and/or re-use a particular Completed Graphic in an Open-Access journal subject to CC-BY sublicensing may do so by clicking on the URL link in the applicable citation for the subject Completed Graphic.

The re-use/modification options below are available after the Reader requests the User to adapt their figure as a BioRender template and the User has granted such access.

1) View-Only/Free Plan Use: A Reader who wishes to only view the Completed Graphic may do so in the BioRender Services as either a BioRender Free Plan user or simply as a viewer. By becoming a BioRender Free Plan user, the Reader may view, modify and re-use the Completed Graphic as permitted under BioRender's Basic License Terms (e.g. personal use only, no publishing or commercial use permitted).

2) Re-Use/Publish with No Modifications: For any re-use and re-publication of a Completed Graphic with no modification(s) to the Completed Graphic made by the Reader, a Reader may do so by citing the original author using the citation noted above with the Completed Graphic. The Reader must also comply with the underlying License Terms which apply to the Completed Graphic as noted above (e.g. no commercial use for Academic License).

3) Re-Use/Publish with Modifications: For any re-use and re-publication of a Completed Graphic with a modification(s) made by the Reader, the Reader may do so by becoming a BioRender user themselves under either an Academic or Industry Plan, citing the original author using the citation noted above with the Completed Graphic and complying with the applicable License Terms.

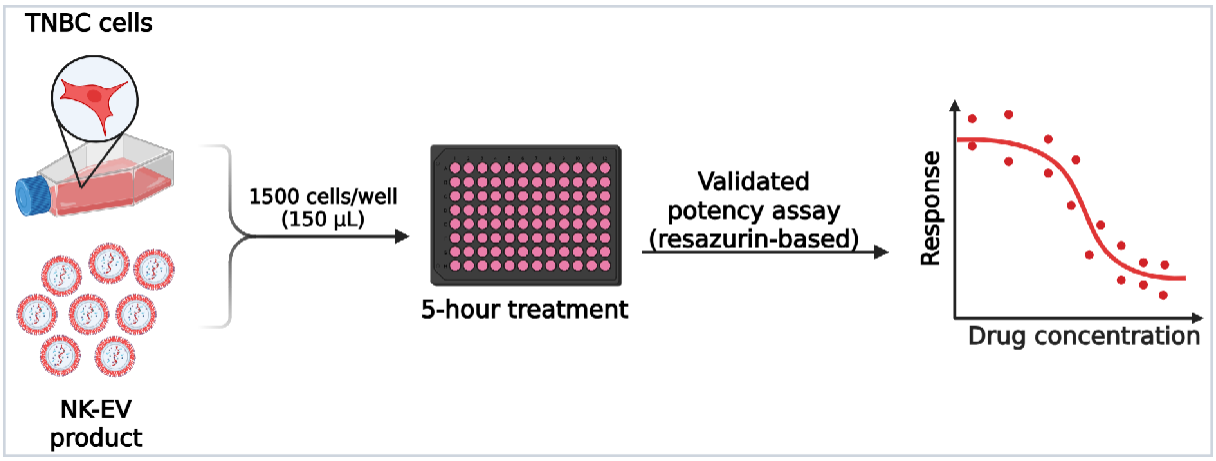

For any questions regarding this document, or other questions about publishing with BioRender, please refer to our BioRender Publication Guide, or contact BioRender Support at support@biorender.com.

49 Spadina Ave. Suite 200
Toronto ON M5V 2J1 Canada
www.biorender.com

Confirmation of Publication and Licensing Rights - Open Access

July 29th, 2025

Subscription Type:	*Lab - Academic*
Agreement number:	*MV28KGEQJC*
Publisher Name:	*University of Ottawa*
Figure Title:	*NK-EVs activate cell-death pathways via an in vitro assay against triple-negative breast cancer cell lines.*
Citation to Use:	*Created in BioRender. St-denis-bissonnette, F. (2025) https://BioRender.com/32v1mw0*

To whom this may concern,

This document ("Confirmation") hereby confirms that Science Suite Inc. dba BioRender ("BioRender") has granted the following BioRender user: Melanie Kirkby ("User") a BioRender Academic Publication License in accordance with BioRender's Terms of Service and Academic License Terms ("License Terms") to permit such User to do the following on the condition that all requirements in this Confirmation are met:

1) publish their Completed Graphics created in the BioRender Services containing both User Content and BioRender Content (as both are defined in the License Terms) in publications (journals, textbooks, websites, etc.); and
2) sublicense such Completed Graphics under "open access" publication sublicensing models such as CC-BY 4.0 and more restrictive models, so long as the conditions set forth herein are fully met.

Requirements of User:

1) All Completed Graphics to be published in any publication (journals, textbooks, websites, etc.) must be accompanied by the following citation either as a caption, footnote or reference for each figure that includes a Completed Graphic:
"Created in BioRender. St-denis-bissonnette, F. (2025) https://BioRender.com/32v1mw0 ".
2) All terms of the License Terms including all Prohibited Uses are fully complied with. E.g. For Academic License Users, no commercial uses (beyond publication in journals, textbooks or websites) are permitted without obtaining or switching to a BioRender Industry Plan.
3) A Reader (defined below) may request that the User allow their figure to be a public template for Readers to view, copy, and modify the figure. It is up to the User to determine what level of access to grant.

Open-Access Journal Readers:

Open-Access journal readers (“Reader”) who wish to view and/or re-use a particular Completed Graphic in an Open-Access journal subject to CC-BY sublicensing may do so by clicking on the URL link in the applicable citation for the subject Completed Graphic.

The re-use/modification options below are available after the Reader requests the User to adapt their figure as a BioRender template and the User has granted such access.

1) View-Only/Free Plan Use: A Reader who wishes to only view the Completed Graphic may do so in the BioRender Services as either a BioRender Free Plan user or simply as a viewer. By becoming a BioRender Free Plan user, the Reader may view, modify and re-use the Completed Graphic as permitted under BioRender's Basic License Terms (e.g. personal use only, no publishing or commercial use permitted).
2) Re-Use/Publish with No Modifications: For any re-use and re-publication of a Completed Graphic with no modification(s) to the Completed Graphic made by the Reader, a Reader may do so by citing the original author using the citation noted above with the Completed Graphic. The Reader must also comply with the underlying License Terms which apply to the Completed Graphic as noted above (e.g. no commercial use for Academic License).
3) Re-Use/Publish with Modifications: For any re-use and re-publication of a Completed Graphic with a modification(s) made by the Reader, the Reader may do so by becoming a BioRender user themselves under either an Academic or Industry Plan, citing the original author using the citation noted above with the Completed Graphic and complying with the applicable License Terms.

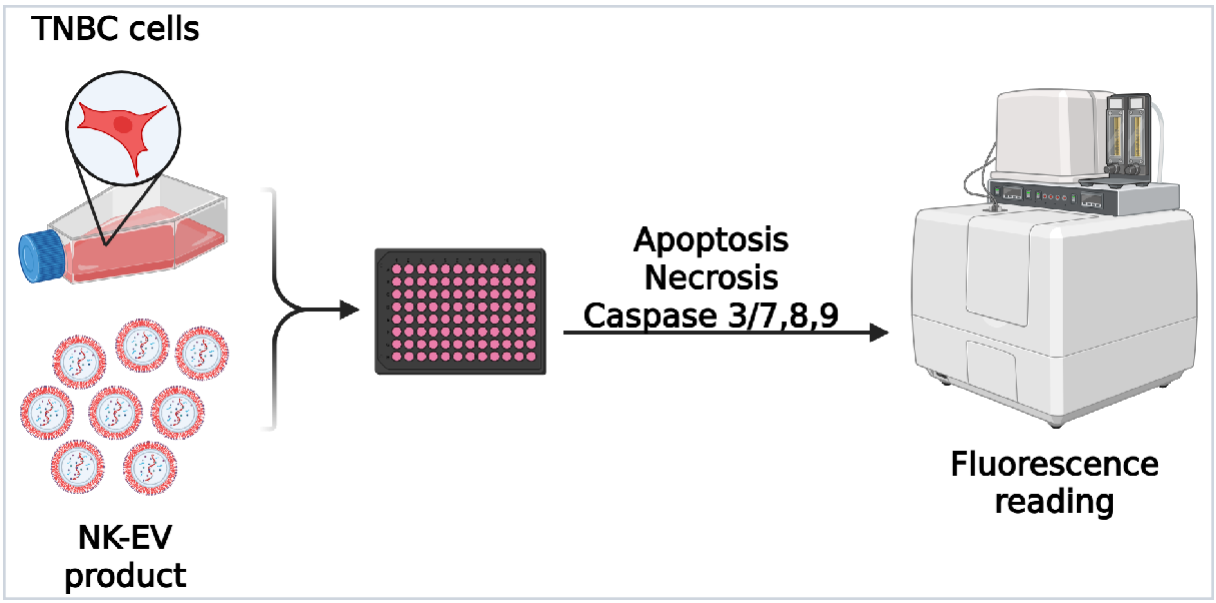

For any questions regarding this document, or other questions about publishing with BioRender, please refer to our BioRender Publication Guide, or contact BioRender Support at support@biorender.com.

49 Spadina Ave. Suite 200
Toronto ON M5V 2J1 Canada
www.biorender.com

Confirmation of Publication and Licensing Rights - Open Access

July 23rd, 2025

Subscription Type:	*Lab - Academic*
Agreement number:	*GP28JMMURM*
Publisher Name:	*University of Ottawa*
Figure Title:	*NK-EV treatment induces apoptosis-mediated cell death in human TNBC-PDX organotypic slice cultures.*
Citation to Use:	*Created in BioRender. Kirkby, M. (2025) https://BioRender.com/jpq9dg6*

To whom this may concern,

This document ("Confirmation") hereby confirms that Science Suite Inc. dba BioRender ("BioRender") has granted the following BioRender user: Melanie Kirkby ("User") a BioRender Academic Publication License in accordance with BioRender's Terms of Service and Academic License Terms ("License Terms") to permit such User to do the following on the condition that all requirements in this Confirmation are met:

1) publish their Completed Graphics created in the BioRender Services containing both User Content and BioRender Content (as both are defined in the License Terms) in publications (journals, textbooks, websites, etc.); and
2) sublicense such Completed Graphics under "open access" publication sublicensing models such as CC-BY 4.0 and more restrictive models, so long as the conditions set forth herein are fully met.

Requirements of User:

1) All Completed Graphics to be published in any publication (journals, textbooks, websites, etc.) must be accompanied by the following citation either as a caption, footnote or reference for each figure that includes a Completed Graphic:
"Created in BioRender. Kirkby, M. (2025) https://BioRender.com/jpq9dg6 ".
2) All terms of the License Terms including all Prohibited Uses are fully complied with. E.g. For Academic License Users, no commercial uses (beyond publication in journals, textbooks or websites) are permitted without obtaining or switching to a BioRender Industry Plan.
3) A Reader (defined below) may request that the User allow their figure to be a public template for Readers to view, copy, and modify the figure. It is up to the User to determine what level of access to grant.

Open-Access Journal Readers:

Open-Access journal readers (“Reader”) who wish to view and/or re-use a particular Completed Graphic in an Open-Access journal subject to CC-BY sublicensing may do so by clicking on the URL link in the applicable citation for the subject Completed Graphic.

The re-use/modification options below are available after the Reader requests the User to adapt their figure as a BioRender template and the User has granted such access.

1) View-Only/Free Plan Use: A Reader who wishes to only view the Completed Graphic may do so in the BioRender Services as either a BioRender Free Plan user or simply as a viewer. By becoming a BioRender Free Plan user, the Reader may view, modify and re-use the Completed Graphic as permitted under BioRender's Basic License Terms (e.g. personal use only, no publishing or commercial use permitted).

2) Re-Use/Publish with No Modifications: For any re-use and re-publication of a Completed Graphic with no modification(s) to the Completed Graphic made by the Reader, a Reader may do so by citing the original author using the citation noted above with the Completed Graphic. The Reader must also comply with the underlying License Terms which apply to the Completed Graphic as noted above (e.g. no commercial use for Academic License).

3) Re-Use/Publish with Modifications: For any re-use and re-publication of a Completed Graphic with a modification(s) made by the Reader, the Reader may do so by becoming a BioRender user themselves under either an Academic or Industry Plan, citing the original author using the citation noted above with the Completed Graphic and complying with the applicable License Terms.

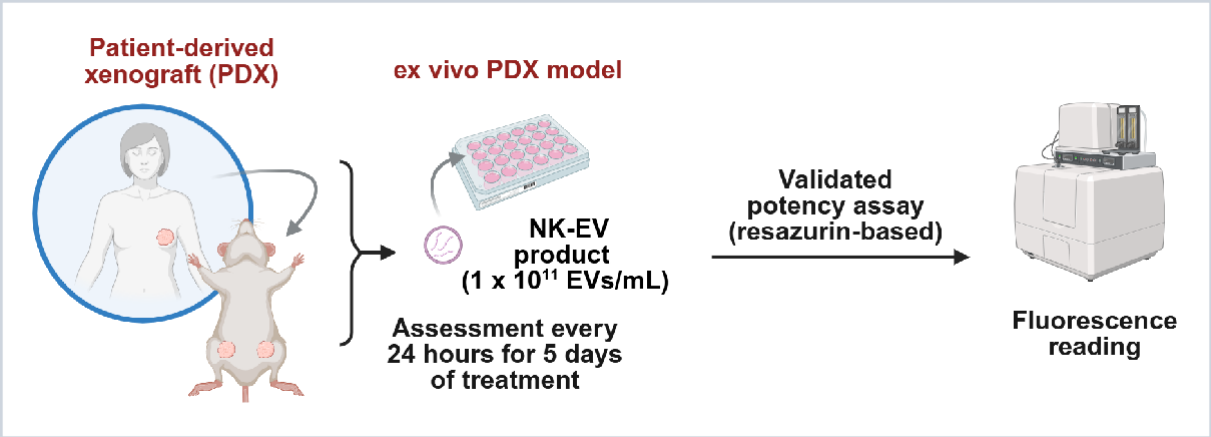

For any questions regarding this document, or other questions about publishing with BioRender, please refer to our BioRender Publication Guide, or contact BioRender Support at support@biorender.com.

49 Spadina Ave. Suite 200
Toronto ON M5V 2J1 Canada
www.biorender.com

Confirmation of Publication and Licensing Rights - Open Access

July 28th, 2025

Subscription Type:	*Lab - Academic*
Agreement number:	*FT28KBZTTB*
Publisher Name:	*University of Ottawa*
Figure Title:	*Evaluation of TNBC PDX tumour growth over four weeks of NK-EV treatment.*
Citation to Use:	*Created in BioRender. Kirkby, M. (2025) https://BioRender.com/mk1zmrq*

To whom this may concern,

This document ("Confirmation") hereby confirms that Science Suite Inc. dba BioRender ("BioRender") has granted the following BioRender user: Melanie Kirkby ("User") a BioRender Academic Publication License in accordance with BioRender's Terms of Service and Academic License Terms ("License Terms") to permit such User to do the following on the condition that all requirements in this Confirmation are met:

1) publish their Completed Graphics created in the BioRender Services containing both User Content and BioRender Content (as both are defined in the License Terms) in publications (journals, textbooks, websites, etc.); and
2) sublicense such Completed Graphics under "open access" publication sublicensing models such as CC-BY 4.0 and more restrictive models, so long as the conditions set forth herein are fully met.

Requirements of User:

1) All Completed Graphics to be published in any publication (journals, textbooks, websites, etc.) must be accompanied by the following citation either as a caption, footnote or reference for each figure that includes a Completed Graphic:
"Created in BioRender. Kirkby, M. (2025) https://BioRender.com/mk1zmrq ".
2) All terms of the License Terms including all Prohibited Uses are fully complied with. E.g. For Academic License Users, no commercial uses (beyond publication in journals, textbooks or websites) are permitted without obtaining or switching to a BioRender Industry Plan.
3) A Reader (defined below) may request that the User allow their figure to be a public template for Readers to view, copy, and modify the figure. It is up to the User to determine what level of access to grant.

Open-Access Journal Readers:

Open-Access journal readers (“Reader”) who wish to view and/or re-use a particular Completed Graphic in an Open-Access journal subject to CC-BY sublicensing may do so by clicking on the URL link in the applicable citation for the subject Completed Graphic.

The re-use/modification options below are available after the Reader requests the User to adapt their figure as a BioRender template and the User has granted such access.

1) View-Only/Free Plan Use: A Reader who wishes to only view the Completed Graphic may do so in the BioRender Services as either a BioRender Free Plan user or simply as a viewer. By becoming a BioRender Free Plan user, the Reader may view, modify and re-use the Completed Graphic as permitted under BioRender's Basic License Terms (e.g. personal use only, no publishing or commercial use permitted).

2) Re-Use/Publish with No Modifications: For any re-use and re-publication of a Completed Graphic with no modification(s) to the Completed Graphic made by the Reader, a Reader may do so by citing the original author using the citation noted above with the Completed Graphic. The Reader must also comply with the underlying License Terms which apply to the Completed Graphic as noted above (e.g. no commercial use for Academic License).

3) Re-Use/Publish with Modifications: For any re-use and re-publication of a Completed Graphic with a modification(s) made by the Reader, the Reader may do so by becoming a BioRender user themselves under either an Academic or Industry Plan, citing the original author using the citation noted above with the Completed Graphic and complying with the applicable License Terms.

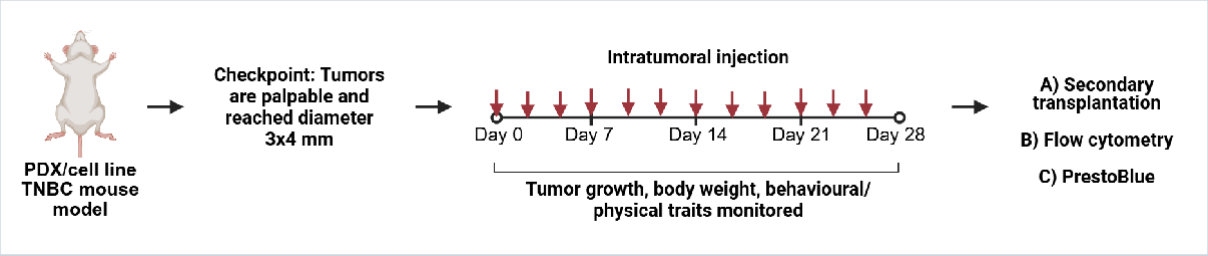

For any questions regarding this document, or other questions about publishing with BioRender, please refer to our BioRender Publication Guide, or contact BioRender Support at support@biorender.com.

49 Spadina Ave. Suite 200
Toronto ON M5V 2J1 Canada
www.biorender.com

Confirmation of Publication and Licensing Rights - Open Access

July 16th, 2025

Subscription Type:	*Lab - Academic*
Agreement number:	*NS28IMY1BG*
Publisher Name:	*University of Ottawa*
Figure Title:	*Secondary transplantation of treated PDX tumours following NK-EV treatment.*
Citation to Use:	*Created in BioRender. Kirkby, M. (2025) https://BioRender.com/k5q2nku*

To whom this may concern,

This document ("Confirmation") hereby confirms that Science Suite Inc. dba BioRender ("BioRender") has granted the following BioRender user: Melanie Kirkby ("User") a BioRender Academic Publication License in accordance with BioRender's Terms of Service and Academic License Terms ("License Terms") to permit such User to do the following on the condition that all requirements in this Confirmation are met:

1) publish their Completed Graphics created in the BioRender Services containing both User Content and BioRender Content (as both are defined in the License Terms) in publications (journals, textbooks, websites, etc.); and
2) sublicense such Completed Graphics under "open access" publication sublicensing models such as CC-BY 4.0 and more restrictive models, so long as the conditions set forth herein are fully met.

Requirements of User:

1) All Completed Graphics to be published in any publication (journals, textbooks, websites, etc.) must be accompanied by the following citation either as a caption, footnote or reference for each figure that includes a Completed Graphic:
"Created in BioRender. Kirkby, M. (2025) https://BioRender.com/k5q2nku ".
2) All terms of the License Terms including all Prohibited Uses are fully complied with. E.g. For Academic License Users, no commercial uses (beyond publication in journals, textbooks or websites) are permitted without obtaining or switching to a BioRender Industry Plan.
3) A Reader (defined below) may request that the User allow their figure to be a public template for Readers to view, copy, and modify the figure. It is up to the User to determine what level of access to grant.

Open-Access Journal Readers:

Open-Access journal readers (“Reader”) who wish to view and/or re-use a particular Completed Graphic in an Open-Access journal subject to CC-BY sublicensing may do so by clicking on the URL link in the applicable citation for the subject Completed Graphic.

The re-use/modification options below are available after the Reader requests the User to adapt their figure as a BioRender template and the User has granted such access.

1) View-Only/Free Plan Use: A Reader who wishes to only view the Completed Graphic may do so in the BioRender Services as either a BioRender Free Plan user or simply as a viewer. By becoming a BioRender Free Plan user, the Reader may view, modify and re-use the Completed Graphic as permitted under BioRender's Basic License Terms (e.g. personal use only, no publishing or commercial use permitted).

2) Re-Use/Publish with No Modifications: For any re-use and re-publication of a Completed Graphic with no modification(s) to the Completed Graphic made by the Reader, a Reader may do so by citing the original author using the citation noted above with the Completed Graphic. The Reader must also comply with the underlying License Terms which apply to the Completed Graphic as noted above (e.g. no commercial use for Academic License).

3) Re-Use/Publish with Modifications: For any re-use and re-publication of a Completed Graphic with a modification(s) made by the Reader, the Reader may do so by becoming a BioRender user themselves under either an Academic or Industry Plan, citing the original author using the citation noted above with the Completed Graphic and complying with the applicable License Terms.

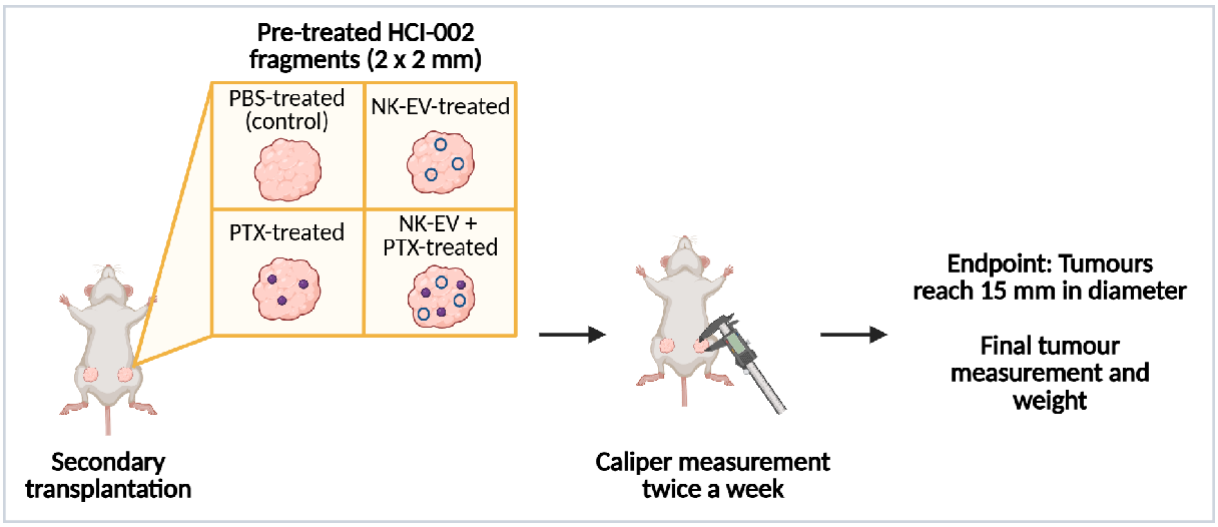

For any questions regarding this document, or other questions about publishing with BioRender, please refer to our BioRender Publication Guide, or contact BioRender Support at support@biorender.com.